Cellular and molecular mechanisms underlying tissue elongation of the developing egg in *Drosophila melanogaster*

by

Saori Lillian Haigo

A dissertation submitted in partial satisfaction of the

requirements for the degree of

Doctor of Philosophy

in

Molecular and Cell Biology

in the

Graduate Division

of the

University of California, Berkeley

Committee in charge:

Professor David Bilder, Chair
Professor Richard Harland
Professor Iswar Hariharan
Professor Jan Liphardt

Spring 2011

Cellular and molecular mechanisms underlying tissue elongation
of the developing egg in *Drosophila melanogaster*

by

Saori Lillian Haigo

Abstract

Cellular and molecular mechanisms underlying tissue elongation
of the developing egg in *Drosophila melanogaster*

by

Saori Lillian Haigo

Doctor of Philosophy in Molecular and Cell Biology

University of California, Berkeley

Professor David Bilder, Chair

The cellular and molecular mechanisms generating the diversity of animal morphologies are still a relatively little explored subject within developmental biology. While changes in cell number help with the growth of tissue, the orientation of cell divisions, migrations, cell rearrangements or changes in cell shape can explain how anisotropies in tissue shape are formed during development. It remains unclear whether the current set of described behaviors can account for all of the diverse morphologies we see in extant metazoan species.

To better understand the mechanisms underlying tissue morphogenesis, my Ph.D. dissertation focused on the development of the ellipsoid egg in *Drosophila melanogaster* as a new, emerging model system to study tissue elongation. Developing egg chambers (follicles) in *Drosophila* originate as a sphere and initially grow isotropically but elongate during oogenesis to form an ellipsoid egg. The cellular and molecular mechanisms underlying follicle elongation were not known, although genetic evidence suggested interactions between the follicle epithelium and the surrounding extracellular matrix (ECM) are somehow involved.

To elucidate how tissue elongation occurs in the *Drosophila* ovary, I utilized live imaging of developing follicles *ex vivo* and discovered that the follicle unexpectedly undergoes several revolutions of polarized, circumferential global tissue rotation – relative to the surrounding ECM – during the major elongation phase of oogenesis. Follicles with epithelia mutant for an Integrin receptor or Collagen IV, an ECM molecule, fail to rotate and result in round eggs. We found that Collagen IV fibrils become circumferentially planar polarized during the rotation phase but become misoriented in non-rotating 'round egg' mutants. Furthermore, acute degradation of Collagen IV rounds previously elongated follicles, suggesting that follicle rotation polarizes a fibrillar matrix that constrains the growing egg in a 'molecular corset', generating its ellipsoid shape. Global tissue rotation is thus a novel morphogenetic behavior, using polarized cell motility to propagate planar polarity information in synchrony to the ECM to control tissue shape.

Many new questions developed from the discovery of global tissue rotation. It is unclear how the follicle epithelium responds to a revolving tissue and a mechanically constraining ECM as

the tissue grows and elongates. Do conventional behaviors of tissue elongation like polarized cell intercalation, cell elongation or cell division occur in the *Drosophila* follicle? Chapter 3 aims to further our understanding of the cellular basis of follicle elongation by developing and performing preliminary quantitative morphometric analysis on the follicle epithelium during the elongation phase. In addition, I examine other known round egg mutants to determine whether they too regulate global tissue rotation or whether these genes regulate additional morphogenetic behaviors necessary for egg elongation.

My final chapter investigates how planar cell polarity (PCP) and global tissue rotation are established in the *Drosophila* follicle. How does molecular planar polarity arise? Does this occur before the onset of polarized follicle rotation? Is there an activation signal to initiate global tissue rotation and from where does this signal originate? I perform an *in silico* enhancer trap screen to identify developmental signaling pathways and other genes that may coincide with the major elongation phase and has led to the identification of the Notch/Delta signaling pathway as a putative regulator of follicle PCP and global tissue rotation, potentially providing an activation signal from the germline.

The findings from my Ph.D. dissertation provide a new framework to think about the cellular and molecular mechanisms underlying tissue elongation of the developing egg, but moreover, challenge current perspectives on metazoan morphogenesis. Global tissue rotation is a novel polarized morphogenetic behavior required for tissue elongation, but the cellular output of this movement remains ambiguous, perhaps because of the follicle's closed topology as an epithelial chamber. It is the first collective cell migration with an obvious individual cell polarity and tissue polarity, but with no obvious collective cell polarity with leader and follower cells. It also raises the possibility that different mechanisms of PCP establishment and propagation may occur in different tissues. These and other issues indicate that continued studies of *Drosophila* egg elongation will provide novel and exciting insights to our understanding of tissue polarity, morphogenesis and development in a variety of organisms.

To my mom,

who is always with me in my heart.

Table of Contents

List of Figures and Table

Acknowledgements

Graduate school has been a long road. A very long road spanning two coasts and 8 years. There are so many people I want to thank who have helped me along my journey but words cannot convey my deepest appreciation for your support. I will try my best.

David, my graduate advisor. Your enthusiasm for science reminds me why I'm in this business. No matter how busy your schedule gets, you always find time for hours of brainstorming, have remarkable speed for editing drafts, and always keep that office door open. All while keeping life in balance with exercise and family; our lab clearly follows your lead. You kept my spirits up when we got those editorial rejections; you were elated to share the news "hot off the presses" when our *Science* reviews came back. Your eagerness to help build new fly stocks makes me laugh. I'll never forget those 3 loud claps. Most importantly, you've given me the freedom to develop this project as independently as I can, and that has given me a tremendous amount of confidence in myself as a young scientist. For that, I am forever grateful.

My thesis committee members: Iswar, Richard and Jan. Iswar, your broad knowledge base, remarkable memory and deep insights make me feel lucky that I can always learn in your presence. Richard, you have been there for me since I started in your lab as an undergraduate nearly a decade ago. Thanks for believing in me before I believed in myself as a scientist. My experience in your lab has led me to become the person and scientist I am today. I look up to you greatly. Thank you Jan for stepping in on such short notice.

The Bilder Lab, my home away from home. So many good memories, so little space. Jen & Han, thanks for introducing me to rock climbing and those words of wisdom when I first joined the lab. Sally, for developing and raising excitement around the round egg project in our lab, for all your entertaining stories and good friendship, for Santa Cruz. Thomas, Anne, and Lucy: your valuable input at lab meetings was one of the main reasons I wanted to join the lab. Lara, for being the best baymate, eh! Holly, your baked goods always hit the spot. Sarah, for reminding me the importance of work/life balance. Brandon, I loved those evening chats in the fly room; thanks for getting me hooked on This American Life. Ale, your unforgettable laugh and general enthusiasm. Laurent, for introducing me to NPR. Josh, for being my tri buddy, purple haze and Lady Gaga. And all the techs and undergrads of past and present – you bring a certain charisma to our lab that cannot be replaced.

My family has been such an instrumental part of my success throughout life. I do not know how to thank them for their constant belief in my abilities and all the sacrifices they have made. It has been hard for our family during grad school – I lost my mom in the middle of it. My sister and my dad's strength through it all has helped me dig deep to keep going. I think of my mom when thoughts of quitting grad school filled my head late at night. She knows I am not a quitter; I stay strong for you. I think of my grandma every time I look at the daruma she had me buy before I started grad school that lives by my desk. I stared at its one eye during my low points in lab. Now, I am very excited that I get to fill in that second eye and send a picture to let her know I've finally finished.

I also am forever indebted to the friendships I've formed during my time at Berkeley. To the Harland lab, for good company, for good laughter, for Bay of Pigs and I'm on a boat, for karma beer. Thanks to all my friends that we've shared laughs, ideas and even a few tears over many dinner parties, game nights, or ventures into the city. To Jose (Joey), my concert buddy! Our conversations over coffee or drinks always give me perspective about the world we live in and life in general that I can easily ignore in the lab. Thank you also for diversifying my musical interests; they paid off in the microscope room. Galo! I love your fun spirit, great laugh and eagerness over Zelda. Kate, my workout buddy! For always being up for cycling, wine tasting and camping. Jess! Such a good friend and great neighbor to have lived by. Melanie! It's been fun to chat over our many walks to Peets to gain perspectives on science and life. I've learned more about birds than I've ever appreciated. Thank you all for helping me during my many injuries at Berkeley – to my face, ankle, or knee – by bringing lunch, ice or driving me around while I healed. I also want to thank the class of 2006 for 5 years of great fun and memories. I value all the friends I've made and look forward to seeing us all grow and prosper.

Last, but not least, I want to thank my boyfriend Pete. You are my best friend and it's been an adventure to share our lives. Your creativity, passion and open heart keep me inspired each day to approach science in ways I didn't necessarily think about until I met you. Thank you for dealing with the odd work hours of an academic scientist and helping me relax and remember the simple yet important things in life when lab gets me down. Thank you for believing in me always. I love you.

Chapter 1

Introduction

1.1 Mechanisms of tissue morphogenesis in metazoans

1.1.1 Overview

The diverse morphologies seen in extant and extinct animal species have long fascinated biologists over time. The collective studies of zoologists and paleontologists have provided the basis for the description of diverse morphologies seen in various animal species, but the mechanisms describing how these morphologies arose has been the study of embryologists and developmental biologists in the last century.

Morphogenesis (from the Greek words *morphê*: shape and *genesis*: creation) is one of the main subjects of developmental biology and describes the cellular and molecular mechanisms leading to the formation of tissue, organ and body shape during development. Morphogenesis is distinct from other main subjects of developmental biology, such as tissue growth and cellular differentiation. These areas focus on the mechanisms that regulate the sizes of organs and the mechanisms that enable cells to gain distinct cell fates during the course of development, rather than the mechanisms that generate form per se. These latter areas have been popular amongst embryologists and have been extensively reviewed (Chuong and Richardson, 2009; Halder and Johnson, 2011; Kondo and Miura, 2010; Stanger, 2008). The remainder of this Ph.D. dissertation will focus on mechanisms of morphogenesis and relate aspects of growth or differentiation of only immediate relevance.

Morphogenesis has been studied in a variety of metazoans from sponges to man but the majority of insights into its cellular and molecular basis have come from studies in the African clawed frog, *Xenopus laevis* and the common fruit fly, *Drosophila melanogaster*. These studies have highlighted that a small repertoire of morphogenetic behaviors seem to give rise to the diverse morphologies seen in these animal model tissues. These include regulated cell proliferation, oriented cell divisions, changes in cell-cell adhesive states, tissue architectural changes from epithelia to mesenchyme or vice versa, directional single or collective cell movements, changes in cell shapes, and changes in cell-cell neighbor relations that control the shapes of tissues (Figure 1.1). In particular, the generation of tissue asymmetries that gives rise to elongate tissues and organs can contribute to the diverse morphologies seen among metazoans. Thus, a better understanding of the mechanisms of tissue elongation is needed to understand how morphological diversity and complexity arose during evolution. I start with an overview of our current understanding of the cellular behaviors and signaling molecules underlying tissue elongation. I then provide an introduction to the model tissue that I chose to study for my dissertation – the elongation of the developing egg in the female *Drosophila* ovary.

1.1.2 Single and collective cell migrations

The migration of single or clusters of cells is necessary to remodel many tissues and is a hallmark of morphogenesis. Cells can move individually or collectively as sheets, strands, clusters or even ducts from one region of the embryo to another (Andrew and Ewald, 2010; Friedl and Gilmour, 2009). These movements enable the extension of organ systems across the entire body axis and the rearrangements of a subset of cells relative to others. Examples include the formation of the lateral line system in zebrafish (Haas and Gilmour, 2006), the migration of

the neural crest in vertebrates (Clay and Halloran, 2011), and branching morphogenesis of the tracheal system in flies (Samakovlis et al., 1996) and of the mammary glands in mammals (Ewald et al., 2008).

Collective cell migrations are of particular interest because they require additional supracellular organization between cells that is still not well understood. Collective cell migration is defined by three criteria: 1) the physical attachment of cells to one another such that cell-cell junctions are properly maintained between cell neighbors during movement, 2) a polarity displayed within the cell group evident by an supracellular organization of the actin cytoskeleton that generates the traction and protrusion force necessary for migration, and 3) modification of the tissue along the migration path through deposition or remodeling the extracellular matrix (ECM) around the cell cluster (Friedl and Gilmour, 2009). Collective cell movements require guidance by extracellular chemical and physical cues and can occur in two-dimensions as a sheet migration or in three-dimensions moving through a tissue scaffold. Oftentimes collective cell migrations exhibit polarity within the group such that 'leader' cells guide their 'follower' cells in the rear. This front-rear asymmetry has been thought to be a defining feature of all migrating collectives thus far (Friedl and Gilmour, 2009).

During the migration process, individual cells must utilize and constantly remodel focal contacts established with the surrounding ECM, and oftentimes in the case of epithelial cells, remodel cell-cell adhesions without completely breaking down cell-cell junctions between neighboring cells within the migrating collective or with surrounding tissues. Cell-ECM adhesions can influence migration speed, and increasing cell-ECM adhesions and cytoskeletal contractility allows motile cells to aggregate these cell-ECM contacts into focal contacts or adhesions that can generate substantial traction force, enabling cells to 'pull' along the ECM substrate (Schmidt and Friedl, 2010). Integrins are the primary mediators of cell-matrix interactions, by controlling the strength and turnover rate of cell-ECM adhesions to regulate migration speed and directional persistence (Schmidt and Friedl, 2010). Remodeling of cell-cell adhesions during morphogenesis often involve cadherins (Gumbiner, 2005) and despite their association in establishing and maintaining stable epithelial architecture (Larue et al., 1994), dynamic turnover of cadherin activity is essential for cell migration and tissue morphogenesis (Bertet et al., 2004; Blankenship, 2006; Classen et al., 2005; Marsden and DeSimone, 2003; Niewiadomska et al., 1999). Migrating epithelial cells in culture can undergo rapid, polarized flow of cadherins (Kametani and Takeichi, 2007) so it is thought that rapid molecular turnover at adherens junctions can change the adhesive states of cadherins (Friedl and Gilmour, 2009), through changes in expression levels or binding partners, to facilitate rapid cell neighbor exchange in some migratory contexts (Cortes et al., 2003). Moreover, there is crosstalk between these adhesion complexes (Chen and Gumbiner, 2006; Weber et al., 2011), either as physical responses to integrin-mediated adhesion or common signaling pathways that link these adhesion complexes through changes in gene expression (Becam et al., 2005) or activity (Marsden and DeSimone, 2003).

1.1.3 Convergent extension by cell intercalation

Convergent extension by cell intercalation is the best-described and documented morphogenetic movement whereby a collective cell behavior has been causally linked to tissue elongation.

Originally described as convergence and extension, these terms were classical definitions for a tissue that undergoes narrowing and lengthening while conserving tissue volume during morphogenesis. Early embryological studies initially described convergence and extension of the dorsal marginal zone of the amphibian gastrula (Mangold, 1920; Spemann, 1902; Vogt, 1922a; Vogt, 1922b), and given that this occurred in the absence of growth, it was postulated that convergent extension occurs by cell-cell rearrangements (Waddington, 1940). The earliest descriptions of the cellular basis of convergence and extension came from the seminal works by Ray Keller in the 1980s, describing mediolateral cell intercalation underlies convergence and extension of the axial mesoderm during *Xenopus* gastrulation (Keller, 1984). In essence, the movement is simply coordinated, polarized cell-cell rearrangements along an axis such that cells intercalate along one axis (convergence), giving rise to more cells in the orthogonal axis and resulting in extension of the entire tissue.

Since those initial studies, convergent extension by cell intercalation has been described in both mesenchymal and epithelial tissues, in a variety of organs and organisms. Examples include archenteron elongation in echinoderms (Ettensohn, 1985; Hardin, 1989; Hardin and Cheng, 1986), germband extension in *Drosophila* (Bertet et al., 2004; Blankenship, 2006; Irvine and Wieschaus, 1994), dorsal hypodermis intercalation in the nematode (Williams-Masson et al., 1998), notochord elongation of ascidians and vertebrates (Miyamoto and Crowther, 1985; Sausedo and Schoenwolf, 1993; Sausedo and Schoenwolf, 1994; Warga and Kimmel, 1990), and neuroectoderm extension of segmented polycheate worms (Steinmetz et al., 2007) and various vertebrates (Elul et al., 1997; Keller et al., 1992; Schoenwolf and Alvarez, 1989).

What has emerged from these works is the variety of subcellular and molecular mechanisms that tissues use to mediate convergent extension by cell intercalation. Mesenchymal cells of the *Xenopus* gastrula or neurula exhibit bipolar or monopolar protrusions, respectively, using neighboring cells as substrates to exert traction on for directed motility (Elul and Keller, 2000; Elul et al., 1997; Keller et al., 1992; Shih and Keller, 1992a). Epithelial cells of the *Drosophila* germband, in contrast, utilize polarized apical cell-cell junction remodeling, following either a stereotypical T1 to T2 to T3 junction transitions (Bertet et al., 2004) or higher order multicellular rosettes (Blankenship, 2006), for polarized cell intercalation. While these model tissues have been the most extensively characterized in the last two decades, studies from other model tissues reveal that epithelial cells can also mediate cell intercalation using protrusive activities on the basolateral domain of the epithelium, such as that seen in the dorsal hypodermal cells of the nematode, *Caenorhabditis elegans* (Williams-Masson et al., 1998) or the notochord of the ascidian (Munro and Odell, 2002). This suggests that we still have much to learn about how different model tissues achieve convergence and extension.

The discovery of higher order multicellular rosette formation and resolution during germband extension in *Drosophila* suggest that cells can mediate very efficient cell intercalation depending on the elongation needs of the tissue (Blankenship, 2006). While most tissues undergo elongation over hours or days to achieve its total elongation, the germband epithelium completes eighty percent of its 2.5-fold elongation within the first forty-five minutes of gastrulation. To accommodate this extensive elongation in a short timeframe, a majority (eight-seven percent) of the germband epithelium form 5 to 11 cell clusters that converge at a common vertex to form a multicellular rosette that resolve their apical cell-cell junctions in a polarized manner

(Blankenship, 2006). This enables up to a 3-fold change in tissue aspect ratio when 10 cells form multicellular rosettes to efficiently change cell neighbors 2 to 5 cell diameters away in contrast to the 1.79-fold change in tissue aspect ratio when cells use type 1 to type 2 to type 3 junctional remodeling for cell intercalation that mediate neighbor exchange only one cell diameter away (Blankenship, 2006). This study reminds us to consider the temporal scale in which elongation occurs, as it may uncover novel strategies used by metazoans to elongate a tissue.

1.1.4 Polarized cell shape changes

Cell shape changes have been described in a subset of elongating tissues. The clearest case has been observed in plants, where individual plant cells elongate along the primary axis and is causally linked to tissue elongation of shoots and roots (Taylor, 2008; Ueda et al., 2005). Cell shape changes in metazoans, however, may be transient changes during a morphogenetic process, or result in permanent changes that can contribute to or is a consequence of tissue elongation. For example, bipolar cell elongation has been described in axial mesodermal convergence and extension (Shih and Keller, 1992a; Shih and Keller, 1992b), but the axis of cell elongation parallels the direction of cell movement, orthogonal to the axis of tissue elongation; these cell shape changes do not contribute to tissue elongation. Initial studies of germband extension in *Drosophila* from fixed samples suggested no change in cell shape within the germband epithelium (Hartenstein and Camposortega, 1985). However, more recent global tissue analysis using individual cell shape and movement tracking has revealed that the germband epithelium undergoes individual cell elongation along the elongating antero-posterior (A-P) axis that is thought to contribute to one-third of tissue elongation during the early phase of germband extension (Butler et al., 2009). These polarized cell elongations are masked somewhat in wild type conditions due to the countering release in tissue tension mediated by polarized cell intercalation within the germband epithelium, but is obviated when mutants defective in convergent extension are examined. Thus, analyzing elongating tissues by tracking "tissue tectonics" (Blanchard et al., 2009) can provide us with additional behaviors and insights that may be missed from traditional methods of morphometric analysis.

1.1.5 Oriented cell divisions

Oriented cell divisions have been observed in elongating tissues, but this behavior has more controversial evidence supporting its causal role in controlling tissue elongation. Oriented cell divisions have been described in the leech germinal bands (Weisblat et al., 1980), the zebrafish gastrula (Concha and Adams, 1998), the chick primitive streak (Wei and Mikawa, 2000) and the mouse kidney (Saburi et al., 2008) in addition to the *Drosophila* germband (da Silva and Vincent, 2007) and imaginal disc (Baena-Lopez et al., 2005) to regulate axial elongation of the developing embryo or the final shape of organs.

In the zebrafish gastrula, it has been suggested that oriented cell divisions rely on PCP genes (Gong et al., 2004) but subsequent experiments randomizing the mitotic spindle orientation plane using loss of function strategies against *nuclear mitotic apparatus* (*NuMA*) or abolishing cell division through inhibition of *early mitotic inhibitor 1* (*emi1*) have shown that oriented cell

divisions are dispensable for the extension of this tissue and body axis elongation (Quesada-Hernandez et al., 2010; Segalen et al., 2010).

1.1.6 Forces underlying morphogenetic behaviors – active versus passive behaviors

An important point to keep in mind in studies of morphogenesis is to appreciate where the forces originate to elongate tissues, as some behaviors may be force-producing active processes while other behaviors may be passive responses to forces generated elsewhere in the developing tissue (Keller et al., 2000). A clear example of this cautionary note comes from studies performed in the zebrafish gastrula (Gong et al., 2004; Quesada-Hernandez et al., 2010; Segalen et al., 2010), where a correlation of oriented cell division was interpreted to play an active, force-producing morphogenetic role in axis elongation from initial studies but subsequent experiments testing this interpretation ruled out the contribution of oriented cell division in tissue elongation. Likewise, one can be led astray if one interprets a genetic loss-of-function phenotype blocks a given behavior – say convergent extension – as revealing that convergent extension is an active process. It is possible that convergent extension is a passive response to other forces in the embryo and the wild type function of the gene may be to increase tissue deformation, enabling it to be sculpted by surrounding active tissues (Aigouy et al., 2010; Keller et al., 2000).

The most rigorous method of determining whether a behavior is an active or passive process is to isolate the tissue of interest from any other forces produced elsewhere in the embryo. The development of tissue explants of the dorsal marginal zone of the *Xenopus* gastrula demonstrated that it could undergo convergent extension in isolation from the rest of the embryo (Keller et al., 1985). Unfortunately, not all developmental tissues undergoing morphogenesis are amenable to explant isolation studies, but use of genetic mutations affecting other potential source tissues of force generation may identify whether some behaviors are passive, as demonstrated in the case of polarized A-P cell elongation of the *Drosophila* germband (Butler et al., 2009), which occurred in response to the invaginating mesoderm. Likewise, use of laser ablation to relieve tension from surrounding tissues identified that the *Drosophila* wing hinge is responsible for the passive responses of proximo-distal (P-D) oriented cell divisions, cell elongation and cell neighbor exchange occurring in the wing blade during pupal morphogenesis (Aigouy et al., 2010).

In the end, many tissue elongation events require a combination of polarized cellular behaviors, and the observation that one behavior may compensate for the defects in another (Butler et al., 2009) demonstrates the robustness of embryos to genetic or environmental challenges that can occur during development. However, it is important to appreciate that some behaviors may be active processes in one context but passive in another, and a further understanding of the forces that contribute to known and uncharacterized morphogenetic processes are needed in order to fully appreciate the mechanisms that control morphogenesis.

1.1.7 Planar cell polarity and tissue elongation

Interestingly, many of the cellular behaviors associated with tissue elongation exhibit tissue polarity, more recently known as planar cell polarity (PCP), where cells across the plane of the tissue display a form of coordinated polarization. The output of PCP can be observed

morphologically by the orientation of hairs or cilia in epithelial tissues or by polarized cell behaviors by mesenchymal cells (Simons and Mlodzik, 2008; Vladar et al., 2009; Wallingford, 2010; Zallen, 2007).

Initial observations of tissues displaying PCP was made in the 1940s to 1970s with the identification of oriented hairs and bristles on the adult insect cuticle (Lawrence, 1966; Wigglesworth, 1940), oriented cell migration during regeneration in *Hydra* (Herlands and Bode, 1974), oriented cilia of ependymal cells of the vertebrate central nervous system (Nakayama and Kohno, 1974), and the orientation of ommatidia within insect eyes (Lawrence and Shelton, 1975).

Genetic screens in *Drosophila* in the 1980s began to elucidate the genetic basis of PCP (Gubb and Garcia-Bellido, 1982) with the isolation of *prickle* (*pk*), *frizzled* (*fz*), and *inturned* (*in*) as the earliest polarity mutants. The availability of genetic mutants and the use of genetic tissue mosaics provided new insights to old observations from transplantation experiments that PCP information was transmitted from neighboring cells and interpreted by individual cells using specific gene products like Fz (Lawrence and Shelton, 1975; Piepho, 1955; Vinson and Adler, 1987; Wigglesworth, 1940). Moreover, this non-autonomous effect was polarized, such that hair polarity was disrupted in wild type cells distal, but not proximal, to mutant clones (Vinson and Adler, 1987). This phenomenon is now known as domineering non-autonomy (Ma et al., 2003). Other tissue mosaic analysis identified genes with cell-autonomous effects: *disheveled* (*dsh*), *in*, and *fuzzy (fy)*, that are involved in the intracellular signal transduction of PCP (Collier and Gubb, 1997; Gubb and Garcia-Bellido, 1982; Park et al., 1996; Theisen et al., 1994).

Since then, additional genetic, molecular and biochemical studies have identified numerous players that relay PCP information across tissues. One possible interpretation of this extensive data posits the existence of three genetic modules (Figure 1.2, H) (Axelrod, 2009). A global module comprising the atypical cadherins Fat (Ft) and Dachsous (Ds) and the golgi kinase Four-jointed (Fj) convert tissue axis information from morphogen gradients into subcellular asymmetries by forming a tissue gradient of Ft-Ds heterodimeric adhesions between cell neighbors along a given axis (Brittle et al., 2010; Simon et al., 2010). Proteins comprising the core module – the seven transmembrane-domain receptor Fz, the cytoplasmic scaffold protein Dsh, the Lim domain protein Pk, the seven-transmembrane atypical cadherin Flamingo (Fmi; also known as Strabismus/Stbm), and the ankyrin repeat protein Diego (Dgo) – receive that global cue through an undefined mechanism and act at adherens junctions of cell-cell boundaries to generate local cell-cell alignments. Polarized Fz transport along microtubules (Shimada et al., 2006) is thought to help initiate an intercellular molecular feedback mechanism that recruit a subset of these core PCP proteins to one edge and others to an adjacent edge of a neighboring cell (Chen et al., 2008; Tree et al., 2002), and through mutual inhibition by these PCP core complexes within the same cell, is thought to be the basis of generating cellular asymmetry and propagating PCP information from cell to cell. Importantly, this propagation of PCP signaling is dependent on cell packing and the geometry of epithelial topology (Ma et al., 2008). Finally, it is thought that these modules feed into the tissue-specific effector module, whose function is to execute some morphological polarization through the output of bristles or polarized cell movement. These modules can be distinguished phenotypically as mutant clones in tissue mosaics affecting global PCP genes will polarize and exhibit local tissue polarity alignment by

neighboring cells, but often fail to align with tissue axes. Clones bearing mutations in tissue effector genes show defects in morphological output formation in individual cells, while mutations in core PCP genes often show defects in both a cell-autonomous morphological polarity and a non-autonomous defect in local cell neighbor polarity alignment (Axelrod, 2009).

While much of our genetic and molecular understanding of PCP has come from studies in *Drosophila*, it is interesting to note that many of these PCP signaling genes play a conserved role in metazoan morphogenesis, and more recently, have been implicated in tissue repair and regeneration (Almuedo-Castillo et al., 2011; Caddy et al., 2010; Roszko et al., 2009; Tada and Kai, 2009; Wang and Nathans, 2007). In the 1990s, genetic screens in the zebrafish identified mutants exhibiting a shortened body axis without major patterning defects that upon positional cloning in the last decade, uncovered the vertebrate homologs of *Drosophila* PCP genes (Hammerschmidt et al., 1996; Heisenberg et al., 2000; Solnica-Krezel et al., 1996). At the same time, several key studies in *Xenopus* provided insights to the generality of the PCP signaling pathway in vertebrate morphogenesis and the molecular mechanism of forming cellular asymmetries needed for PCP. Expressing dominant negative constructs that delete *Xenopus* Dsh protein domains required for PCP signaling in *Drosophila* resulted in a shortened body axis and defects in convergent extension movements (Sokol, 1996) that were subsequently shown to be due to defects in stable bipolar, mediolateral lamellopodia needed by intercalating mesoderm cells of the dorsal marginal zone (Wallingford et al., 2000). Moreover, use of a heterologous system expressing *Drosophila* Dsh protein domain deletions in *Xenopus* identified cytoplasmic, vesicular and membrane-associated pools of Dsh, of which membrane-localization was associated with PCP signaling (Axelrod et al., 1998) and shown to be the molecular basis for convergent extension by cell intercalation (Wallingford et al., 2000). Since those initial vertebrate studies, many groups have taken a candidate gene approach to examine vertebrate homologs of *Drosophila* PCP genes and have demonstrated a general role for PCP genes in vertebrate morphogenesis.

Despite the conserved function of numerous members of the PCP signaling pathway in *Drosophila* and vertebrate morphogenesis, observations unique to vertebrates have made it unclear the extent to which vertebrates use a similar molecular mechanism of PCP propagation identified in *Drosophila*. Vertebrates use Wnt ligands, glypicans and the apico-basal polarity determinant Scribble (Scrb) which has not been implicated in *Drosophila* PCP (Tada and Kai, 2009). Moreover, the PCP pathway in *Drosophila* has only been described in epithelia while the vertebrate PCP pathway is involved in both epithelial and mesenchymal cells, resulting in monopolar or bipolar morphological outputs. These differences have made it challenging to appreciate whether asymmetric protein localization of some core PCP proteins in *Drosophila* should be expected in vertebrate tissues. The vestibular epithelium of the mammalian inner ear display a monopolar oriented kinocillium and stereocilia and support a general conservation of asymmetric membrane localization of core PCP proteins examined thus far (Vladar et al., 2009). However, bipolar mesenchymal cells of the axial notochord of zebrafish and *Xenopus* show Pk localization to the anterior edge of intercalating cells while Dsh has had more controversial subcellular localization along the A-P and/or medio-lateral axes (Kinoshita et al., 2003; Wallingford et al., 2000; Yin et al., 2008). Thus, it remains unclear how bipolar cells establish cellular asymmetry using PCP proteins, whether planar information is propagated to neighboring

cells in both epithelia and mesenchyme, whether domineering non-autonomy is also observed, and the molecular mechanism establishing PCP in vertebrates.

It should be noted that while most molecular attention has been directed towards the PCP signaling pathway in tissue elongation, PCP signaling is not involved in all cases. Germband extension does not require *dsh*, a key PCP component (da Silva and Vincent, 2007), but rather involves actomyosin polarization and contractility and involves polarized remodeling of apico-basal polarity regulators and cell adhesion molecules at adherens junctions (Bertet et al., 2004; Blankenship, 2006; Rauzi et al., 2010; Zallen and Wieschaus, 2004). Interestingly, many of these genes show bipolar asymmetric subcellular localization, either enriched along A-P cell boundaries or on the orthogonal dorso-ventral (D-V) cell boundaries, and it remains unclear whether the germband epithelium propagates planar information like that seen in the wing epithelium. Likewise, cell-matrix interactions are required for the bipolar protrusions that drive mediolateral cell intercalation for convergent extension of the dorsal mesoderm in *Xenopus* (Davidson et al., 2006). Continued research to build our understanding of PCP in different tissues will help us elucidate the similarities and diversity of the molecular and cellular mechanisms underlying PCP and tissue elongation during metazoan morphogenesis.

1.1.8 Summary

There is an emerging rise in the developmental biology literature that describes the basic cellular mechanisms that give rise to tissue morphogenesis. It is noteworthy that certain attributes – elongation along the A-P axis, the use of PCP to mediate polarized cell intercalation, cell division orientation and cell shape changes – seem to be hallmarks of these morphogenetic events. However, it remains to be elucidated whether these behaviors can account for the diverse morphologies seen amongst animal species and the extent of mechanistic conservation at a molecular level. As such, continued exploration of morphogenesis of a variety of model tissues is required in order to have a sufficient appreciation for the diversity of morphogenetic mechanisms utilized by metazoans.

1.2 Elongation of the developing egg in *Drosophila melanogaster* as an emerging model system to study tissue elongation

The development of the ellipsoid shape of the egg is a beautiful but underappreciated model system to study tissue elongation. Insects, reptiles and birds are the primary animal lineages that have evolved the production of ellipsoid eggs (Figure 1.3). It is thought that the ellipsoid egg is an adaptation to reproduction on land compared to the spherical eggs laid by aquatic organisms like fish and amphibians. The ellipsoid shape is thought to keep eggs from a single clutch together, promote maximal gas exchange for the developing embryo, and is an adaptive compromise for maximal maternal deposition to offspring within the constraints of a smaller body size (Elgar and Heaphy, 1989; Gilbert, 1979; Grant, 1982; Mao et al., 2007; Smart, 1991). Given these studies on evaluating the adaptive value of the ellipsoid egg, it is surprising that there has been little attention given to how an ellipsoid shaped egg is formed during oogenesis.

Developing eggs, also known as egg chambers or follicles, initially begin as a sphere. In some insects and birds, this morphological radial symmetry is broken such that there is preferential growth along the A-P axis relative to the orthogonal D-V axis. While the elongate egg has been recognized in various insect species (Parthasarathy et al., 2010; Tucker and Meats, 1976; Went, 1978), relatively little work has been made towards understanding the morphogenesis of egg shape in insects. The initial description of *Drosophila melanogaster* oogenesis was performed by Robert King and colleagues in the 1950s to 1970s (King, 1970). Since then, the abundance of resources generated by the *Drosophila* community has made the study of oogenesis a simple, genetically tractable model of tissue morphogenesis. The basic anatomy and processes occurring during oogenesis will be summarized briefly below.

1.2.1 Anatomy and physiology of the ovary

Each adult female bears two ovaries in the posterior abdomen (Figure 1.4). The ovaries are connected by individual lateral oviducts that converge at a common oviduct. Peristaltic contractions push mature eggs into the uterus where fertilization occurs prior to oviposition of fertilized eggs. Each ovary contains 16-20 ovarioles, each representing an assembly line of developmentally older follicles that are spatiotemporally ordered and separated by interfollicular stalk cells. The germarium, stalk cells, and individual egg chambers are surrounded by a follicular basement membrane that keep each ovariole intact. Each ovariole is encased by the epithelial muscle sheath, and all ovarioles are held together by the peritoneal sheath, a connective tissue vascularized by tracheoles to provide oxygen necessary for ovarian metabolism. The epithelial and peritoneal muscle sheaths contract rhythmically to help facilitate posterior movement of egg chambers through the ovary towards the oviduct.

The anterior tip of the ovary is known as the germarium, the tissue that include germline and somatic stem cells that give rise to individual follicles (Figure 1.4, F). Each follicle is comprised of a 16-cell germline cyst that contains the prospective oocyte and 15 accompanying nurse cells, whose connections through large intercellular bridges enable deposition of maternal components into the oocyte necessary for early embryonic development. This germline cyst is surrounded by a somatic follicle cell epithelium, derived from the gonadal mesoderm, which produces the yolk and secrete the eggshell onto the developing oocyte. The apical domain of the follicle membrane is in contact with the internal germ cells, while the basal domain of the epithelium is in close contact with the superficial follicle basement membrane (Figure 1.4, G). After budding from the germarium, each follicle will progress through fourteen morphologically defined stages comprising oogenesis (King, 1970; Spradling, 1993) that span across three or more days and involves a 5,000-fold increase in total volume (Figure 1.4, D-E) (King, 1970). Secretion of the eggshell and subsequent apoptosis by the supporting nurse cells and follicle cells marks the end of oogenesis and the formation of the mature egg. This whole process yields an ellipsoid egg approximately half a millimeter long and one-fifth a millimeter wide (Figure 1.4, C), and while these absolute numbers vary between different wild type strains, there is always a minimal 2.5-fold elongation along A-P axis in all wild type genotypes thus examined (data not shown).

1.2.2 The mystery of egg elongation

How follicles initially grow isotropically as an enlarging sphere but break this radial symmetry to grow anisotropically along the A-P axis from stage 4 of oogenesis (King, 1970; Spradling, 1993) is not understood. This is surprising given that over half a century of research has been dedicated to studies in the *Drosophila* ovary. While total follicle growth and elongation are complete by stage 12-13 (King, 1970; Spradling, 1993), no complete study describing the phase or kinetics of elongation during oogenesis has been made, nor the molecular mechanisms underlying this elongation are completely understood. This clear and simple case of tissue elongation that each follicle undergoes, starting as a sphere and ending as an ellipsoid, forms the basis of my dissertation. I provide an introduction to the known morphogenetic processes that control egg morphology, then describe our understanding of the genetic control of egg shape at the time I started my dissertation. Finally, I provide an introduction the developments leading to our laboratory's interest in this question and list outstanding questions that I address in the remainder of my dissertation.

1.2.3 Morphogenesis during oogenesis

Many morphogenetic processes occur during *Drosophila* oogenesis, some which are executed by the follicle cells, others by the germ cells, but most events depend on signaling between the germline and soma to initiate these movements. While all of the known morphogenetic behaviors described below ultimately affect some aspect of egg morphology, none of these movements are thought to directly affect egg shape without an effect on egg volume.

The first morphogenetic process involves the formation of individual egg chambers in the germarium. After one of the two germline stem cells divide to form a daughter cystoblast cell, this cell will continue to divide four more times, and through incomplete cytokinesis, form an inter-connected 16-cell germline cyst (Spradling, 1993). Concurrently, two somatic follicle stem cells divide and form progenitor follicle cells that proliferate and migrate to generate the 16-80 cells that encapsulate the germline cyst to form the stage 1 follicle (King and Vanoucek, 1960; Spradling, 1993). During this time, a subset of follicle cells become specified to terminal polar cell and interfollicular stalk cell fates, and using the A-P polarity information of adjacent, older follicles, relays A-P polarity information to the posterior polar cells of the newly forming egg chamber. This triggers an increase in cadherin expression by posterior follicle cells to capture the prospective oocyte at the posterior pole, thus orienting the germline cyst (Torres et al., 2003). Mutations affecting these processes can result in fused egg chambers, mispositioned oocytes, or non-encapsulated germline cysts (Spradling, 1993).

Following proliferation of the follicle epithelium to reach 650-1000 cells by the end of stage 6 (King and Vanoucek, 1960; Margolis and Spradling, 1995), the next wave of morphogenetic processes occurs in mid-oogenesis, during stage 9, when the follicle cell epithelium undergoes a dramatic shift in epithelial architecture to form 3 distinct populations. The anterior 50 follicle cells undergo a cuboidal to squamous epithelial transition to form stretch cells overlying the nurse cells and shift from spanning approximately 9 percent of the surface area of a stage 8 follicle to spanning 50 percent of the surface area of the follicle by stage 10A. The remaining 650-950 follicle cells undergo a cuboidal to columnar shape transition to become the main body follicle cells that overlie the oocyte and shift from spanning 91 percent to 50 percent of follicle surface area to occupy the posterior half of the follicle by stage 10A (Kolahi et al., 2009). This

change in distribution of the follicle cells relative to the internal germ cells was for a long time proposed to result from apical constriction and active posterior migration of the main body follicle cells towards the growing oocyte (Grammont, 2007; Horne-Badovinac and Bilder, 2005; King, 1970; Spradling, 1993; Zarnescu and Thomas, 1999). However, a recent quantitative approach to the problem found that main body follicle cells do not undergo apical constriction and increase their total surface area during stage 9 modestly. These observations suggest instead that germline growth, most notably the dramatic increase of the oocyte, accounts for the majority of posterior displacement of main body follicle cells, which was further supported by mathematical modeling (Kolahi et al., 2009), and renamed as "anterior accommodation." Live imaging of stage 9 main body follicle cells confirms a lack of obvious posterior migration by these cells (He et al., 2010). Finally, a third group of 6 to 10 follicle cells at the anterior pole delaminate and undergo posterior migration through the nurse cells towards the oocyte, known as border cell migration. While these processes are normally coordinated, mutations reveal that these behaviors can be uncoupled (King, 1970; Montell et al., 1992; Zarnescu and Thomas, 1999). Defects in border cell migration result in defects in micropyle formation, while defects in proper positioning of main body follicle cells over the oocyte result in defects in eggshell and dorsal appendage formation, affecting final egg morphology, fertilization of the egg, or gas exchange for the developing embryo (King, 1970; Spradling, 1993).

A third major morphogenetic process occurs during stages 10B and 11. Centripetal migration of a subset of anterior main body follicle cells results in invasion at the nurse cell:oocyte boundary to enclose the oocyte at its anterior edge. At the same time, nurse cells transfer their entire cytoplasmic contents into the growing oocyte. These two processes must be coordinated, and dumpless mutants displaying defects in nurse cell dumping can result in "small egg" or short egg phenotypes (see Table 1.1 for clarification) (Cant et al., 1994; Cooley et al., 1992; Mahajanmiklos and Cooley, 1994; Robinson and Cooley, 1997), where the mature egg is shortened along the A-P length but generally have a generally wild type D-V length, leading to a reduction in egg volume. Defects in centripetal migration can result in an open chorion phenotype, where the anterior eggshell structures fail to be made on the mature egg. It remains to be elucidated whether the main body follicle cells that overlie the growing oocyte, now occupying the majority of total follicle volume, actively migrates with the oocyte, or like that during mid-oogenesis, is a passive response to the growing oocyte.

Secretion of the eggshell is performed by the main body follicle cells, beginning with production of the vitelline membrane at stage 9 while chorion secretion occurs at stage 12 and later. Additional modifications to the eggshell at stage 12 enable the vitelline membrane to support egg shape when other eggshell components are removed from the mature egg (Spradling, 1993), and a wax layer, preventing desiccation of the egg, is deposited between the vitelline membrane and chorion upon exit of the ovary (King, 1970). Defects in eggshell production can compromise eggshell integrity and often result in collapsed egg phenotypes (Orr et al., 1989; Schupbach and Wieschaus, 1991).

The formation of specialized eggshell structures also occurs near the end of oogenesis, using a subset of anterior main body follicle cells. 90-120 dorso-anterior follicle cells will undergo convergent extension during stage 12 to form the dorsal appendages that extend beyond the anterior pole of the mature egg, which serve as breathing tubes and can extract oxygen from

water for the developing embryo when the egg is submerged in water. 50-70 centripetal follicle cells give rise to the operculum, which is a specially weakened collar that enables larval hatching. Finally, nurse cell nuclei and follicle cell apoptosis are complete at stage 14, yielding the mature egg. Defects in these processes only subtly affect egg morphology but have greater impact on embryonic development and function.

1.2.4 The somatic follicle cell epithelium is required for the ellipsoid shape of the egg

The first hint that the follicle cell epithelium may play a role in the control of insect egg shape came from work on the gall midge, *Heteropeza pygmaea*, and the cockroach, *Periplaneta americana* (Tucker and Meats, 1976), in which a coordinated planar polarity of microtubules in the follicle epithelium was hypothesized to control egg elongation (see further description below). Went tested the requirement of the follicle epithelium to control egg shape using X-ray irradiation, mechanical or chemical removal of the follicle epithelium in *Heteropeza* follicles *ex vivo* and found that instead of being oval they become spherical (Went, 1978; Went and Junquera, 1981). Moreover, these spherical eggs could undergo some early embryonic development, forming a blastoderm and showing some signs of attempted gastrulation (Went, 1978; Went and Junquera, 1981), suggesting that the activities controlling egg shape may be uncoupled from other activities that control pattern formation in the oocyte necessary for early embryonic development. A similar study was performed in *Drosophila*, using X-ray irradiation to generate genetic mosaics in the ovary using a known mutation affecting egg shape, *short egg* (*seg*), and found that germline mutant *seg* clones showed normal egg shape, thus indirectly attributing a requirement by the somatic follicle epithelium for *seg* function (Wieschaus et al., 1981). Additional reports using FLP/FRT-mediated genetic mosaics also support a requirement by the follicle epithelium to control egg shape (Bateman et al., 2001; Frydman and Spradling, 2001).

1.2.5 Early models on egg elongation

The second hint that a specific activity of follicle cells may control insect egg shape came from the inspiration to examine the insect follicle cytoskeleton (Tucker and Meats, 1976). Studies in the 1960s and 1970s had been examining the role of microtubule cytoskeletal organization in individual cell shape control in a variety of cell lines, animals and plants. Elongated cells were known to orient microtubules parallel to the long axis of the cell, but whether microtubules also exhibited a similar polarity in multicellular tissues was not clear. Examination of *Heteropeza* follicle cells revealed that these cells orient their microtubules parallel to the long axis of individual cells (Tucker and Meats, 1976), but more importantly, this microtubule polarity occurred at a supracellular level – through coordinated polarity across multiple follicle cells, encircling the circumference of the *Heteropeza* follicle, perpendicular to its long axis. These observations provided the first description of planar polarity emerging at the basal domain of an epithelium in an animal model (Tucker and Meats, 1976). The oriented microtubules, through spot desmosomes located near the basal surface, were postulated to transmit tissue wide tensile strength to constrain growth of the follicle along its circumference. The growth of the *Heteropeza* follicle was speculated to occur primarily along its length rather than its width. Thus, the circumferential microtubules of the *Heteropeza* follicle provided the first notion of a supracellular 'molecular corset' in an animal model. Moreover, the concept that the mechanical

properties of the superficial epithelial layer can influence the shape of the cells it encloses were inklings of appreciation for the sources of force generation to shape tissues that were to develop in the morphogenesis community in the 1980s.

Wieschaus recognized this pioneering study in his own efforts to understand the contributions of the germline versus soma in affecting egg morphology in *Drosophila*. He published the first description of a round egg mutant, *seg*, which showed a mild defect in egg shape without affecting egg volume, where *seg* eggs were shorter and wider by 20 and 10%, respectively, and like that in *Heteropeza*, these eggs were capable of fertilization and undergoing embryonic development (Wieschaus et al., 1981). Given that a majority of oocyte elongation occurs during nurse cell dumping, and that genetic mosaic data pointed at a probable involvement of the somatic follicle epithelium, his recognition that main body follicle cells elongate along their A-P length during this process suggested that this activity may be involved in oocyte elongation. However, *seg* mutant eggs seemed to undergo normal nurse cell dumping, weakening this hypothesis. Likewise, genetic screens identifying additional mutations generating round egg phenotypes (Table 1.1) showed a similar short and wide egg shape defect but normal nurse cell dumping (Schupbach and Wieschaus, 1991; Tearle and Nusslein-Volhard, 1988), suggesting that other activities during oogenesis are instead involved in the control of egg elongation.

1.2.6 The actin cytoskeleton as a molecular corset to constrain Drosophila egg shape

The most influential contributions to the control of *Drosophila* egg elongation came from Gutzeit, who, after years of studying various aspects of *Drosophila* oogenesis (Gutzeit, 1980; Gutzeit, 1986; Gutzeit and Gehring, 1979), became interested in the potential role that follicle cells have in regulating egg shape. No characterization of the cytoskeleton in *Drosophila* follicle cells had been made, and examination of both the microtubule and the actin cytoskeleton revealed that microfilaments, not microtubules, were circumferentially oriented, orthogonal to the long axis on the basal domain of the follicle cell epithelium during vitellogenic stages of oogenesis (Gutzeit, 1990; Gutzeit et al., 1993). Interestingly, monopolar actin-rich protrusions were also noted on the basal surface, highlighting the first case of a monopolar output of PCP on the basal side of an epithelium (Gutzeit, 1992). Using the same general ideas proposed by Tucker (Tucker and Meats, 1976), Gutzeit hypothesized that actin filaments may have been co-opted to act as a "circumferential corselette" (Gutzeit et al., 1991) to control *Drosophila* egg elongation (Gutzeit, 1990; Gutzeit, 1992; Gutzeit et al., 1991; Gutzeit et al., 1993). Despite his own reservations for this hypothesis (Tucker and Meats, 1976), the F-actin molecular corset model became associated with Gutzeit for all subsequent papers discussing egg shape (Bateman et al., 2001; Conder et al., 2007; Frydman and Spradling, 2001; Haigo and Bilder, 2011; He et al., 2010; Viktorinova et al., 2009).

Gutzeit recognized that several of his own observations were difficult to reconcile with his model: microfilaments were not always oriented in the right way at the right time nor clearly required. Stage 7 to early 9 follicles showed planar polarized basal microfilaments, but F-actin re-organizes to a thin mesh network in stretch cells of the anterior half, such that only the centripetal cells of stage 10 follicles maintain its clear circumferential orientation (Gutzeit, 1990; Gutzeit, 1992). Posterior main body follicle cells also show a breakdown in circumferential polarity, and the high degree of variation in basal F-actin orientation between different follicle

cells without a consequence on follicle shape during nurse cell dumping seemed to weaken the model further. Moreover, other insects like *Bradysia* bearing oval follicles did not have any planar polarized basal microfilaments (or microtubules) (Gutzeit and Haas-Assenbaum, 1991). Functionally, loss of actin filaments at the basal surface using the actin depolymerizing drugs, Cytochalasin B or D, have no effect on follicle shape at stage 10 (Gutzeit, 1990; Gutzeit, 1992). Given these observations, an alternative role for polarized microfilaments was proposed as a counteracting pressure to withstand the mechanical deformations the follicle faces upon peristaltic contractions by the ovarian muscle sheaths, through its adhesion to the basement membrane (Gutzeit, 1990).

Gutzeit then shifted his attention towards the basement membrane that encases each follicle. In noticing the strong adhesion of the basement membrane to the basal surface epithelium in resisting mechanical separation (Gutzeit, 1990), examination of the Laminin matrix revealed that Laminin fibrils displayed circumferential planar polarity around the A-P axis, parallel to the basal microfilaments in the follicle cells (Gutzeit et al., 1991). Use of Collagenase to remove the basement membrane of stage 10 *Drosophila* and late stage follicles of the fungus gnat, *Bradysia tritici,* resulted a subtle rounding of follicle shape (Gutzeit and Haas-Assenbaum, 1991). Despite the lack of appropriate controls in those experiments, Gutzeit suggested that the orientation of Laminin or basal microfilaments may be involved to control egg shape. This hypothesis was tested using a novel round egg mutant called *kugelei (kugel, kug*) that produced short and wide or even spherical eggs (Tearle and Nusslein-Volhard, 1988). Homozygous *kug* follicles showed no circumferential polarity of actin filaments, loss of monopolar protrusions, and abnormal Laminin fibril orientation (Gutzeit et al., 1991). By the end of his work on egg shape, Gutzeit believed that coordinated polarization of the Laminin ECM and the basal actin cytoskeleton was mediated by Integrin receptors, that through unknown molecular mechanisms were propagating planar information between neighboring follicle cells to synchronize tissue orientation and somehow control follicle shape (Gutzeit et al., 1991; Gutzeit et al., 1993).

1.2.7 Cell-matrix genes control egg shape

Gutzeit's intuitions proved correct, as a handful of reports in the last decade have demonstrated a genetic requirement for cell-matrix genes in the control of *Drosophila* egg shape. These round egg mutants are genes encoding basement membrane molecules (Laminin A), ECM receptors ($\alpha_{PS1,2}$ and β_{PS} Integrins, Dlar/Lar) and adaptor proteins to the actin cytoskeleton (Tensin, Talin, Dpak) (Bateman et al., 2001; Becam et al., 2005; Conder et al., 2007; Duffy et al., 1998; Frydman and Spradling, 2001; Lee et al., 2003). Moreover, additional cell-matrix components have defects in follicle PCP, though their phenotypic effects on egg shape are less clear (Delon and Brown, 2009; Deng et al., 2003; Mirouse et al., 2009; Schneider et al., 2006).

Those reports that focus on the round egg phenotype support the common disruption in planar polarization of actin filaments at the basal epithelium, and invoke Gutzeit's F-actin molecular corset model. Despite their limitations in providing a molecular mechanism, these reports do provide important observations. Through use of tissue mosaics, the non-autonomous disruption in basal actin filament orientation demonstrated that propagation of PCP also occurs in the follicle epithelium, possibly through transient storage of PCP information in the basement membrane (Bateman et al., 2001; Frydman and Spradling, 2001). Emergence of microfilament

planar polarity occurred during stage 5, first forming near the poles, and suggested a role for polar cells in providing the polarity cue for follicle PCP (Frydman and Spradling, 2001). β_{PS} integrin and Enabled were shown to have bipolar enrichment at dorsal and ventral faces on the basal surface epithelium of late stage follicles while Dlar was observed to have a similar pattern earlier at stage 8, but it remained unclear what this output meant. Likewise, both β_{PS} integrin and Dlar formed puncta at tricellular junctions (Bateman et al., 2001). While these data implicate the importance of planar polarized cell-matrix interactions for the control of egg elongation, the underlying molecular mechanisms for their requirement remained to be elucidated.

1.3 Overview of Ph.D. dissertation

Our lab became interested in the question of the genetic, molecular and cellular basis of *Drosophila* egg elongation upon the recovery of a large number of mutations that result in round eggs using a forward genetic screen targeted to generate homozygous recessive mutations in the follicle cells in an otherwise heterozygous female using the FLP/FRT, GAL4/UAS systems (Figure 1.5) (S. Horne-Badovinac, unpublished results, (Duffy et al., 1998)). While preliminary results from this forward genetic approach points to the identification of novel genes involved in this process (S. Horne-Badovinac, unpublished results), many basic parameters of *Drosophila* egg elongation were not defined at the start of my dissertation. For example, when is the elongation phase of oogenesis? Does the rate of elongation differ during distinct phases of oogenesis? Do the follicle cells undergo any morphogenetic behaviors during the elongation phase? What is the molecular mechanism underlying the necessity of cell-matrix genes for egg elongation? How does planar cell polarity of the actin cytoskeleton control egg shape? Is the establishment and propagation of PCP similar to other tissues undergoing morphogenesis or are there features unique to the *Drosophila* follicle?

These and many other questions helped form the basis of questions I chose to pursue during my Ph.D. In Chapter 2, I define the major elongation phase of oogenesis and using live cell imaging, discovered a novel polarized morphogenetic behavior, global tissue rotation, required for tissue elongation and egg shape. I provide a molecular mechanism for the requirement of Integrin receptors and Collagen IV – for collective cell migration to build a polarized ECM matrix that acts as a molecular corset to constrain egg shape. This mechanism can account for the majority of egg elongation in *Drosophila*.

Many new questions emerge from the discovery of global tissue rotation. One major enigma is that polarized cell shape changes and/or polarized cell intercalation occurs during tissue elongation in all other developmental tissues studied thus far. Whether these behaviors also occur and contribute to follicle elongation is unclear. It also remains unclear whether all known round egg mutants are involved in global tissue rotation or are required for other morphogenetic behaviors necessary for egg elongation. Chapter 3 aims to better characterize the cellular basis of follicle elongation during the rotation phase using quantitative morphometric analysis. In addition, preliminary characterization of other known round egg mutants, *rhea/talin*, *Dpak, Dlar* and *fat2*, indicate that these genes may also be required for global tissue rotation, suggesting that further genetic screening or improved screening strategies may help uncover novel genes and behaviors that are involved in egg elongation.

Another fascinating enigma is how PCP and global tissue rotation is established in the *Drosophila* follicle, an issue at the crux of the PCP field. Does PCP emerge at the molecular level prior to the onset of morphological tissue polarization like that seen in the *Drosophila* germband? Is there an activation signal to initiate global tissue rotation and from where does this signal originate? Chapter 4 aims to tackle these issues by more detailed examination of the emergence of molecular PCP at stage 5. Furthermore, an *in silico* enhancer trap screen to identify developmental signaling pathways and other genes that may coincide with the major elongation phase has led to the identification of the Notch/Delta signaling pathway as a putative regulator of follicle PCP and global tissue rotation, potentially providing an activation signal from the germline at stage 5.

The findings from my Ph.D. dissertation have challenged the ways in which we think about morphogenesis during metazoan development. Global tissue rotation is a novel polarized morphogenetic behavior required for tissue elongation, but the cellular output of this movement remains ambiguous, perhaps because of the follicle's closed topology as an epithelial chamber. It is the first collective cell migration with an obvious individual cell polarity and tissue polarity, but with no obvious collective cell polarity with leader and follower cells. It also raises the possibility that different mechanisms of PCP propagation may occur depending on the timescale to form morphological polarization, given the relatively short time needed to coordinate global movement in the *Drosophila* follicle and other elongating tissues while morphological polarization to orient hairs in the *Drosophila* wing occur over many hours. These and many other issues indicate that continued studies of *Drosophila* egg elongation will provide novel and exciting insights to our understanding of tissue polarity, morphogenesis and general development in a variety of organisms.

Figure 1.1
Known cellular behaviors underlying morphogenesis of metazoan tissues.

Developing tissues are known to undergo one or more morphogenetic behaviors to form the final shape of the tissue. These behaviors include regulated cell proliferation, changes in tissue architecture, single or collective cell movements, changes in cell shapes through apical constriction or cell length, and cell intercalation. These can result in morphogenetic movements such as condensation (**A**), tissue bending processes like involution or invagination (**B**), cavitation (**C**), epithelial to mesenchymal transitions (**D**) or its reverse (**E**), convergent extension of tissues (**F**), epiboly (**G**), or more complex movements like branching morphogenesis (**H**). From (Slack, 2006).

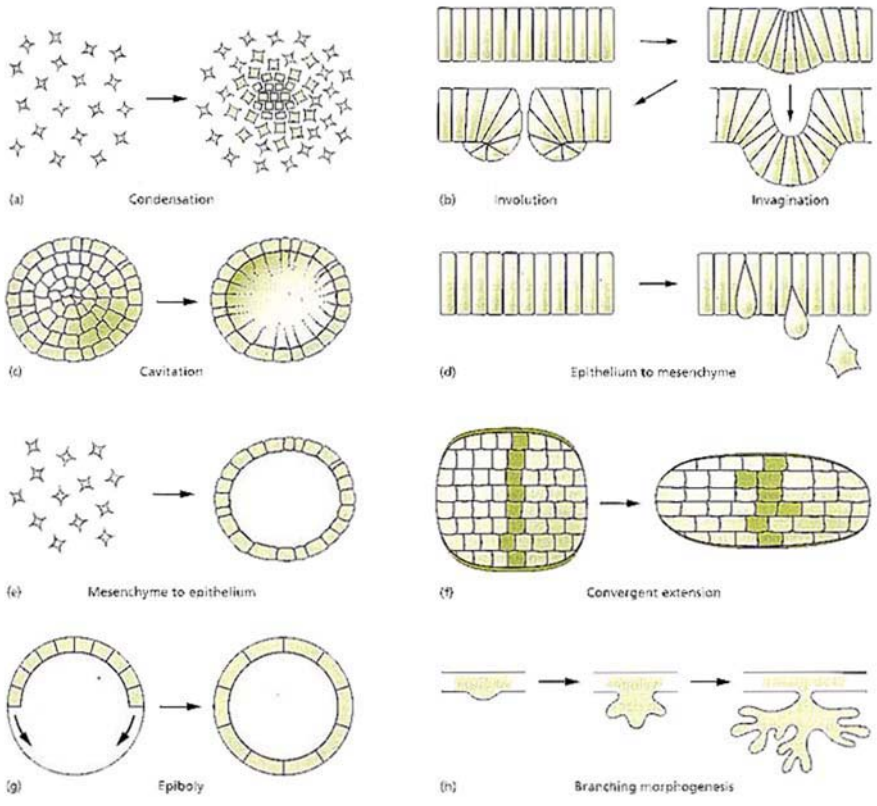
(a) Condensation
(b) Involution
Invagination
(c) Cavitation
(d) Epithelium to mesenchyme
(e) Mesenchyme to epithelium
(f) Convergent extension
(g) Epiboly
(h) Branching morphogenesis

Figure 1.2
Planar cell polarity is involved in metazoan morphogenesis.

(**A-F**) Planar cell polarity (PCP) is manifested by coordinated morphological outputs like the distal orientation of hairs on the *Drosophila* wing (**A**), the distal orientation of fur on the mouse paw (**B**), or the orientation of stereocilia in sensory receptor cells of the cochlea in the mammalian inner ear (**C**). Mutations in PCP signaling components result in disorganized polarity in these tissues (**B, D, F**). (**G**) PCP signaling pathway components in flies and vertebrates. (**H**) Schematic of the PCP signaling pathway, which is composed of a global module that converts morphogen gradients to a tissue polarity gradient, a core module to generate cellular asymmetry and propagate polar information locally from cell to cell, and tissue specific effectors to execute morphological polarization. (**I**) Subcellular distributions of PCP proteins and morphological outputs show similarities and differences in various polarized tissues. (**A-F**) from (Zallen, 2007), (**G-I**) adapted from (Vladar et al., 2009).

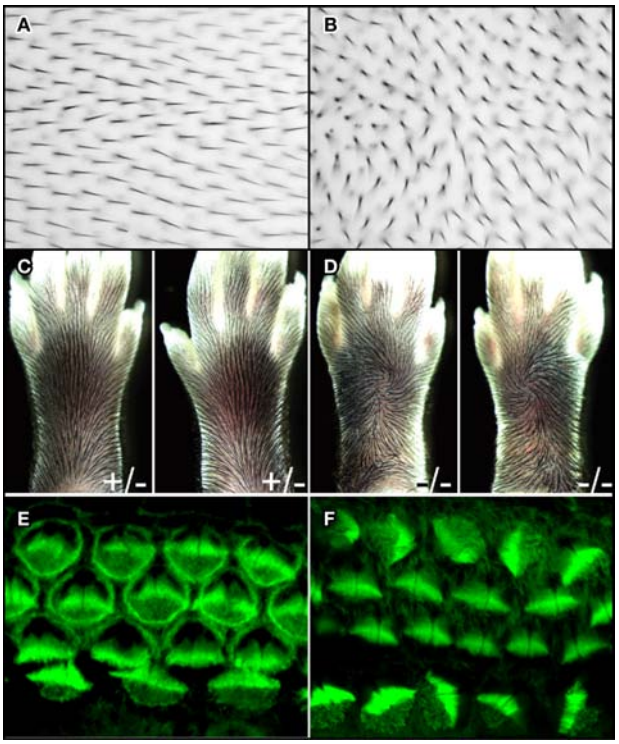

G

Table 1. PCP components in files and vertebrates

Drosophila	Vertebrates
Van Gogh (Vang) *Strabismus (Stbm)*[1]	Van Gogh-like 1 (Vangl1) Van Gogh-like 2 (Vangl2)
Prickle (Pk)	Prickle1 (Pk1) Prickle1 (Pk2)
Frizzled (Fz)	Frizzled3 (Fz3) Frizzled6 (Fz6) Frizzled7 (Fz7)
Dishevelled (Dsh)	Dishevelled1 (Dvl1) Dishevelled2 (Dvl2) Dishevelled3 (Dvl3)
Flamingo (Fmi) *Starry Night (Stan)*[1]	Celsr1 Celsr2 Celsr3
Diego (Dgo)	Inversin
Fuzzy (Fy)	Fuzzy
Inturned (In)	Inturned
Rho1 *RhoA*[1]	RhoA
Drok	Rok/Rock
Fat (Ft)	Fat1 Fat2 Fat3 Fat4
Dachsous (Ds)	Dachsous1 (Dchs1)[3] Dachsous2 (Dchs2)[3]
Four-jointed (Fj)	Fjx
Wingless (Wg)[2]	Wnt4 Wnt5a Wnt7a Wnt11

[1]Italicized text indicates alternative name in *Drosophila*.
[2]Wg does not directly regulate PCP in *Drosophila*.
[3]Role in PCP not determined.

H

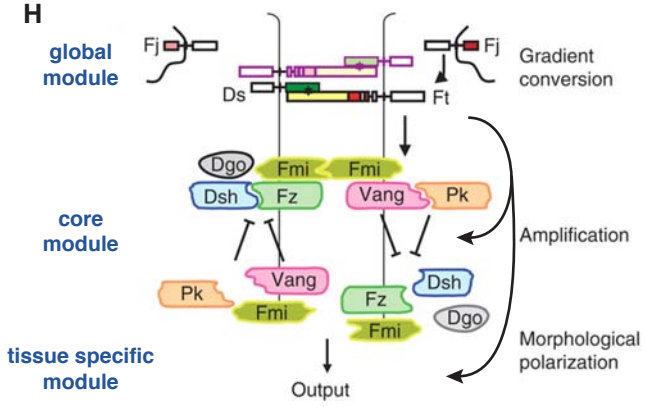

I

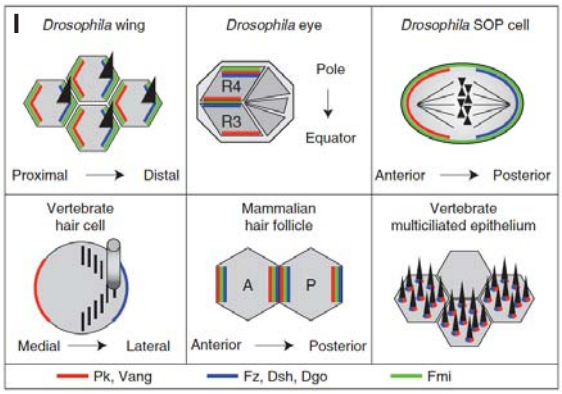

Figure 1.3
A variety of organisms are known to produce ellipsoid shaped eggs.

Insects, reptiles and birds are the primary animal lineages that produce ellipsoid eggs, but some basally-derived chordates also produce elongate eggs. Illustration of eggs from a variety of birds (**1-50**), turtles (**51-52**), sharks (**53-55**), chimaera (**56**), lamprey (**57**), mollusk (cuttlefish) (**58**), and insects (**59-72**). From (Millot, 1897-1904).


NOUVEAU LAROUSSE ILLUSTRÉ
1
3
29
46
37
38
43
4
45
44
28
2
35
5
47
27
7
8
6
26
25
32
42
36
24
9
10
23
30
11
33
41
39
48
49
12
22
31
16
20
21
40
34
13
18
19
14
53
56
50
17
57
15
58
55
59
69
54
60
61
62
66
67
68
52
63
64
65
70
71
72
51

Figure 1.4
Overview of oogenesis in *Drosophila melanogaster*.

(**A**) Illustration of dorsal view of *D. melanogaster* adult female. (**B**) Illustration of the female reproductive system in *D. melanogaster*. (**C**) Dorsal view of a mature egg of *D. melanogaster*. Wild type eggs are approximately 520 μm long and 200 μm wide. (**D**) Illustration depicting a wild type ovariole. Fourteen morphological stages define progression through oogenesis following formation of an individual egg chamber (follicle) in the germarium. Anterior is to the left, posterior to the right; this orientation will be maintained throughout this dissertation unless otherwise noted. Somatic follicle cells are in yellow, specialized follicle cells known as polar cells in green, and the germline in light blue. Note the posterior location of the prospective oocyte (blue). The time spent in each given stage of oogenesis are estimates based on (Spradling, 1993) and (Margolis and Spradling, 1995). (**E**) Relative timing of critical patterning events and morphogenetic behaviors that affect final egg morphology. (**F**) Structure of the germarium shows the spatial organization of germline stem cells (purple) and somatic follicle stem cells (light green) that give rise to individual egg chambers. Interfollicular stalk cells differentiate early in oogenesis to help separate adjacent follicles. (**G**) Illustration of the follicle cell epithelium at higher magnification. The apical domain faces internally towards the germline, while the basal domain has a unique planar polarization of actin filaments (red) and cell-matrix components (blue) around its circumference. The basal surface is in direct contact with the follicle basement membrane (green) that encases each follicle. (**A-B**) from Flybase (Tweedie et al., 2009) (**D-F**) adapted from (Horne-Badovinac and Bilder, 2005).

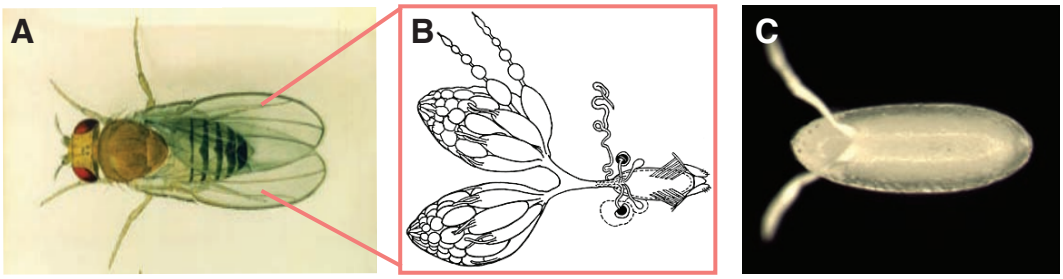
A
B
C

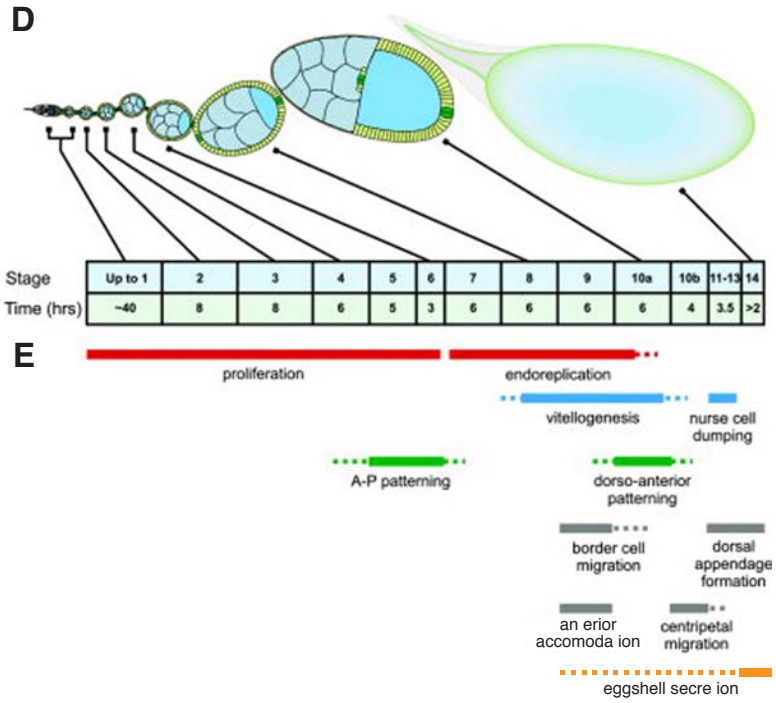
D
Stage
Time (hrs)
Up to 1
~40
2
8
3
8
4
6
5
5
6
3
7
6
8
6
9
6
10a
6
10b
4
11-13
3.5
14
>2
E
proliferation
endoreplication
vitellogenesis
nurse cell dumping
A-P patterning
dorso-anterior patterning
border cell migration
dorsal appendage formation
an erior accomoda ion
centripetal migration
eggshell secre ion

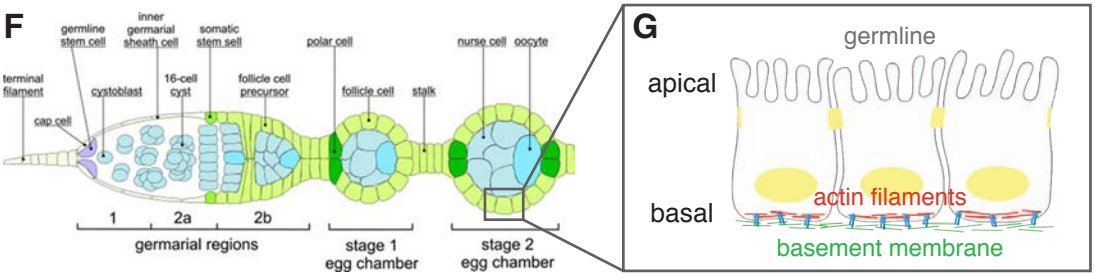
F
germline stem cell
inner germarial sheath cell
somatic stem cell
polar cell
nurse cell
oocyte
terminal filament
cap cell
cystoblast
16-cell cyst
follicle cell precursor
follicle cell
stalk
1
2a
2b
germarial regions
stage 1 egg chamber
stage 2 egg chamber
G
germline
apical
basal
actin filaments
basement membrane

Figure 1.5
The follicle cell epithelium is required to control egg shape in *Drosophila melanogaster*.

(A) Illustration depicting a modern directed tissue mosaic approach using a combination of the FLP/FRT and GAL4/UAS systems to produce homozygous mutant follicle cells in an otherwise heterozygous animal. Use of a GAL4 enhancer trap expressed specifically in the follicle cells enables expression of FLP recombinase to induce recombination in mitotic follicle cells, and following appropriate chromosomal segregation during anaphase, can generate two daughter cells – one that is homozygous wild type and a sister that is homozygous mutant for a gene of interest. (B) Preliminary results from a pilot screen performed in our lab using this directed tissue mosaic approach uncovered a striking class of mutations where females instead of producing ellipsoid eggs (B), produced round eggs (C). We refer to them as round egg mutants.

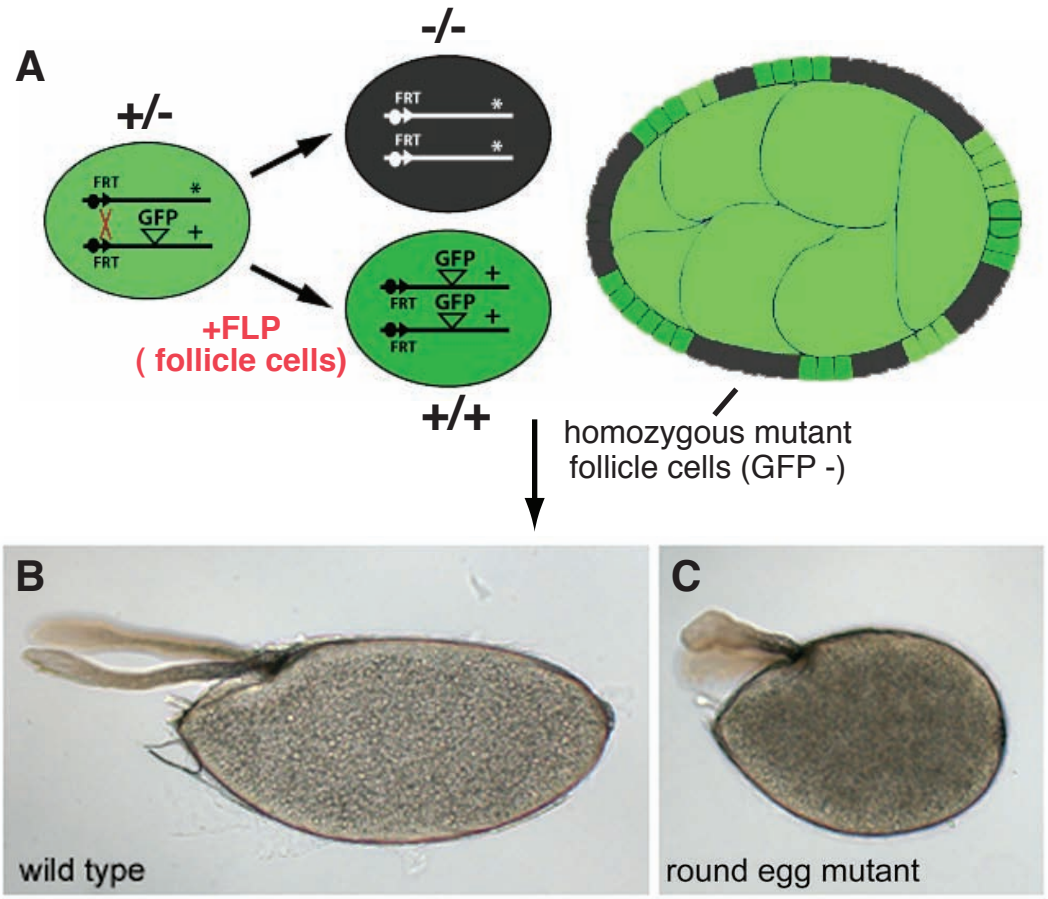
A
-/-
+/-
FRT
*
FRT
*
GFP
+
FRT
GFP
+
FRT
GFP
+
FRT
+FLP
(follicle cells)
+/+
homozygous mutant
follicle cells (GFP -)
B
wild type
C
round egg mutant

Table 1.1
Classification of published mutations affecting egg shape in *Drosophila melanogaster*.

Isolation of various mutations affecting egg shape was performed by independent groups, resulting in some confusion in egg shape classification and nomenclature in the literature. The table lists a suggested re-organization of known egg shape mutants by their effect on A-P length, D-V width, and/or changes in egg volume. These classifications will be followed throughout this dissertation.

Class	Phenotype	Previously known as
Round egg	Short A-P length, wider D-V width, no change in egg volume	Short egg phenotype

Gene	Gene activity required in	Known molecular function	Reference
short egg/seg	Follicle cells *	Unknown	Wieschaus et al 1981
kugelei/kugel/kug/fat2	Follicle cells *	Global regulator of planar cell polarity	Viktorinova et al 2011
myospheroid/mys	Follicle cells	Integrin βPS; collective cell migration	Haigo & Bilder 2011
bola/Dlar	Follicle cells	ECM receptor	Frydman & Spradling 2001
blistery/by/tensin†	-	Focal complex adaptor protein	Lee et al 2003
rhea/talin	Follicle cells	Focal complex adaptor protein	Becam et al 2005, unpub. obs.
PAK-kinase/Dpak	Follicle cells *	F-actin assembly	Conder et al 2007
Laminin A/LanA	Follicle cells	ECM molecule; molecular corset	6-7, 12
viking/vkg/collagen IV α2	Follicle cells	ECM molecule; molecular corset	Haigo & Bilder 2011

Short egg — Short A-P length, no defect in D-V width, reduced egg volume — Dumpless or small egg phenotype

Gene	Gene activity required in	Known molecular function	Reference
chickadee/chic	Germline cells	F-actin assembly; nurse cell dumping	Cooley et al 1992
singed/sn	Germline cells	F-actin bundling; nurse cell dumping	Cant et al 1994
kelch/kel	Germline cells	Ring canal stability; nurse cell dumping	Robinson & Cooley 1997
quail/qua	Germline cells	F-actin bundling; nurse cell dumping	Mahanjan-Miklos & Cooley 1994

Small egg — Short A-P legnth, short D-V width, reduced egg volume

Gene	Gene activity required in	Known molecular function	References
tiny/ty	Unknown	Follicle growth	Falk & King 1964

* Not directly tested

† Round egg phenotype not reproducible using two independent genetic null alleles (unpub. obs.)

Part of the following chapter was originally published as a Report in
Science. 2011 Feb 25; 331(6020): 1071-4;
published online 2011 Jan 6 (*10.1126/science.1199424*).

Chapter 2

Global tissue revolutions in a novel morphogenetic behavior required for tissue elongation and egg shape in *Drosophila*

2.1 Abstract

Polarized cell behaviors including cell intercalation, cell shape changes and cell division are associated with the elongation of a variety of tissues during metazoan development, but the mechanisms underlying elongation of many tissues remain unknown. The development of the ellipsoid *Drosophila* egg is an elegant case of tissue elongation, but the mechanisms of *Drosophila* egg elongation are not known. Using live imaging of developing egg chambers (follicles), we show that the follicle unexpectedly undergoes repeated rounds of circumferential rotation, relative to the surrounding extracellular matrix (ECM), during the elongation phase of oogenesis. Follicle epithelia mutant for *myospheroid* (integrin β_{PS}) or *viking* (Collagen IV α_2) fail to rotate and result in round eggs. We found that Collagen IV fibrils become circumferentially planar polarized during the rotation phase but become misoriented in non-rotating round egg mutants. Furthermore, acute degradation of Collagen IV rounds previously elongated follicles, suggesting that follicle rotation polarizes a fibrillar extracellular matrix that constrains the growing egg in a molecular corset, generating its ellipsoid shape. Thus, global tissue rotation is a morphogenetic behavior that uses planar mechanotransduction through a static ECM to control tissue elongation. We integrate this movement with known patterning and morphogenetic processes during oogenesis and we speculate how this discovery adds to our understanding of collective cell migrations, planar cell polarity, and the general mechanisms underlying morphogenesis.

2.2 Introduction

Elongation of a tissue along a major body axis is a central and conserved feature of animal development. Epithelial sheets and tubes as well as mesenchymal cell populations undergo elongation (Andrew and Ewald, 2010; Keller, 2002), and defects in this process can cause human developmental abnormalities (Wallingford, 2005). Studies of elongating tissues have uncovered morphogenetic behaviors such as convergent extension, part of a small repertoire of cell movements known to shape animal body plans (Keller, 2006). However, for many animal tissues, the mechanism underlying their elongation remains unknown.

The development of the ellipsoid *Drosophila* egg is an elegant case of tissue elongation. *Drosophila* eggs develop from individual follicles, each consisting of a somatic follicle cell epithelium that surrounds the oocyte and accompanying 15 nurse cells. Newly formed follicles are spherical and initially grow isotropically but acquire anisotropic growth along the antero-posterior (A-P) axis from stage 4 of oogenesis to form a mature (stage 14) egg half a millimeter long and one-fifth millimeter wide (Frydman and Spradling, 2001; Spradling, 1993). How the developing follicle breaks radial symmetry to channel a 5,000-fold increase in total volume (King, 1970) from a stage 1 sphere to an elongated ellipsoid by stage 12 is poorly understood. Physical ablation studies in Dipteran insects indicate that the ellipsoid shape of the egg requires the follicle epithelium (Went, 1978), and genetic studies in *Drosophila* have shown that proteins linking intracellular actin to the extracellular matrix (ECM) are required in follicle cells to control egg shape (Bateman et al., 2001; Becam et al., 2005; Conder et al., 2007; Frydman and Spradling, 2001; Gutzeit et al., 1991; Lee et al., 2003; Mirouse et al., 2009). However, the specific activity that the follicle cells confer to shape the egg has remained elusive. To better understand this activity, we sought to define the elongation phase of oogenesis and characterize the behaviors the follicle cells undergo during this period.

2.3 Results

2.3.1 The major elongation phase of oogenesis occurs from stages 5-9

Many measurements defining the basic morphological characteristics of oogenesis have been made (King, 1970) but the one that is surprisingly neglected is that characterizing the elongation of the developing egg. By using a measure of elongation we call follicle aspect ratio – the maximal A-P length relative the maximal D-V length – we have found that elongation occurs from 4 to 12 of oogenesis (Figure 2.1). 74 percent of this 2.5-fold elongation is achieved from stages 5 to 9 of oogenesis (Figure 2.1, B). These stages only comprise 20 hours of the 3+ days spanning oogenesis following the formation and budding of an individual follicle in the germarium. Thus, we define stage 5 to 9 as the major elongation phase of oogenesis.

2.3.2 Polarized follicle rotation coincides with the major elongation phase

To better understand the activity required by the follicle cells to control egg shape, we characterized the behaviors of the follicle cells during the elongation phase of oogenesis. Cell behaviors associated with the elongation of other developmental tissues include polarized cell

division, polarized cell intercalation and polarized cell shape changes (Butler et al., 2009; Gong et al., 2004; Irvine and Wieschaus, 1994; Shih and Keller, 1992a). We reasoned that polarized cell division cannot be the major cellular behavior driving follicle elongation since most of the elongation occurs after stage 6, when the follicle epithelium has ceased proliferation (Figure 1.4) (Spradling, 1993). To determine whether dynamic cell behaviors are involved, we utilized live imaging of developing follicles (Bianco et al., 2007; Prasad and Montell, 2007) using the *i'm not dead yet* (*indy*) GFP protein trap line as a marker of the plasma membrane in the follicle cells (Kelso et al., 2004) (Figure 2.2, A-B). Surprisingly, this analysis revealed a novel and unexpected behavior during the elongation phase of oogenesis (Movie 2.1). We observed that the entire follicle epithelium undergoes a dramatic migration, in a circumferential direction around the elongating A-P axis, leading to rotation of the geometrically continuous tissue (Figure 2.2, C; Movie 2.2).

This rotation is developmentally regulated, occurring from mid-stage 5 to early stage 9 (Figure 2.1, B), terminating upon the delamination and onset of border cell migration (Spradling, 1993). Strikingly, this corresponds closely to the major phase of follicle elongation (Figure 2.1, B). The polarized rotation is observed in > 95% of wild type follicles (n > 100). Both left- and right-handed chiralities of rotation in adjacent follicles are observed (Figure 2.3, Movie 2.3), suggesting that the chirality of rotation is autonomous to each follicle. In addition, individual follicles isolated from the rest of the ovariole and the surrounding muscle sheath undergo polarized rotation, further supporting the active nature and autonomy of each follicle for rotation. Interfollicular stalk cells that connect adjacent follicles can accommodate rotating follicles within a given ovariole (Movie 2.3). This is possible because the stalk cells are not in direct contact with the migrating follicle cells of the egg chamber, but are instead, in direct contact with the static basement membrane that surrounds each follicle (Appendix A). The velocity of follicle cell rotation varies by stage from 0.26-0.78 μm/min (Appendix A), peaking during stages 6 to 8, and averaging 0.5 μm/min. Taking into account the estimated durations each follicle spends in each stage of oogenesis, the data suggest that a developing follicle undergoes approximately 3 revolutions during the 20 hours in which it achieves 74 percent of its total elongation.

The rotation of the follicle epithelium raises the question of what substrate these cells are moving along. Apically, the follicle epithelium contacts the germline cells (Figure 2.1, A). We used a Histone H2A variant (*His2Av*) mRFP fusion protein transgene to monitor germline nuclear movement and found that germline cells move in concert with the follicle cells, both in the direction and angular velocity of rotation (Figure 2.3, Movie 2.3). Basally, the follicle epithelium contacts a basement membrane that encases each follicle (Figure 2.1, A; Figure 2.9, A). To observe how the follicle cells behave relative to this basement membrane, we used a GFP protein trap line in *viking* (*vkg*; Collagen IV α2), which shows striking polarized fibrillar organization at this stage (Figure 2.4, A"; Figure 2.9, D-H). We found that follicle cells move across static Collagen IV fibrils (Figure 2.4; Movie 2.4), suggesting the active nature of the rotation. This 'follicle rotation' therefore consists of concerted movement of the somatic follicle cell and germline components of the growing egg, against the surrounding basement membrane, during the elongation phase of oogenesis. Follicle rotation is a novel type of collective cell migration and this global tissue rotation is unprecedented in any developing animal tissue studied thus far.

2.3.3 myospheroid (integrin βPS) and viking (collagen IV α2) do not undergo polarized follicle rotation and do not elongate

The strong correlation between the kinetics of egg elongation and the phase of follicle rotation suggested that this novel cellular behavior might play a role in egg morphogenesis. To investigate this possibility, we analyzed null mutants in the integrin β_{PS} subunit encoded by *myospheroid* (*mys*). *mys* is required in follicle cells for egg elongation but the underlying mechanism has not been investigated (Bateman et al., 2001; Duffy et al., 1998). As *mys* also regulates follicle stem cell proliferation and integrity of the epithelial monolayer (Fernandez-Minan et al., 2007; O'Reilly et al., 2008), we restricted our analysis to mosaic follicle cell clones with minimal disruptions in epithelial architecture. We first asked when *mys* was required for egg shape and found that *mys* mutant follicles are significantly rounder than wild type controls from stage 5 (one-way ANOVA, Tukey-Kramer test, $P \leq 0.014$, Figure 2.5, B, D). The defect in shape is not due to a change in egg volume or a defect in oocyte patterning (Figure 2.6), and round follicles are seen with only a fraction of the epithelium mutant for *mys* (Appendix A). Interestingly, this places the defect in follicle shape at the time period when follicle rotation normally occurs. We therefore carried out live imaging of round *mys* mutant follicles at these stages. Strikingly, we found that these follicles fail to rotate or undergo defective, off-axis rotation in most samples (Figure 2.7, B, D, Movies 2.5-2.7). The off-axis rotation explains the occasional observation of a *mys* mutant follicle with a misoriented oocyte from stage 7 onward (Figure 2.8; Movie 2.7) but not in younger stages (data not shown) (Becam et al., 2005).

The requirement for *mys* in both follicle rotation and follicle shape suggested that cell-matrix interactions, mediated by integrins, are required for the epithelial movement that may contribute to elongation of the egg. We examined the organization of three known *Drosophila* ECM molecules in the follicular basement membrane: Laminin, whose loss results in low-penetrant defects in egg shape (Frydman and Spradling, 2001), Perlecan, and Collagen IV. Among these, only Collagen IV forms and maintains striking polarized fibrils from stages 5-12, during the entire phase of follicle elongation (Figure 2.9, D-H, Appendix A) (Gutzeit et al., 1991). This observation, along with the requirement of Collagen IV to maintain basement membrane integrity in vertebrates (Poschl et al., 2004), led us to hypothesize that Collagen IV may also be involved in the control of *Drosophila* egg shape. To test this hypothesis, we analyzed females carrying follicle cell clones of vkg^{ICO}, a null allele of Collagen IV α_2, and found that they produce round eggs with normal egg volume and oocyte patterning (Figure 2.6). During oogenesis, follicles with an epithelium entirely mutant for *vkg* deviate in shape, with high penetrance, from stage 8 and have a final defect in elongation comparable to that of *mys* and other characterized round egg mutants (one-way ANOVA, Tukey-Kramer test, $P \leq 0.019$, Figure 2.5, A, C-D) (Bateman et al., 2001; Frydman and Spradling, 2001; Viktorinova et al., 2009). Interestingly, live imaging of *vkg* mutant follicles revealed that mutant follicles rotate normally up until stage 7, when there is a notable breakdown in follicle rotation (Figure 2.7, A, C-D; Movies 2.8-2.9). These data demonstrate that mutations in genes that block follicle rotation also block follicle elongation in a similar time frame, suggesting a tight coupling of these two processes.

2.3.4 A polarized fibrillar Collagen IV matrix is being built during follicle rotation

How might polarized follicle rotation shape the developing egg? We were intrigued to find that the length and density of fibrils of the basement membrane increase during the phase of follicle rotation (Figure 2.9). We measured the relative intensity of basement membrane Collagen IV-GFP during oogenesis and found that peak intensity coincides with the phase of follicle rotation (Figure 2.9, B-C) and peak *vkg* transcription during oogenesis (Appendix A). In addition, the Collagen IV matrix undergoes a dynamic change in organization during this period. Collagen IV forms an initial basal matrix around the germarium and the youngest follicles (Fig. 2.1, A, Appendix A) (Wang et al., 2008) with distinct puncta through stage 4 that mature into circumferentially oriented fibrils from stage 5 onward (Figure 2.9, D-H) that reach a maximal length and density at stage 8 (Figure 2.9, J-K). As no significant difference was found in Collagen fibril diameter in all stages examined (data not shown), this suggests that Collagen fibrils increase in length and density primarily from *de novo* polymerization rather than remodeling of puncta into fibrils. Importantly, fibril orientation is tightly regulated, and is established and maintained in the same orientation ($89.8^{o} \pm 27.2^{o}$ relative to the A-P axis at stage 8; Figure 2.9, I) that the follicle rotates. Moreover, by stage 8, individual Collagen IV fibrils can span across multiple follicle cells (Figure 2.10, A). Together, these data raised the possibility that the displacement of migrating follicle cells during rotation may direct the polarization of the fibrillar matrix.

To evaluate a possible link between polarized follicle rotation and Collagen IV fibrillogenesis *in vivo*, we examined the contribution of migrating follicle cells to matrix deposition. We carried out clonal analysis with a chromosome in which Collagen IV-GFP is genetically linked to a red fluorescent nuclear marker (Figure 2.10, B). By generating tissue mosaics using this chromosome in an otherwise unmarked, wild type follicular epithelium, the position of RFP-marked follicle cells can be compared with the distribution of Collagen IV-GFP that they have secreted (Figure 2.10, B). We observed that Collagen IV-GFP fibrils are present in unmarked domains of the follicle, indicating labeled follicle cells moved relative to these fibrils. To determine whether the observed distribution could be a consequence of follicle rotation, we examined follicles with marked follicle cells occupying either an A-P half or dorso-ventral (D-V) half of the follicle. When Collagen IV-GFP producing follicle cells are distributed across the A-P axis of the follicle, they produce a continuous distribution of Collagen IV-GFP fibrils across this axis (Figure 2.10, C). In contrast, if Collagen IV-GFP producing follicle cells occupy primarily the anterior or posterior half of the follicle, a non-uniform Collagen IV-GFP fibril distribution is seen, where GFP positive fibrils are associated with the portion containing marked follicle cells (Figure 2.10, D). These data are consistent with a model in which rotation plays a key role in forming the polarized basement membrane that surrounds developing follicles.

2.3.5 The actin cytoskeleton is dispensable as a molecular corset to maintain follicle shape

The emergence of a polarized basement membrane during the phase of follicle rotation raised the question of what role this fibrillar matrix may have. One possible model is that of a 'molecular corset.' A molecular corset has been proposed to control *Drosophila* egg shape by constraining growth along the D-V axis and permitting the majority of follicle growth along the A-P axis. Previous investigations have ascribed such a function for the actin cytoskeleton (Bateman et al., 2001; Conder et al., 2007; Frydman and Spradling, 2001; Gutzeit, 1990; Viktorinova et al., 2009), due to the striking polarization of stress fibers at the basal surface of the follicular

epithelium. However, basal actin filaments lose their circumferential orientation during the later phase (stages 9-11) of follicle elongation, raising the question of whether F-actin alone could serve this role throughout oogenesis (Appendix A) (Delon and Brown, 2009; Gutzeit, 1992). Furthermore, acutely disrupting polarized basal actin filaments in elongated stage 12 follicles with the actin depolymerizing agents Latrunculin A (Figure 2.11, C-E; 2.12, B-B") or Cytochalasin D (data not shown) did not perturb follicle shape (Gutzeit and Haas-Assenbaum, 1991). In contrast, the extracellular Collagen IV matrix establishes and maintains its fibrillar orientation from stages 5 to 12 of oogenesis during the entire elongation phase (Figure 2.9), making it an attractive candidate for a molecular corset.

2.3.6 The fibrillar Collagen IV matrix is required to maintain follicle shape

We first asked whether basement membrane integrity was compromised in *vkg* mutant follicles. We found that *vkg* is not required to establish the polarized matrix of the follicular basement membrane, as the Perlecan fibrillar matrix is intact and polarized in stage 7 *vkg* mutant follicles, which display wild type shape (Figure 2.13, A-B, A'-B'). At stage 8, however, when *vkg* mutants first show a defect in follicle shape (Figure 2.5), the Perlecan matrix has lost all of its polarized fibrils (Figure 2.13, C-D, C'-D'). Loss of Laminin fibrils, as detected by the binding of the lectin Concanavalin A (Gutzeit et al., 1991), was also seen in stage 8 *vkg* mutant follicles (data not shown). This is consistent with studies in vertebrates that type IV Collagens are required to maintain, but not establish, ECM organization (Poschl et al., 2004) and suggest that the integrity of a polarized fibrillar matrix is required for egg shape.

We then reasoned that if the Collagen IV matrix acts as a molecular corset, then acute loss of this fibrillar matrix should affect the shape of elongated follicles. To test this hypothesis, we treated follicles with Collagenase to determine whether such treatment affects late stage follicles, which have completed follicle rotation and established the polarized Collagen IV matrix. Indeed, we found that acute loss of Collagen IV within an hour of Collagenase treatment can result in a defect in follicle shape, rounding stage 12 follicles without affecting oocyte volume (paired t-test, $P << 0.001$, Figure 2.11, A-B, E; 2.12, C-C"). These data support the role of the Collagen IV matrix acting as a molecular corset to maintain the ellipsoid shape of the *Drosophila* egg.

2.3.7 Formation of a polarized fibrillar extracellular matrix is dependent on polarized follicle rotation

We next asked what happens to the basement membrane when follicle rotation is blocked. We analyzed round *mys* mutant follicles and found that the Collagen IV matrix is present but its organization is perturbed (Figure 2.14). Collagen IV clumped and formed aggregates (Figure 2.14, A-B) and the shape of individual fibrils was significantly altered (Mann-Whitney U-test, $P=0.0017$; Figure 2.14, E-F). Importantly, while neither the fibrillar density nor the length of the longest fibrils were statistically deviant from wild type controls (Appendix A), the uniform orientation of Collagen IV fibrils appeared completely lost (Mann-Whitney U-test, $P<<0.001$; Figure 2.14, A-D). These results suggest that the polarized organization of the Collagen IV fibrillar matrix, built by follicle rotation, is required to elongate the *Drosophila* egg.

To test the generality of this model to the entire follicle basement membrane, we tested the functional link between polarized global tissue rotation to Perlecan fibrillogenesis *in vivo* using a similar tissue mosaic strategy described earlier for Collagen IV-GFP (Figure 2.15, A). As Perlecan-GFP and *mys* are both located on chromosome X, this enabled us to analyze whether RFP-marked source cells could deposit polarized Perlecan-GFP fibrils into the unmarked territories of follicle mosaics in wild type or *mys* mutant backgrounds. As expected, we found that Perlecan-GFP is deposited as circumferentially polarized fibrils in wild type unmarked clones (Figure 2.15, B-B'). In contrast, Perlecan-GFP was not polarized and showed major defects in deposition into *mys* mutant unmarked clones (Figure 2.15, C-C'), although some non-cell autonomous deposition was seen at clone borders, likely due to overall follicle growth (Appendix A). Given that the majority of *mys* mutant follicles fail to undergo polarized rotation (Figure 2.7, D), these data support a model in which polarized follicle rotation is required to build a polarized fibrillar ECM to constrain tissue shape.

2.3.8 Basal microfilament circumferential polarity correlates with polarized follicle rotation

Finally, since basal microfilament polarity had long been associated with a molecular corset hypothesis (Bateman et al., 2001; Conder et al., 2007; Frydman and Spradling, 2001; Gutzeit, 1990; Viktorinova et al., 2009) that our data failed to support (Figure 2.11, 2.12), what role could planar polarized actin filaments have in the control of egg shape? We observed that basal F-actin circumferential polarity correlates with the ability of follicles to undergo polarized rotation. Typically, in wild type conditions, actin filaments exhibit planar polarity around its circumference, perpendicular to the long A-P axis during the rotation phase (Bateman et al., 2001; Delon and Brown, 2009; Frydman and Spradling, 2001; Gutzeit, 1979). In contrast, basal actin filaments polarized within individual wild type follicle cells of round *mys* follicles, but did not achieve global tissue planar polarity (Figure 2.16, A-A', lines) (Bateman et al., 2001). F-actin aggregates at the periphery of the basal surface in *mys* mutant cells but not in neighboring wild type cells within these follicles (Figure 2.16, A-A', arrow), suggesting that *mys* mutant cells were compromised in actin-based motility. When a sufficient portion of the tissue is mutant for integrin-based motility, it appears that the entire follicle fails to rotate and becomes round in shape (Appendix A).

Likewise, examination of *vkg* mutant follicles show that that basal microfilament polarity correlates with polarized tissue rotation and follicle shape. At stage 7, when *vkg* mutant follicles are still wild type in shape (Figure 2.5, D), basal microfilament polarity is circumferential to the A-P axis (Figure 2.16, B), albeit some irregularities compared to control genotypes (data not shown). In contrast, stage 8 follicles that begin to deviate in follicle shape (Figure 2.5, D) show a loss in planar polarity of basal microfilaments, where neighboring mutant cells fail to show local cell neighbor polarity alignment (Figure 2.16, C).

To test whether the actin filaments play a role in global tissue rotation more directly, we used the actin depolymerizing drug Cytochalasin D in wild type follicles undergoing polarized rotation. Within minutes after treatment, Cytochalasin D potently blocked follicle rotation (data not shown). This experiment supports the model where basal actin filaments play a role in actomyosin based motility that underlies global tissue rotation of the *Drosophila* follicle to control egg shape.

2.3.9 Summary & Model

In this chapter, we have identified a novel polarized morphogenetic behavior – global tissue rotation – that is strongly linked to the elongation of the developing egg in *Drosophila*. Together, our data indicate that polarized tissue revolutions mediated by the follicle epithelium over the ECM substratum, build polarized fibrils, like Collagen IV and Perlecan, within the follicle basement membrane. The anisotropic tensile strength of the polarized fibrillar ECM network acts as a 'molecular corset' to allow anisotropic growth of developing egg chambers, and maintain its ellipsoid shape until elongation and growth are complete at stage 12 (Figure 2.17). When follicles fail to undergo polarized rotation – due to defects in integrin-mediated cell motility – ECM fibril deposition is misoriented, leading to isotropic growth during oogenesis and production of a mature round egg. Our data suggest that global tissue rotation can account for the majority of elongation of the *Drosophila* egg.

2.4 Discussion

2.4.1 Polarized epithelial rotation as a novel collective cell movement

Here we describe a novel morphogenetic movement that elongates a developing tissue. Follicle rotation is a type of collective cell migration (Friedl and Gilmour, 2009; Rorth, 2009) that shares hallmarks common to these morphogenetic movements but also involves unique features that distinguish it as a novel class of morphogenetic movement. Like other types of collective cell migrations, follicle rotation is an intact epithelial sheet migration, maintaining cell-cell junctions with little evidence of cell neighbor exchange. It involves a multicellular polarity of cell-matrix interactions at the basal surface of the epithelium to set up a supracellular actin filament polarity, thought to generate the polarized traction and protrusive force necessary for migration. Follicle rotation generates traction against the static basement membrane to modify the tissue during migration by facilitating polarized ECM fibrillogenesis. However, because of the follicle's unique closed topology as a spheroid with no leading edge, this migration has a treadmill effect, leading to no net translocation of the epithelium. It is the first collective cell migration described with an obvious individual cell polarity and tissue polarity, but with no obvious collective cell polarity with leader and follower cells from our current analyses. Thus, the signal(s) that dictate the chirality, onset and cessation of global tissue rotation in each follicle and how coordinated migration occurs in this tissue occurs from a subcellular and molecular level remain interesting areas of future research.

2.4.2 Follicle planar cell polarity

Planar cell polarity (PCP) in this system was first noted by the striking supracellular polarity of basal actin filaments in follicle cells two decades ago (Gutzeit, 1990), and additional work identified a polarized cell-matrix network involved in this tissue polarity (Bateman et al., 2001; Conder et al., 2007; Delon and Brown, 2009; Deng et al., 2003; Frydman and Spradling, 2001; Gutzeit et al., 1991; Mirouse et al., 2009). The handful of studies on *Drosophila* egg shape (Bateman et al., 2001; Conder et al., 2007; Frydman and Spradling, 2001; Gutzeit et al., 1991)

have revealed that this cell-matrix PCP shares some features with other PCP tissues, including non cell-autonomous propagation of planar information through local polarity alignment (Bateman et al., 2001; Frydman and Spradling, 2001), asymmetric protein localization (Bateman et al., 2001; Delon and Brown, 2009) and a monopolar morphological output; however, the control of egg shape and PCP in the *Drosophila* ovary is independent of *fat* or the core PCP signaling pathway (Bastock and Strutt, 2007; Viktorinova et al., 2009). This is not surprising given that follicle PCP occurs at the basal domain of the epithelium, while core PCP signaling components (Fz, Dsh, Pk, Stbm, Fmi) localize to the apical domain in other planar polarized epithelia, such as the wing. Thus, it appears that distinct genetic and molecular cassettes may be involved in establishing planar polarity in the apical versus basal domains of epithelia (Figure 2.18).

Interestingly, it was found that one of the original round egg mutants, *kugelei* (Gutzeit et al., 1991; Tearle and Nusslein-Volhard, 1988) is allelic to *fat2*/*fat*-like, part of a the cadherin superfamily of Ca^{2+} dependent cell adhesion molecules (Viktorinova et al., 2009) whose family member, *fat*, plays a critical role as a global modulator of PCP in other tissues (Ma et al., 2003; Yang et al., 2002). This study suggests that a similar modular cascade for tissue PCP (Axelrod, 2009) may exist in this system, though the genes and molecular mechanisms involved appear to be distinct (Figure 2.18). Fat2 is expressed dynamically in both the germline and follicle cells during oogenesis though its function in egg elongation is associated with its activity in the follicle epithelium. Fat2 is localized at the basal surface and shows monopolar enrichment, like that seen for actin-based protrusions (Viktorinova et al., 2009). While a follow up report from this group proposed *fat2* acts as a global modulator of follicle PCP with the tissue axes (Viktorinova et al., 2011), the analysis was performed at late stage follicles when elongation is complete, so it remains to be resolved how global polarity emerges in the follicle during the major elongation phase at stage 5. It is unclear what global cue might break the initial symmetry in the follicle to form the molecular polarity of cell-matrix proteins and to initiate follicle rotation. How tissue polarity is established in this system will be an interesting and exciting area for future research.

2.4.3 Planar mechanotransduction through a static ECM to relay polarity information across a tissue

Our discovery of follicle rotation and the central role of cell-matrix interactions in this process suggest that the core module to amplify asymmetry in individual cells in the follicle epithelium involves a positive biomechanical feedback loop using cell-matrix genes rather than a molecular inhibitory feedback mechanism mediated by core PCP proteins between adjacent cells in other tissues. At a subcellular level, we envisage actomyosin contractile forces are generated by follicle cells in the direction of motility to exert traction through focal adhesions on to the basement membrane, organizing the orientation of ECM fibrillogenesis (Appendix A). The increase in fibril length and density of the matrix increases ECM rigidity, and the elevated ECM tension is reciprocally sensed by integrin-based contacts in the follicle cells to elevate cellular tension and reinforce actin filament polarity. This positive biomechanical feedback loop amplifies receptor-cytoskeleton asymmetry within a cell (Colognato et al., 1999), while the closed geometry and circumferential rotation of the follicle epithelium coordinates polarized ECM fibrillogenesis. At the supracellular level, the polarized ECM can communicate PCP

information (Frydman and Spradling, 2001; Skoglund and Keller, 2010) to feed back to follicle cells to promote directed tissue migration. Since individual follicle cells move over ECM fibrils previously oriented by neighbors, global rotation can both amplify and reinforce coordination of PCP across the entire tissue in a relatively short timeframe.

When follicle rotation does not occur, for instance in follicles containing *mys* clones, basal actin filaments within wild type cells align locally but cannot form a uniform global orientation. The loss of F-actin polarity within *mys* mutant cells demonstrates the requirement for integrin in establishing cellular asymmetries in individual follicle cells and demonstrates integrin's required function in global tissue rotation. Moreover, our work suggests its global non-autonomous effect on follicle PCP is primarily biomechanical. We propose that a small *mys* clone is sufficient to alter local tissue polarity of the F-actin cytoskeleton without completely disrupting tissue migration, resulting in defective off-axis rotation. However, if the mutant clone size is large enough in *mys* round follicles, it seems that the loss of polarized F-actin in mutant cells and the non-autonomous effects in neighboring wild type cells is sufficient to block follicle rotation entirely. The decision to rotate or not to by a given follicle, may be telling of how tissue polarity is conveyed at a supracellular level and remains to be explored.

In summary, the system described here in the *Drosophila* follicle has thematic parallels to the canonical PCP signaling cascade, but propagates the asymmetry primarily through cell-ECM contacts rather than cell-cell contacts. It raises the possibility that different tissues may relay planar information using different mechanisms, depending on the timescale needed to execute an output of morphological polarization. Most notably, rather than involving a cue that dynamically propagates through the plane of a static epithelium, in the follicle, coordination of polarity is provided by moving an epithelium dynamically across a stable cue – the ECM. It is possible that this cell-matrix relay mechanism may be employed in other morphogenetic tissues, for example during convergent extension of the dorsal mesoderm in the *Xenopus* gastrula (Davidson et al., 2008; Davidson et al., 2006). Given our relatively naive understanding of PCP propagation in most tissues, it will be quite interesting to see how other tissues propagate planar information in migrating and static tissues.

2.4.4 A revised function for circumferential basal microfilaments in the control of egg shape

Our work sheds light on the long-standing view of the proposed function of the circumferential polarity of the actin cytoskeleton on the basal domain of the follicle epithelium. Early work proposed that circumferentially polarized basal microfilaments mechanically constrains follicle shape to bias growth along the A-P axis (Gutzeit, 1990; Gutzeit et al., 1991), and this model has become the dogma within the field for many years (Bateman et al., 2001; Conder et al., 2007; Delon and Brown, 2009; Frydman and Spradling, 2001; He et al., 2010; Mirouse et al., 2009; Viktorinova et al., 2011).

There have been conflicting observations – that microfilaments are not always circumferentially oriented, that loss of actin filaments does not affect overall follicle shape – that has led to proposed alternative functions for basal actin filaments: as a counteracting pressure via focal adhesions to withstand the mechanical deformations the follicle faces upon ovarian muscle contractions (Gutzeit, 1990), to strengthen integrin-based adhesion in late oogenesis (Delon and

Brown, 2009), or for A-P cell lengthening of follicle cells during nurse cell dumping (Viktorinova et al., 2011). While some of these hypotheses may be true for the function of basal actin during mid to late oogenesis where the analyses were performed, more functional experiments need to be performed to directly test these hypotheses. Still, the prevailing model assumes that actin functions as a molecular corset, and recent work has identified oscillating contractions of a basal actomyosin network in stage 9 to 10 follicles that have been implicated as part of the F-actin molecular corset (He et al., 2010). The functional data supporting this proposed role at stage 9-10 is weak due to caveats in the experimental design and is inconsistent with our own observations (Appendix A). Despite these reservations, it will be interesting to elucidate the function of these basal follicle cell oscillations for oogenesis.

Perhaps the greatest challenge in making progress by the community has been due to limited efforts to elucidate the function of polarized microfilaments during the major elongation phase from stage 5 to 9. The discovery of polarized follicle rotation provides one function, and we propose that a primary requirement of the actin cytoskeleton in egg elongation is due to a role in polarized collective cell motility, not as a molecular corset. While we believe our proposed mechanism can account for the majority of follicle elongation, our data from *mys* and *vkg* mutant follicles suggest that it is only one of several mechanisms that establish final egg shape and it will be exciting to identify other activities in the follicle that control its elongation.

2.4.5 The importance of the polarity of the extracellular matrix to shape tissues

Our work highlights the importance of the ECM in sculpting tissues and organs. The elegant circumferential polarity of the Collagen IV matrix during the entire elongation phase has identified a clear, yet simple function as a molecular corset to control *Drosophila* egg shape. The use of a polarized ECM is not unique to the *Drosophila* follicle, as oriented fibronectin fibrils promote convergent extension and elongation of the *Xenopus* notochord (Adams et al., 1990; Davidson et al., 2006; Koehl et al., 2000) and circumferential cellulose fibrils form around plant cells necessary for plant cell and axial elongation (Paredez et al., 2006). It is interesting to note that animals use motility to form such an elegant ECM structure, while stationary plant cells have found an alternate mechanism to form oriented cellulose fibrils by rotating the cellulose synthase complex within the plasma membrane (Paredez et al., 2006). Likewise, the structural organization of the exoskeleton is important to control body shape in *C. elegans* and *Drosophila* larvae and adults, where defects can result in dumpy or tubby phenotypes. Interestingly, body shape involves nematode Collagens or insect Tweedles, a novel cuticle protein family (Guan et al., 2006; Johnstone, 1994), suggesting that the polarity and structural integrity of the extracellular matrix supporting tissues or whole bodies play a critical role in morphogenesis in a variety of organisms.

2.4.6 The generality of polarized tissue rotation to shape tissues in metazoans

To the best of our knowledge, a morphogenetic movement with the attributes of follicle rotation has not been described in other animal tissues. We note that the discovery of follicle rotation was not anticipated by the rich history of studies on *Drosophila* oogenesis from fixed specimens and that live time-lapse microscopy was required to reveal its existence. Intriguingly, developing chicken eggs rotate in the portion of the oviduct when egg shape is being conferred,

but the relationship of chicken egg rotation to egg shape is not understood and seems to occur in the absence of a supporting migratory follicle epithelium (Gilbert, 1979; Kochav and Eyalgila, 1971; Smart, 1991). We suggest that live imaging of other morphogenetic events may uncover additional instances where, as we have shown here for the *Drosophila* egg, polarized tissue rotation influences tissue and organ shape.

2.5 Materials & Methods

***Drosophila* genetics**

vkg^{ICO} was a gift from D. Kimbrell (Rodriguez et al., 1996). The allele was confirmed as a genetic null by lethal phase complementation analysis to the chromosomal deficiency *Df(2L)BSC172*. Other fly stocks included *mys*^{XG43} *FRT101*, *w; ubi::eGFP FRT40A, T155::GAL4 UAS::FLP* (N. Perrimon) (Duffy et al., 1998), *GR1::GAL4 UAS::FLP* (T. Schupbach) (Gupta and Schupbach, 2003), *myc*^{PG45}*::GAL4* (D. Stein) (Zhu and Stein, 2004) and GFP protein traps in *indy* (YC0017) (Kelso et al., 2004) *vkg* (CC00791) and *trol* (CA06698) (Buszczak et al., 2007). *ubi::nls-mRFP* transgenes were kindly provided by J. Lipsick. Additional stocks were obtained from the Bloomington *Drosophila* Stock Center; information is available on Flybase (Tweedie et al., 2009). *mys*^{XG43} was recombined onto *FRT19A*, while *vkg*^{ICO}, *vkg-GFP* and *ubi::nls-mRFP* were recombined onto *FRT40A* using standard techniques. Mosaic follicle cells were generated as previously described (Duffy et al., 1998). All crosses were performed at 25 ºC and adult females were fed on an abundant yeast diet for 2-7 days prior to dissection.

Experimental Genotypes:

Figure 2.1:

A. y *w; vkg-GFP*

B. *w; His2Av-mRFP*

Figure 2.2:

B, C. *w; indy-GFP*

Figure 2.3:

A. y *w/w; His2Av-mRFP/+; indy-GFP/+*

Figure 2.4:

A-A". *myc*^{PG45}*::GAL4/w; vkg-GFP/+; UAS::myr-mRFP FRT80B/+*

Figure 2.5:

A, D. *w; ubi::eGFP FRT40A; GR1::GAL4 UAS-FLP/+*

B, D. *w mys*^{XG43} *FRT101/y w ubi::nls-GFP FRT101; e22c::GAL4 UAS::FLP/+*

C, D. *y w/w; vkg*^{ICO} *FRT40A/ubi::eGFP FRT40A; GR1::GAL4 UAS::FLP/+*

D. *y w ubi::nls-GFP FRT101; e22c::GAL4 UAS::FLP/+*

Figure 2.6:

A, E-G. *y w ubi::nls-GFP FRT101; e22c::GAL4 UAS::FLP/+*

B, E-G. *w; ubi::eGFP FRT40A; GR1::GAL4 UAS::FLP/+*

C, E-G, H. *w mys*^{XG43} *FRT101/y w ubi::nls-GFP FRT101; e22c::GAL4 UAS::FLP/+*

D, E-G, I. *y w/w; vkg*^{ICO} *FRT40A/ubi::eGFP FRT40A; GR1::GAL4 UAS::FLP/+*

Figure 2.7:

A, D. *w; ubi::eGFP FRT40A; GR1::GAL4 UAS::FLP/indy-GFP*

B, D. *w mys*^{XG43} *FRT101/y w ubi::nls-GFP FRT101; e22c::GAL4 UAS::FLP/+; indy-GFP/+*

C, D. *w; vkg*^{ICO} *FRT40A/ubi::eGFP FRT40A; GR1::GAL4 UAS::FLP/indy-GFP*

D. *y w ubi::nls-GFP FRT101; e22c::GAL4 UAS::FLP/+; indy-GFP/+*

Figure 2.8:

A. *w mys*^{XG43} *FRT101/y w ubi::nls-GFP FRT101; e22c::GAL4 UAS::FLP/+*

B. *w mys*^{XG43} *FRT101/y w ubi::nls-GFP FRT101; e22c::GAL4 UAS::FLP/+; indy-GFP/+*

Figure 2.9:
A-K. *y w; vkg-GFP*
Figure 2.10:
A. *y w; vkg-GFP*
C, D. *w; ubi::nls-mRFP vkg-GFP FRT40A/FRT40A; T155::GAL4 UAS::FLP/+*
Figure 2.11:
A-E. y *w; vkg-GFP*
Figure 2.12:
A-C". y *w; vkg-GFP*
Figure 2.13:
A-A', C-C'. y *w trol-GFP/w; ubi::nls-mRFP FRT40A; GR1::GAL4 UAS::FLP/+*
B-B', D-D'. y *w trol-GFP/w; vkg^{ICO} FRT40A/ubi::nls-mRFP FRT40A; GR1::GAL4 UAS::FLP/+*
Figure 2.14:
A, C, E, G. *w ubi::nls-mRFP hs::FLP^{122} FRT19A; e22c::GAL4 UAS::FLP/vkg-GFP*
B, D, F, G. *w mys^{XG43} FRT19A/w ubi::nls-mRFP hs::FLP^{122} FRT19A; e22c::GAL4 UAS::FLP/vkg-GFP*
Figure 2.15:
B-B'. *w sn FRT19A/y w trol-GFP ubi::nls-mRFP hs::FLP^{122} FRT19A; e22c::GAL4 UAS::FLP/+*
C-C'. *w mys^{XG43} FRT19A/y w trol-GFP ubi::nls-mRFP hs::FLP^{122} FRT19A; e22c::GAL4 UAS::FLP/+*
Figure 2.16:
A-A'. *w mys^{XG43} FRT101/ y w ubi::nls-GFP FRT101; e22c::GAL4 UAS::FLP/+*
B, C. *y w/w; vkg^{ICO} FRT40A/ubi::eGFP FRT40A; GR1::GAL4 UAS::FLP/+*
Movie 2.1:
w; indy-GFP
Movie 2.2:
w; indy-GFP
Movie 2.3:
y *w/w; His2Av-mRFP/+; indy-GFP/+*
Movie 2.4:
myc^{PG45}::GAL4/w; vkg-GFP/+; UAS::myr-mRFP FRT80B/+
Movie 2.5:
w mys^{XG43} FRT101/y w ubi::nls-GFP FRT101; e22c::GAL4 UAS::FLP/+; indy-GFP/+
Movie 2.6:
y w ubi::nls-GFP FRT101; e22c::GAL4 UAS::FLP/+; indy-GFP/+
Movie 2.7:
w mys^{XG43} FRT101/y w ubi::nls-GFP FRT101; e22c::GAL4 UAS::FLP/+; indy-GFP/+
Movie 2.8:
w; vkg^{ICO} FRT40A/ubi::eGFP FRT40A; GR1::GAL4 UAS::FLP/indy-GFP
Movie 2.9:
w; ubi::eGFP FRT40A; GR1::GAL4 UAS::FLP/indy-GFP

Fixation & Immunohistochemistry
All follicles were manually dissected from the epithelial muscle sheath as described (Prasad et al., 2007) to preserve follicle shape in Schneider's *Drosophila* medium (GIBCO) and fixed within 15 minutes using 4% formaldehyde or an alternate fixative used to enhance preservation

of the basal F-actin cytoskeleton in follicle cells (Frydman and Spradling, 2001). Immunostaining followed standard protocols and the following primary antibodies were used: mouse anti-Grk (1D12 concentrate, 1:100, DSHB), rabbit anti-GFP (1:200, Molecular Probes) and rabbit anti-GFP-AlexaFluor 488 (1:100, Molecular Probes). AlexaFluor- conjugated secondary antibodies (Molecular Probes) were used at 1:200. F-actin was visualized using phalloidin-TRITC (1:500, Sigma), Laminin was visualized using Concanavalin A-AlexaFluor 647 (100μg/ml, Molecular Probes) and DNA was visualized using TOPRO-3 (1:200, Molecular Probes).

***Ex vivo* follicle culture**

Live imaging of cultured follicles were performed largely as described (Prasad et al., 2007) with the following modification. For egg chamber mounting, a 18x18 mm #1 cover glass (Fisher Sci.) was cushioned using high vacuum grease (Dow Corning) and gently placed over dissected follicles in 30 μl of culturing medium to reduce the working distance required for use with certain objective lenses.

Actin Pharmacological Inhibitors and Collagenase treatments

Latrunculin A (10 μM in DMSO, Enzo Life Sciences) or Collagenase (1000 Units/ml CLSPA; Worthington Biochemical Corp.) were added to a final volume of 100 μl of culturing medium. DMSO (1%) was used as a control for Latrunculin A experiments. Collagenase reactions were stopped with 10mM L-cysteine (Sigma) prior to fixation.

Microscopy and Image Processing

Fixed and live time-lapse images were acquired on a TCS SL (Leica) using 16x/NA 0.5, 40x/NA 1.25 or 63x/NA 1.4 oil immersion lenses, a LSM 5 Live (Zeiss) using 20x/NA 0.5 or 40x/NA 1.3 oil immersion lenses, or a Axio Imager.M1 (Zeiss) using 10x/NA 0.3 air objective lens. For time-lapse imaging, 2, 5 or 15 minute time points were acquired with single xy or multiple z-step xy planes imaged over a total scan time of < 1 min per time point. Cell tracking was performed using object tracking algorithms or manual object tracking in Volocity (Perkin Elmer). Collagen fibril analysis used Volocity object recognition software and Image J (NIH). Other data quantitation used Volocity and/or Image J.

Data Analysis

All experiments were performed on at least 3 independent dates. All data graphs are reported as mean $\pm$ standard deviation. Images were processed and assembled using Creative Suite 4 (Adobe), Volocity and Image J. Statistical analysis was performed using StatPlus (Analyst Soft, Inc.) with alpha levels for all statistical tests set to 5%. Graphs were produced using Excel 2008 (Microsoft) and rose diagrams were plotted using Rozeta 2.0 (Pazera-Software).

Data Statistics

Figure 2.5, D: one-way ANOVA, Tukey-Kramer test, $P \leq 0.014$ for all stages indicated between mys^{XG43} and *ubi::GFP* controls.
Figure 2.5, D: one-way ANOVA, Tukey-Kramer test, $P \leq 0.019$ for all stages indicated between vkg^{ICO} and *ubi::eGFP* controls.
Figure 2.11, E: paired t-test, $P << 0.001$ between Collagenase treated and untreated controls.
Figure 2.14, C-D: Mann-Whitney U-test, $P << 0.001$

Figure 2.14, G: Mann-Whitney U-test, P=0.0017

Follicle Aspect Ratio Measurements

Staging of *D. melanogaster* egg chambers followed the field guide provided in (Spradling, 1993). Follicle AR was calculated as a ratio of follicle A-P maximal length: D-V maximal length for stage <11 follicles. Stage 12-13 follicle A-P maximal length was measured from the anterior follicle cells overlying the micropyle to the posterior pole. Dorsal appendage follicle cells and nurse cells were excluded in AR measurements for stage 12-13 follicles. Midsagittal views were acquired to determine AR measurements.

Collagen IV Relative Intensity Analysis

Images of follicles from ovarioles were acquired using uniform imaging conditions within an emission range of 0-255 intensity units. The Collagen IV intensity per follicle was calculated by averaging intensity through the basement membrane at three independent regions of a given follicle. All ovarioles had the same relative intensity trendline as a function of developmental stage but contained a subset of differentially staged follicles; the graph pooled average intensity as a function of developmental stage in oogenesis.

Collagen IV Fibril Analysis

Data quantification for Collagen IV fibril analysis was performed on 30 x 30 μm squares in Figure 3 or 40 x 40 μm squares in Figure 4. Images were acquired at 300 nm steps at 1.0 airy unit. Following cropping of representative areas for further analysis, image z-stacks were deconvolved and 3D fibrils were identified using an intensity threshold algorithm for each sample. Noise was removed from analysis using a minimal volume threshold. The accuracy of fibril object recognition was verified manually for each sample. Objects touching the edges of images were excluded from further analysis. The skeletal length of identified objects was determined by thinning each object from all sides until single voxel line was left and the direction of the line was elongated to meet the edges of the object. The accuracy of the skeletal length was verified by computing the skeletal diameter, which is defined as the diameter of a cylinder if it had a length (l) equal to the object's measured skeletal length with a volume (V) equal to the object's measured volume, using $V=\pi_{*}r^{2}{}_{*}l$, where r is the cylinder's radius (r). Using this strategy, Volocity-recognized objects has an average skeletal diameter of 344 $\pm$ 84 nm in both wild type and mutant follicles, which closely approximates the known diameter of Collagen fibrils at 260-410 nm (Bozec et al., 2007). Volocity recognized objects were flattened from 3D to 2D objects for use in ImageJ to calculate object shape factor and orientation. Objects were converted to a best-fit ellipse to calculate the major and minor axis to compute the object's aspect ratio (AR). The angle of the major axis of each object is reported in degrees relative to the x-axis of each image (A-P axis of each follicle) at 0 degrees.

Figure 2.1
The major elongation phase of oogenesis in *Drosophila melanogaster.*

(**A**) Follicles elongate along the A-P axis during successive stages of oogenesis. Midsagittal section showing Collagen IV-GFP (green), F-actin (red), and DNA (cyan). (**B**) Quantification of follicle aspect ratio reveals a major elongation phase between stages 5 and 9. Stage duration (measurements from (Spradling, 1993)) and percent elongation are reported below. The periods of follicle rotation (blue), polarized basal actin filaments (red), and polarized Collagen IV fibrils (green) are indicated as solid lines, with dotted lines indicating the presence of movement or structure without clear circumferential polarity.

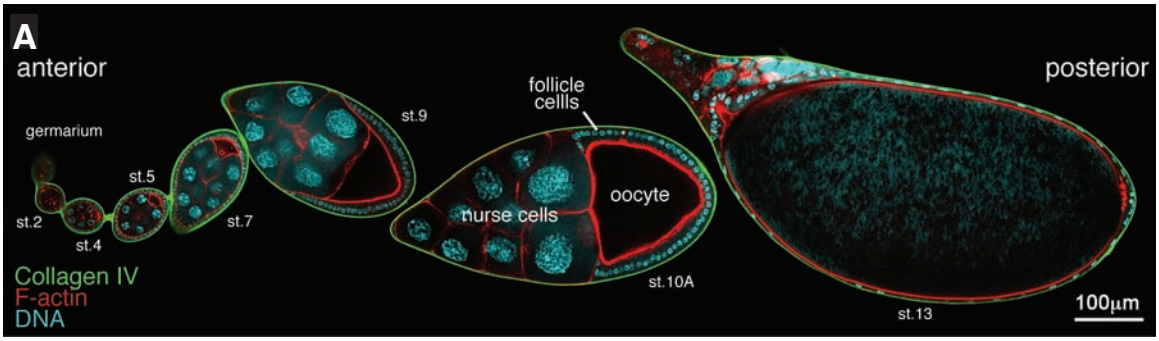

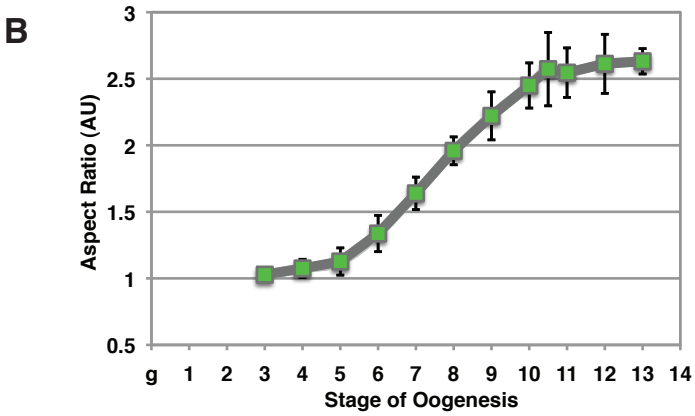

hours per stage	n/a	8	8	6	5	3	6	6	6	10	0.5	2	1	>2
% e ongat on per stage			4	5	19	23	19	13	10	5	2			
% tota e ongat on			4	9	28	51	70	83	93	98	100			
po ar zed fo c e rotat on														
po ar zed F-act n (basa)														
po ar zed Co agen IV f br s														

Figure 2.2
Follicle cells undergo a polarized, concerted migration around the A-P axis.

(**A**) General microscope setup used for live imaging of developing follicles *ex vivo*. Planes commonly shown in figures and supporting movies are indicated by the red dotted lines. (**B-C**) Live imaging of follicles expressing Indy-GFP (green) to outline follicle cell membranes (**B**) reveals that follicle cells move continuously in an orthogonal axis to the A-P axis. A subset of follicle cells are pseudo-colored red for cell tracking purposes. Frames taken from Movie 2.2. Scale bar in (**B-C**) 25 μm.

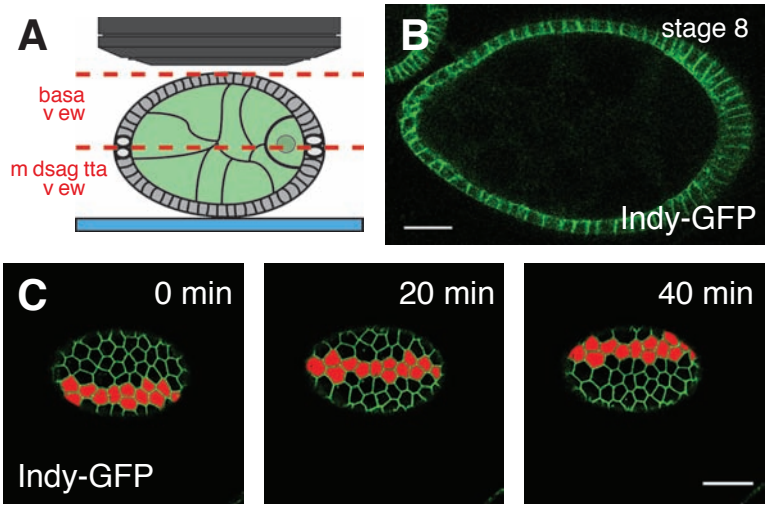
A
basa
v ew
m dsag tta
v ew
B
stage 8
Indy-GFP
C
0 min
Indy-GFP
20 min
40 min

Figure 2.3
Global tissue rotation coincides with the elongation of the *Drosophila* egg.

87 μm maximal projection 4D time-lapse of follicle rotation. Tracking of follicle cells (white and yellow dots, arrowheads in (**A**) and germline nuclei (large RFP nuclei, red; numbered in **A'**) reveals that the germline and follicle epithelium rotate together. Depth code scale for (**A')** is shown to the right, where red indicates superficial depths and blue indicates the deepest depths along the z-axis of the time-lapse. Note that the stage 6 and stage 7 follicles are moving in opposite chiralities, and that the stage 9 follicle does not rotate. Frames taken from Movie 2.3. Scale bar 50 μm.

A
A'
0 min
20 min
40 min
60 min
st. 3
st. 4
st. 6
st. 7
st. 9
Indy-GFP
His2Av-mRFP
depth coded nuclei
µm
80
70
60
50
40
30
20
10
0

Figure 2.4
Follicle cells undergo a polarized migration against a static basement membrane.

4D live imaging of a stage 8 follicle's basal surface. 26μm maximal projection reveals follicle cells (red; tracked cells outlined in blue) move against static Collagen IV fibrils (green, arrowheads). Gray-scale channel for each marker is shown below. Frames taken from Movie 2.4. Scale bar 10 μm.

0 min
12 min
24 min
36 min
A
A′
A″
Collagen IV-GFP
myc >> myr-mRFP
Collagen IV-GFP
myc >> myr-mRFP

Figure 2.5
***mys* or *vkg* mosaic follicles show defects in follicle shape during the rotation phase of oogenesis.**

(**A-D**) Follicles with epithelial clones of *mys* or *vkg* (GFP negative) show shape defects during rotation. *mys* mutant follicles (**B**) are rounder from stage 5; *vkg* mutant follicles (**C**) are rounder from stage 8. Follicle aspect ratio is displayed in (**D**). Asterisks indicate $P<0.05$. Scale bar in (**A-C**) 100 μm.

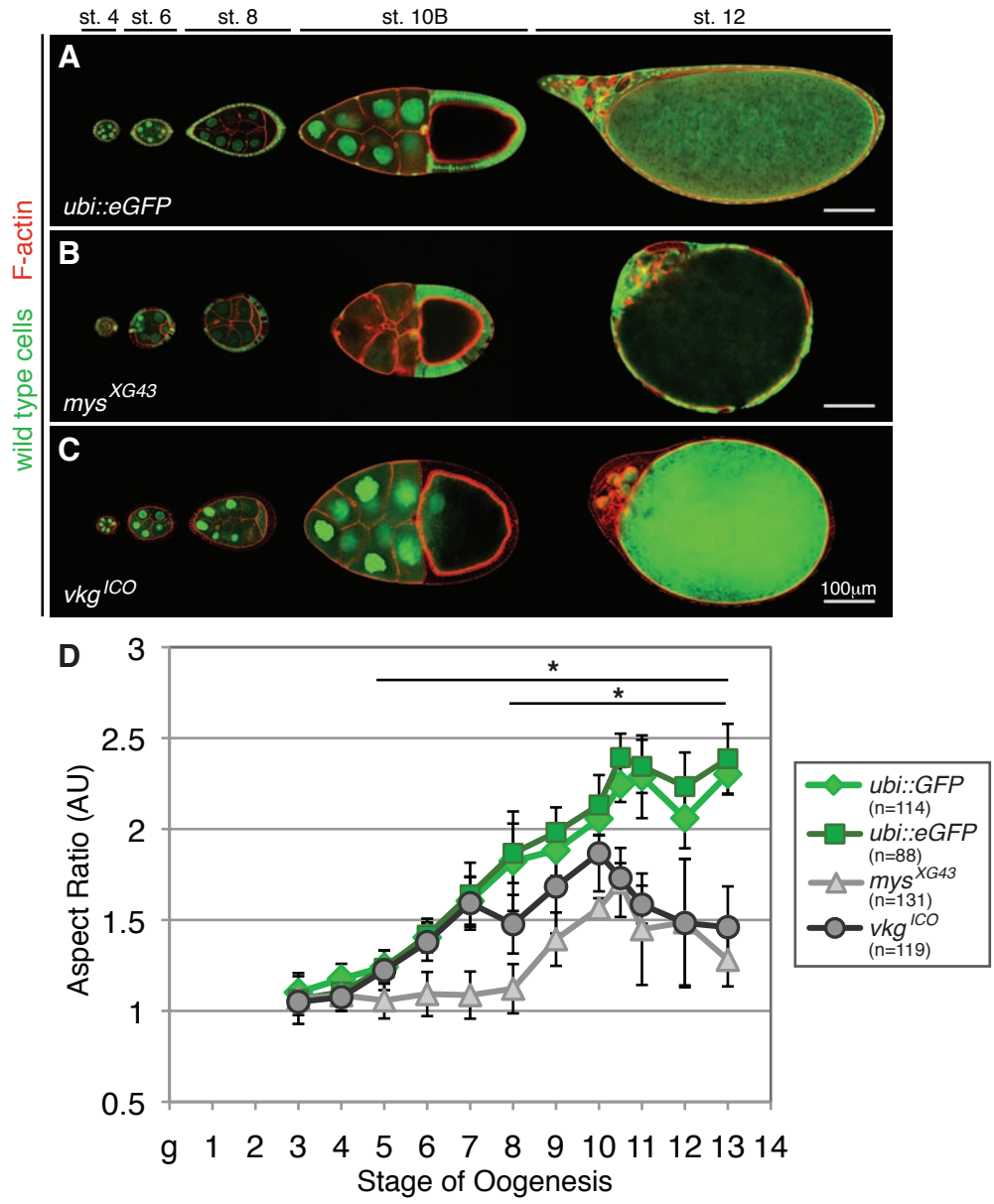
st. 4
st. 6
st. 8
st. 10B
st. 12
A
ubi::eGFP
B
mys XG43
C
vkg ICO
100µm
wild type cells
F-actin
D
Aspect Ratio (AU)
3
2.5
2
1.5
1
0.5
*
*
g 1 2 3 4 5 6 7 8 9 10 11 12 13 14
Stage of Oogenesis
ubi::GFP
(n=114)
ubi::eGFP
(n=88)
mys XG43
(n=131)
vkg ICO
(n=119)

Figure 2.6
Specific egg elongation defects produced by *mys* or *vkg* mutant follicle cell clones.

(**A-D**) Darkfield images of eggs produced by control (**A, B**), *mys* (**C**)**,** or *vkg* (**D**) mutant follicle epithelia. Quantitation of dimensions (**E**), aspect ratio (**F**) and volume (**G**) reveals that elongation is specifically altered. Polarity of the oocyte (assayed by asymmetric localization of Gurken (Grk; cyan) is unaltered in round *mys* (**H**) and *vkg* (**I**) mutant follicles.

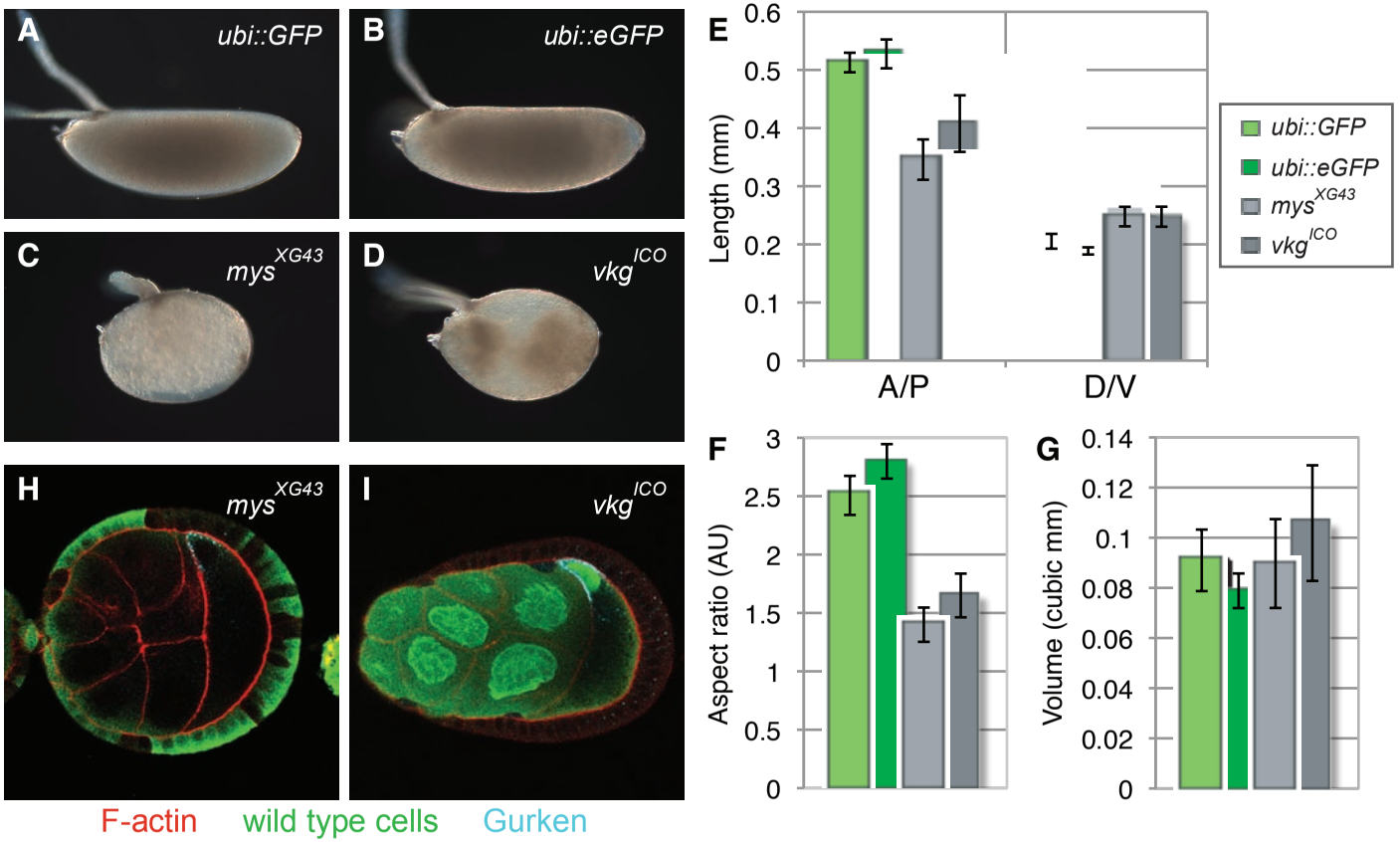
A
ubi::GFP
B
ubi::eGFP
C
mys XG43
D
vkg ICO
H
mys XG43
I
vkg ICO
F-actin
wild type cells
Gurken
E
Length (mm)
0.6
0.5
0.4
0.3
0.2
0.1
0
A/P
D/V
ubi::GFP
ubi::eGFP
mys XG43
vkg ICO
F
Aspect ratio (AU)
3
2.5
2
1.5
1
0.5
0
G
Volume (cubic mm)
0.14
0.12
0.1
0.08
0.06
0.04
0.02
0

Figure 2.7
***mys* or *vkg* mosaic follicles do not undergo polarized rotation and do not elongate.**

(**A-C**) Round follicles with *mys* (**B**) and *vkg* (**C**) clones are defective in rotation compared to control (**A**). Wild type cells (green intracellular); Indy-GFP (green membrane); tracked cells are pseudocolored red. (**D**) Percentage of follicles undergoing polarized, off-axis, or no rotation from live imaging. Frames for (**A-C**) taken from Movie 2.5, Movie 2.8 and Movie 2.9. Scale bar in (**A-C**) 25 μm.

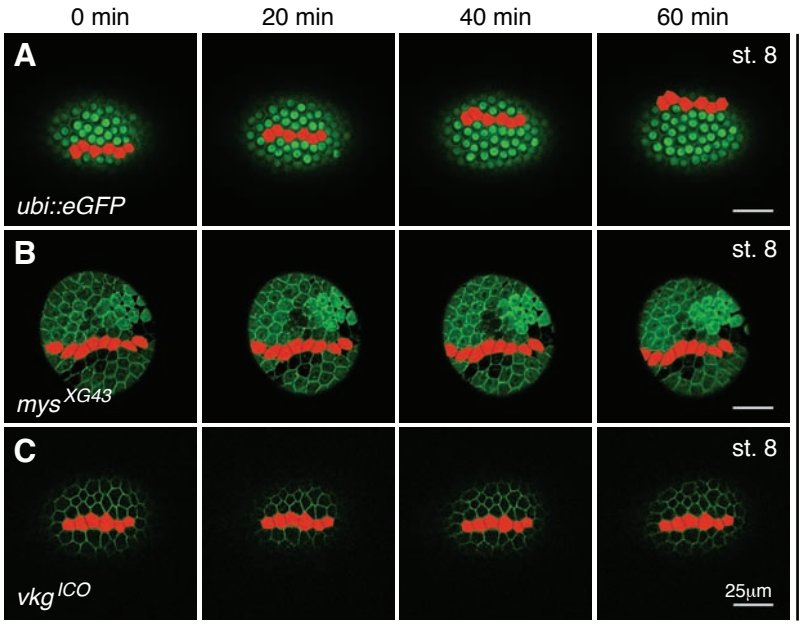

D

percentage (%), by stage

	stage	5	6	7	8
ubi::GFP (n=19)	↕	**71.4**	**100**	**100**	**100**
	↝	0	0	0	0
	—	28.6	0	0	0
ubi::eGFP (n=30)	↕	**83**	**100**	**100**	**100**
	↝	0	0	0	0
	—	17	0	0	0
mys XG43 (n=18)	↕	25	0	14	0
	↝	25	33	**43**	25
	—	**50**	**67**	**43**	**75**
vkg ICO (n=19)	↕	**100**	**50**	**57**	12.5
	↝	0	**50**	0	12.5
	—	0	0	43	**75**

↕ polarized rotation
↝ off-axis rotation
— no rotation

Figure 2.8
Off-axis rotation of *mys* mutant mosaic follicles can lead to follicle misorientation.

(**A**) WT follicles are oriented with the A-P axis, evidenced by the posterior oocyte (asterisks), generally aligned with the ovariole axis, evidenced by the position of interfollicular stalks. Occasional aberrant rotation in follicles with *mys* mutant clones (arrow) can lead to positioning of a follicle A-P axis divergent from the ovariole axis. (**B**) Live imaging of an off-axis rotation event in a follicle with *mys* mutant clones (lacking cytoplasmic GFP; Indy-GFP shows follicle cell membranes in green). Frames taken from Movie 2.7. Scale bar in (**A**) 100 μm; (**B**) 25 μm.

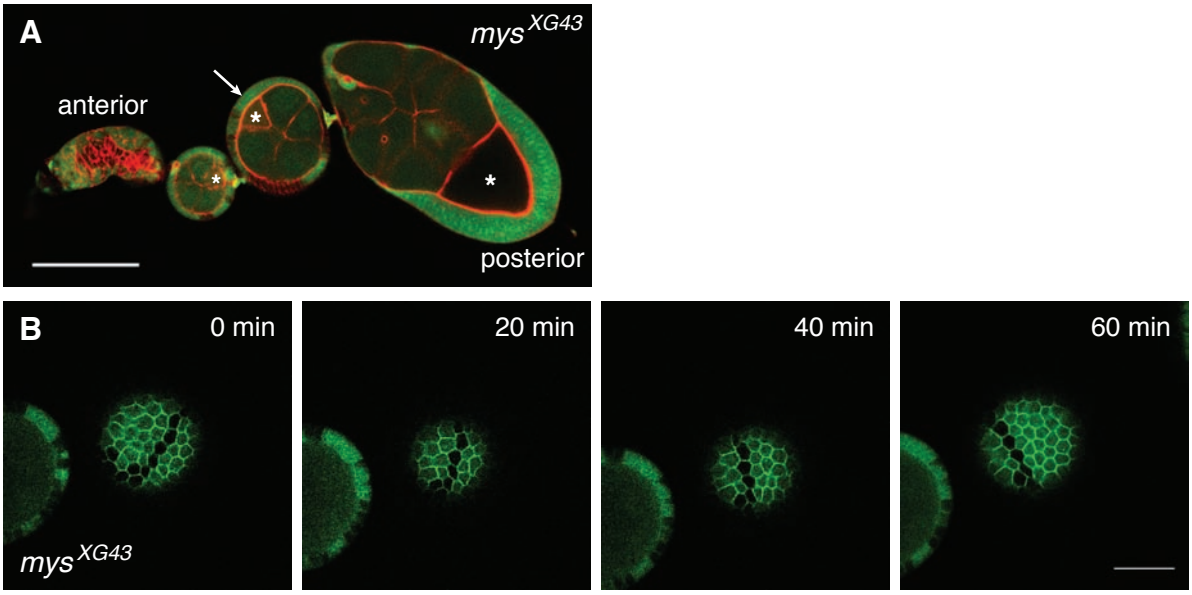
A
mys XG43
anterior
posterior
B
0 min
20 min
40 min
60 min
mys XG43

Figure 2.9
A polarized fibrillar Collagen IV matrix is built during follicle rotation.

(**A**) 76μm maximal projection of the Collagen IV matrix (green) revolved around the y-axis reveals circumferentially oriented fibrils around the A-P axis. (**B**) Maximal projection of sagittal cross sections shows that the Collagen IV matrix (green) peaks in relative abundance during follicle rotation stages, quantified in (**C**). Representative images of Collagen IV-GFP (**D-H**) and rose diagrams below (**I**) reveal that Collagen fibrils orient perpendicular to the A-P axis during the rotation phase. (**J-K**) Collagen fibrils reach maximal length (**J**) and density (**K**) at stage 8. Scale bar in (**A**) 25 μm; (**B**) 100 μm; (**D-H**) 5 μm.

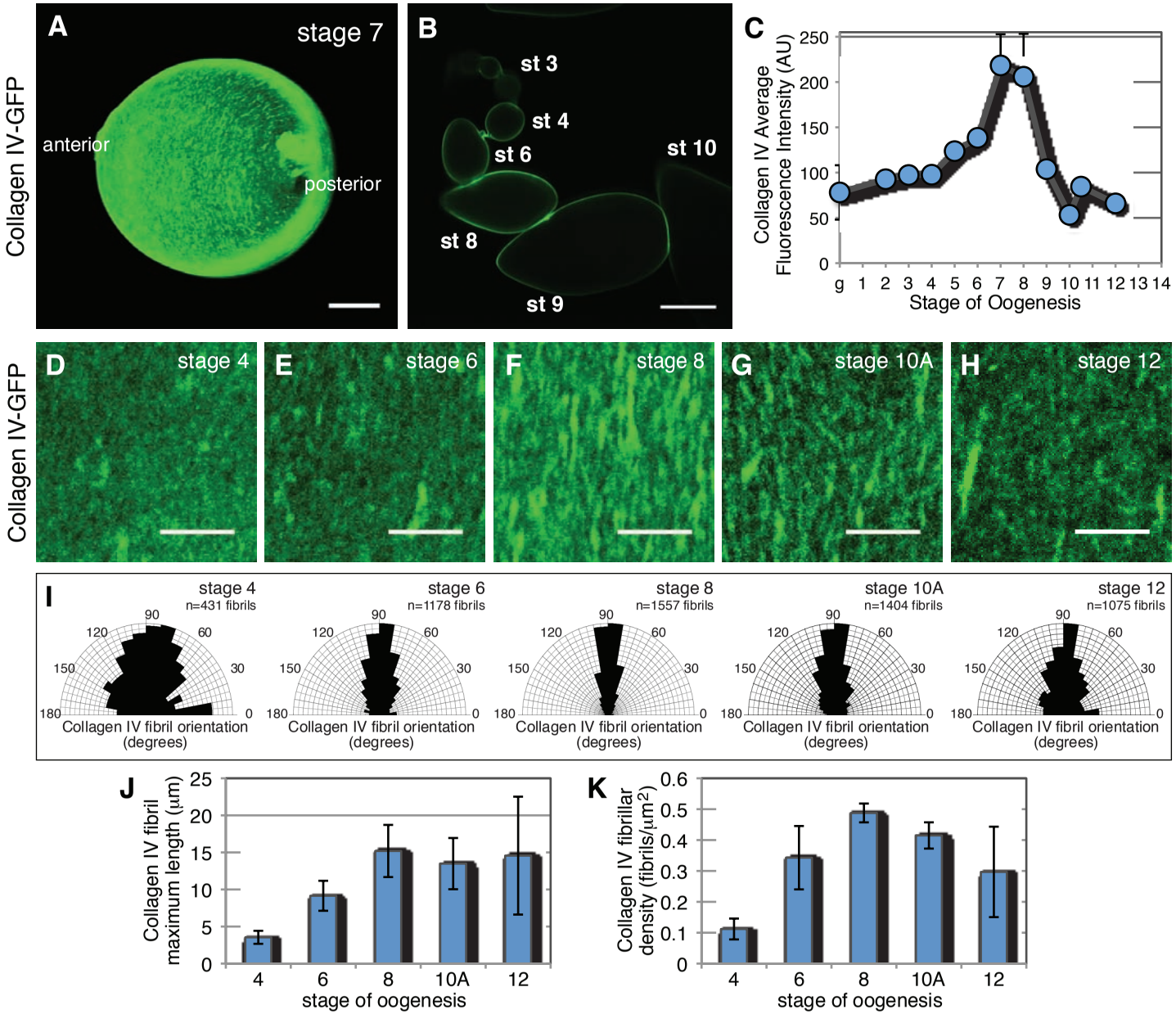
A
stage 7
anterior
posterior
Collagen IV-GFP
B
st 3
st 4
st 6
st 10
st 8
st 9
C
Collagen IV Average Fluorescence Intensity (AU)
250
200
150
100
50
0
g 1 2 3 4 5 6 7 8 9 10 11 12 13 14
Stage of Oogenesis
Collagen IV-GFP
D
stage 4
E
stage 6
F
stage 8
G
stage 10A
H
stage 12
I
stage 4
n=431 fibrils
stage 6
n=1178 fibrils
stage 8
n=1557 fibrils
stage 10A
n=1404 fibrils
stage 12
n=1075 fibrils
90
120
60
150
30
180
0
Collagen IV fibril orientation (degrees)
J
Collagen IV fibril maximum length (μm)
25
20
15
10
5
0
4
6
8
10A
12
stage of oogenesis
K
Collagen IV fibrillar density (fibrils/μm2)
0.6
0.5
0.4
0.3
0.2
0.1
0
4
6
8
10A
12
stage of oogenesis

Figure 2.10
Polarized global tissue rotation builds a polarized Collagen IV fibrillar matrix.

(**A**) Collagen IV-GFP fibrils (arrows) can span multiple cells (red) in stage 8 follicles. (**B**) Strategy used to create RFP-marked follicle cells producing Collagen IV-GFP in genetic mosaics. (**C-D**) RFP-positive follicle cells distributed across the A-P axis (**C**) produce a uniform distribution of Collagen IV-GFP fibrils, while RFP-positive follicle cells restricted to the posterior of the follicle (**D**) produce labeled fibrils only in the posterior. Scale bar in (**A**) 5 μm; **(C-D**)25 μm.

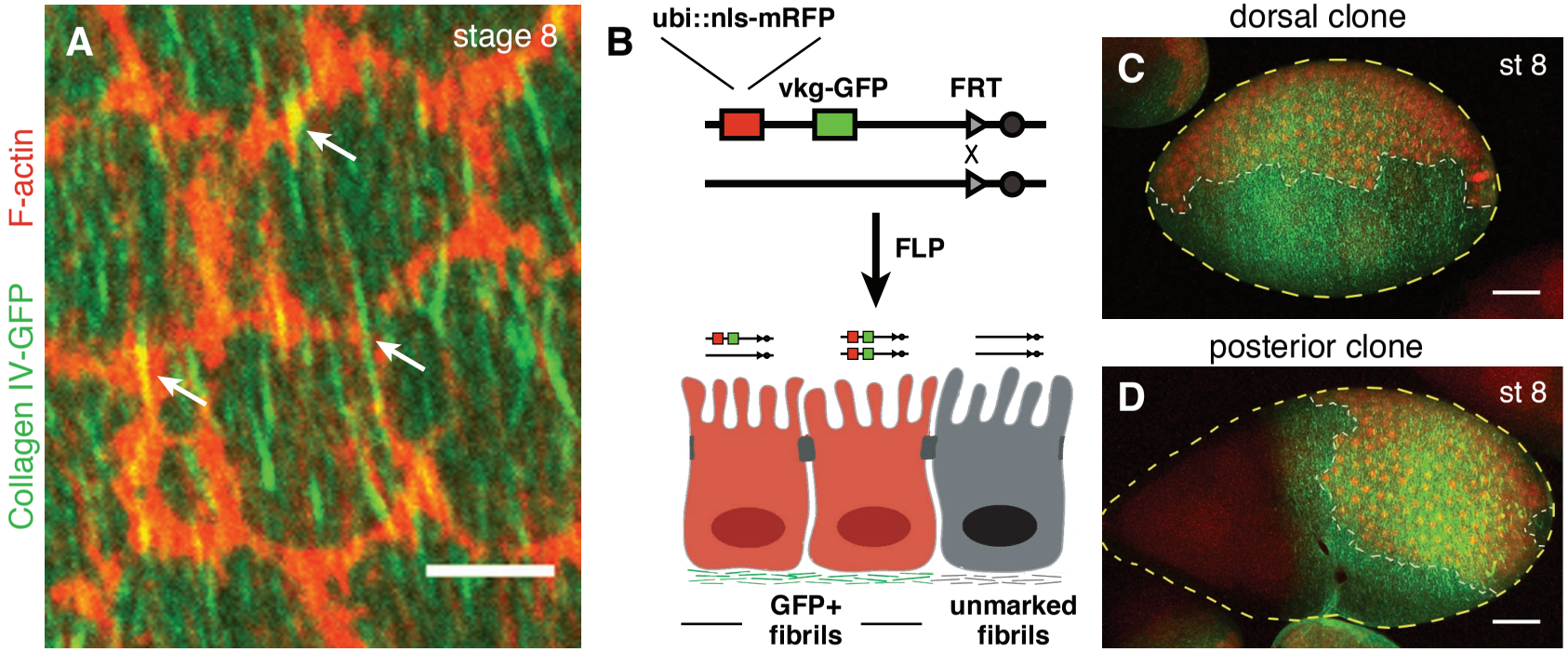
A
stage 8
F-actin
Collagen IV-GFP
B
ubi::nls-mRFP
vkg-GFP
FRT
X
FLP
GFP+
fibrils
unmarked
fibrils
dorsal clone
C
st 8
posterior clone
D
st 8

Figure 2.11
Elongated follicles treated with Collagenase, but not Latrunculin A, show gross defects in follicle shape.

(**A-D**) Acute drug treatment of elongated stage 12 follicles for 60 min. Collagenase (**B**) but not Latrunculin A (**D**) perturbs follicle shape compared to their respective controls (**A,C**), quantified in (**E**). Triple asterisks indicate P<<0.001. Scale bar in (**A-D**) 100 μm.

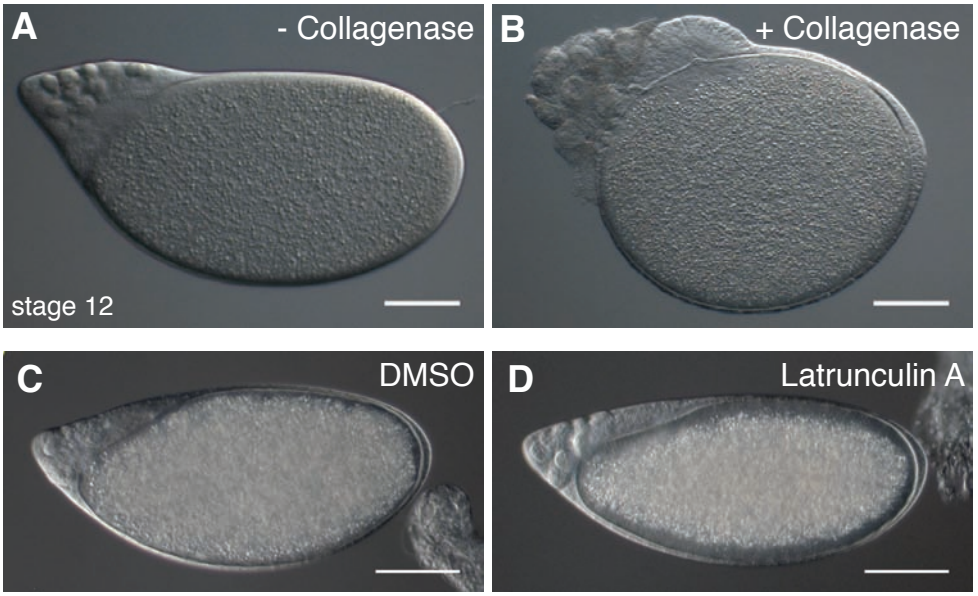
A
- Collagenase
stage 12
B
+ Collagenase
C
DMSO
D
Latrunculin A

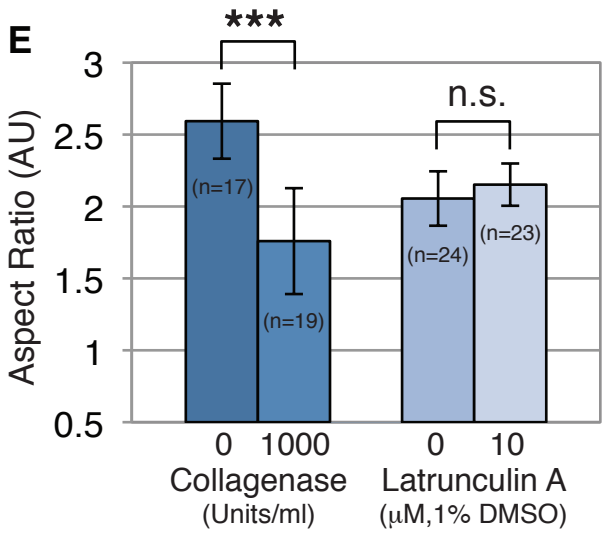
E
***
n.s.
Aspect Ratio (AU)
3
2.5
2
1.5
1
0.5
(n=17)
(n=19)
(n=24)
(n=23)
0
1000
Collagenase
(Units/ml)
0
10
Latrunculin A
(μM,1% DMSO)

Figure 2.12
A polarized fibrillar Collagen IV matrix is required to maintain follicle shape.

Midsagittal (**A-C**) and basal surface views (**A'-C"**) of stage 12 follicles treated with DMSO, Latrunculin A or Collagenase. Collagen IV-GFP (green) is intact in control (**A"**) or Latrunculin A treated follicles (**B"**), but is severely lost in Collagenase treated follicles (**C"**). In contrast, actin stress fibers (red) are severely lost at the follicle epithelium basal surface in Latrunculin A treated follicles (**B'**) compared to controls (**A'**). Actin stress fibers aggregate to cell peripheries upon exposure to Collagenase, concomitant with an alteration in cell shape (**C'**). Scale bar in (**A-C'**) 10 μm.

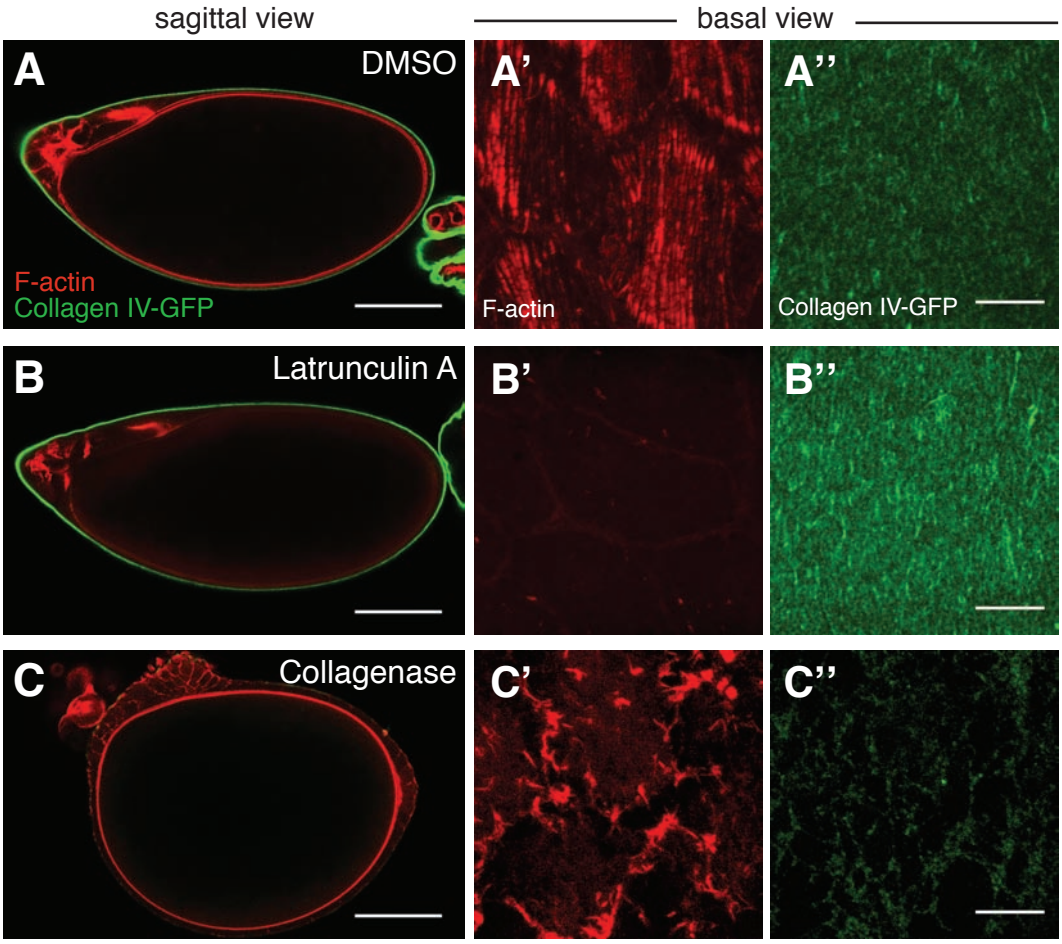
sagittal view
basal view
A
DMSO
F-actin
Collagen IV-GFP
A'
F-actin
A''
Collagen IV-GFP
B
Latrunculin A
B'
B''
C
Collagenase
C'
C''

Figure 2.13
***vkg* is required for the maintenance of polarized Perlecan fibrils and basement membrane integrity.**

(**A-D**) The Perlecan fibrillar matrix (green) is present in WT shaped stage 7 *vkg* mutant follicles (**B'**) but is lost at stage 8 when shape deviates from WT (**D'**) compared to controls (**A', C'**). (Scale bar in (**A-D**) 25μm; (**A'-D'**) 3 μm.

stage 7
stage 8
A
ubi::mRFP
A'
B
vkg ICO
B'
C
ubi::mRFP
C'
D
vkg ICO
D'
wild type cells
Perlecan-GFP

Figure 2.14
Polarized follicle rotation is required to build the polarized, fibrillar Collagen IV matrix to maintain follicle shape.

(**A-B**) The Collagen IV matrix (green) is present but disorganized in round *mys* mutant follicles (**B**) compared to a control genotype (A). (**C-D**) Rose diagrams plotting Collagen fibril orientation shows that Collagen IV polarity is completely lost in *mys* mutant follicles. Fibrils normally elongated in WT (**E**) fail to elongate in *mys* mutants (**F**); largest fibril shapes quantitated in (**G**). Double asterisks indicate $P<0.01$. Scale bar in (**A-B**) 10 μm; (**E-F**) 3 μm.

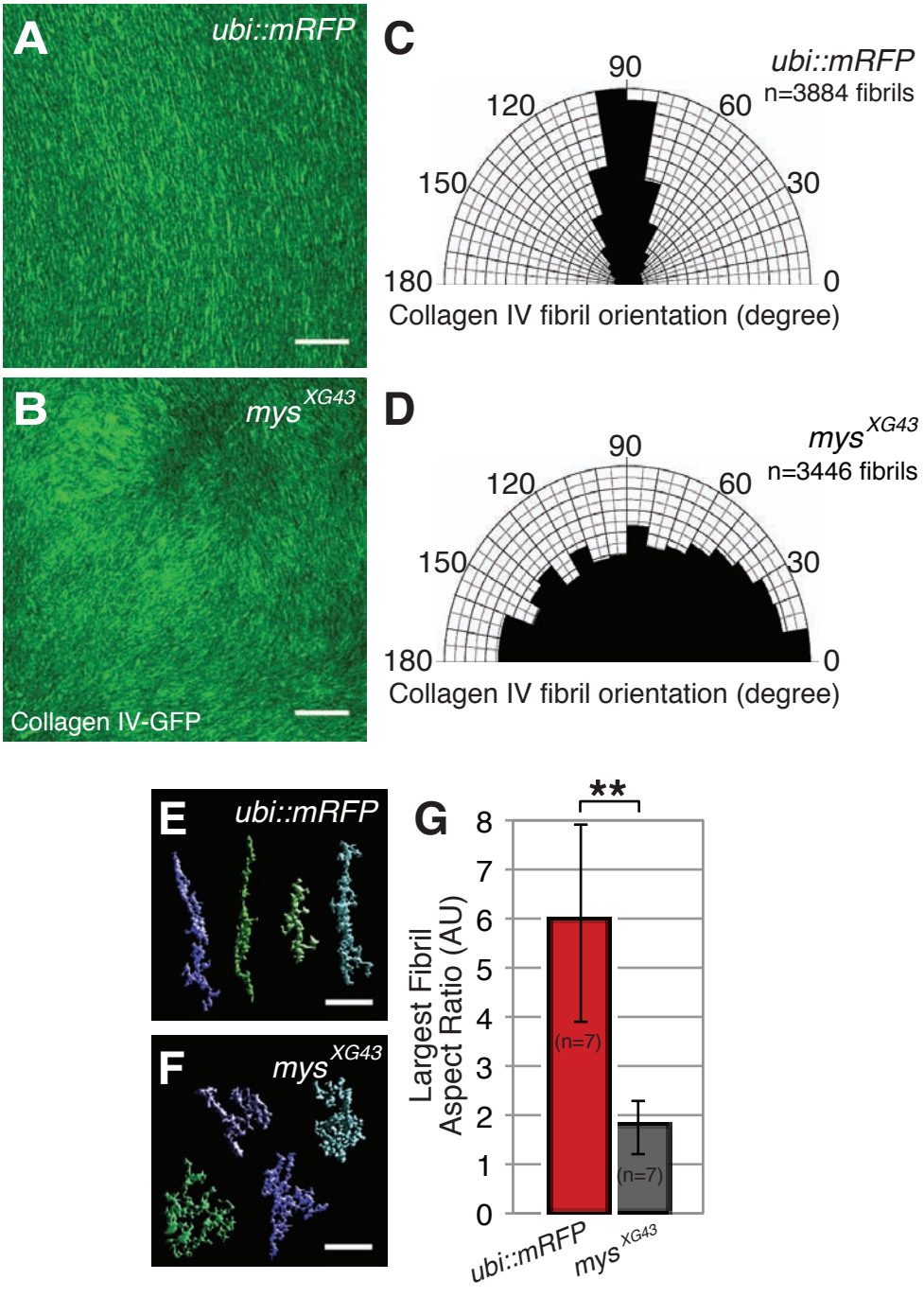
A
ubi::mRFP
B
mys XG43
Collagen IV-GFP
C
ubi::mRFP
n=3884 fibrils
90
120
60
150
30
180
0
Collagen IV fibril orientation (degree)
D
mys XG43
n=3446 fibrils
90
120
60
150
30
180
0
Collagen IV fibril orientation (degree)
E
ubi::mRFP
F
mys XG43
G
**
Largest Fibril Aspect Ratio (AU)
0
1
2
3
4
5
6
7
8
(n=7)
(n=7)
ubi::mRFP
mys XG43

Figure 2.15
Polarized Perlecan fibrils cannot be deposited into mutant clone territories in *mys* mosaic follicles.

(**A**) Strategy to create RFP-marked follicle cells producing Perlecan-GFP in genetic mosaics. (**B-C**) Polarized Perlecan-GFP fibrils are deposited into the matrix overlying unmarked domains in WT control clones (**B'**) but are not deposited into the matrix overlying *mys* mutant mosaic clones (**C'**, asterisk) and are misoriented in the rest of the follicle. Scale bar in (**B-C**) 10 μm.

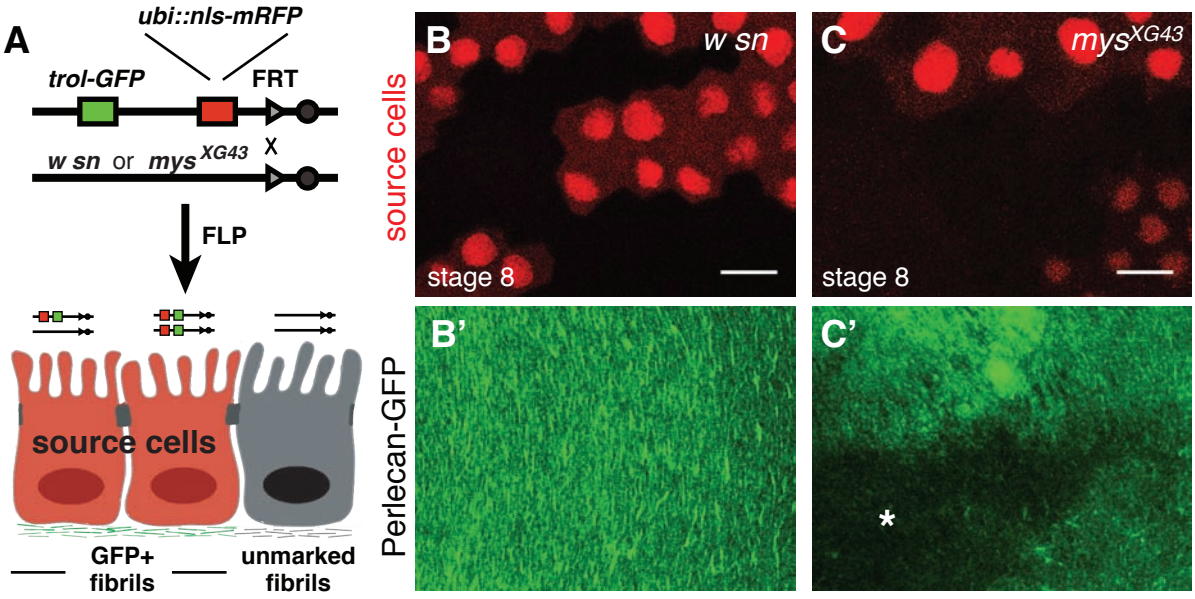
A
ubi::nls-mRFP
trol-GFP
FRT
w sn or mys XG43
X
FLP
source cells
GFP+ fibrils
unmarked fibrils
source cells
Perlecan-GFP
B
w sn
stage 8
C
mys XG43
stage 8
B'
C'
*

Figure 2.16
Microfilament orientation correlates with polarized follicle rotation.

(**A-B**) F-actin (red in (**A**), white in (**A'**)) aggregates to the periphery of *mys* mutant follicle cells (arrow), revealing defective focal complex formation. Neighboring WT cells (green in (**A)**) maintain intact polarized stress fibers but lose their global tissue polarity. White lines indicate stress fiber orientation of WT cells in (**A**). (**B-C**) F actin tissue polarity is generally maintained in WT shaped stage 7 *vkg* mutant follicles (**B**) but is lost at stage 8 when the majority of *vkg* mutant follicles fail to rotate (**C**). Scale bar in (**A-C**) 10 μm.

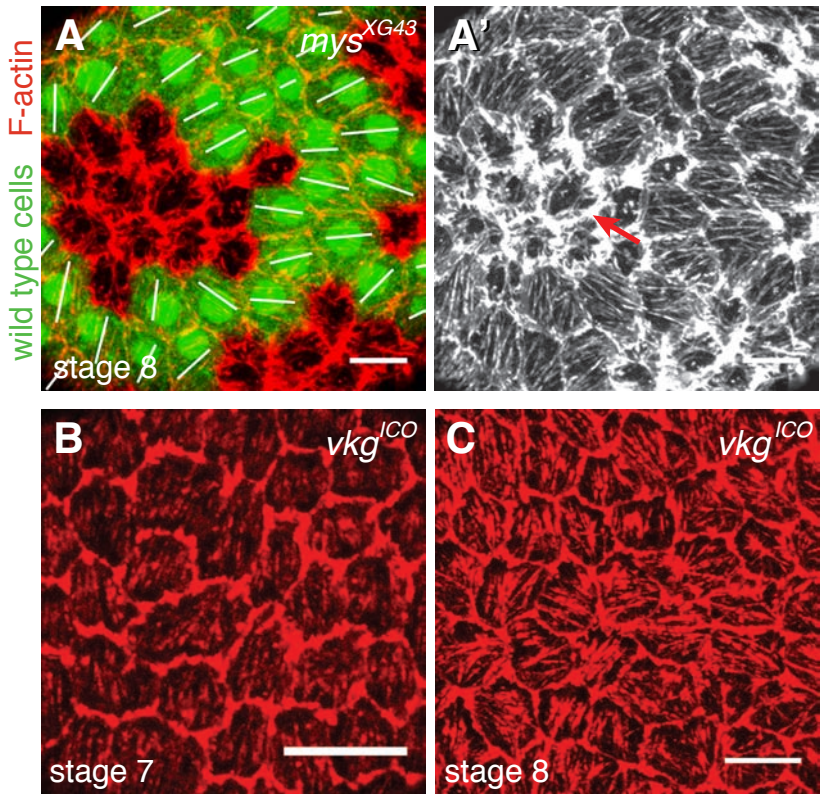
A
mys XG43
A'
wild type cells
F-actin
stage 8
B
vkg ICO
stage 7
C
vkg ICO
stage 8

Figure 2.17
Model for the function of global tissue rotation in the control of *Drosophila* egg elongation.

(**A**) Polarized global tissue rotations around the elongating A-P axis, mediated by coordinated migration of the follicle cells over the ECM substratum, build polarized fibrils of ECM including Collagen IV (green). The anisotropic tensile strength of the polarized Collagen IV fibrillar network acts as a 'molecular corset' to promote elongation of the growing egg, and maintain its ellipsoid shape once elongation and growth are complete at stage 12. (**B**) When follicles fail to undergo polarized rotation, ECM fibrils are misoriented, leading to isotropic growth during oogenesis and production of a mature round egg.

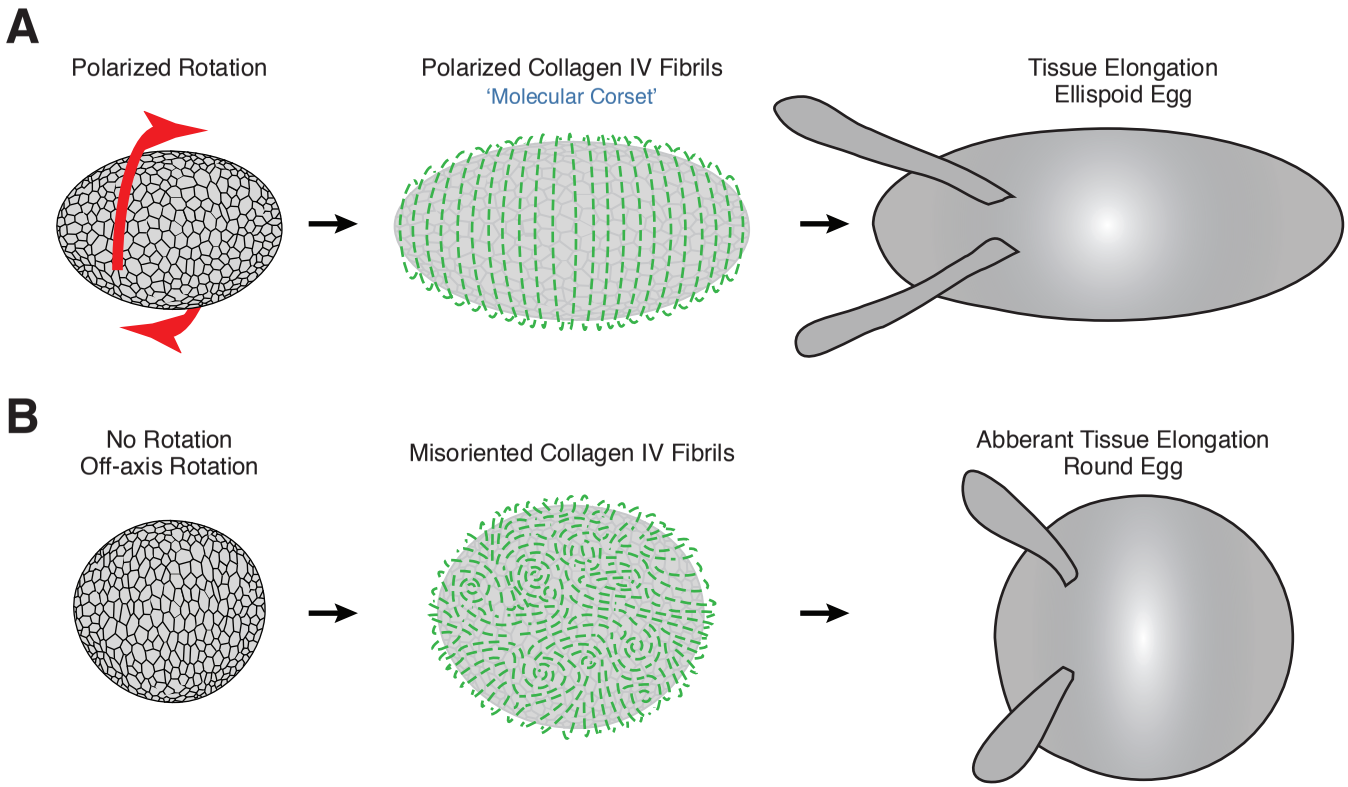
A
Polarized Rotation
Polarized Collagen IV Fibrils
'Molecular Corset'
Tissue Elongation
Ellispoid Egg
B
No Rotation
Off-axis Rotation
Misoriented Collagen IV Fibrils
Abberant Tissue Elongation
Round Egg

Figure 2.18
Working model for genetic regulation of planar cell polarity in the wing epithelium versus the follicle epithelium in *Drosophila*.

(**A**) The wing epithelium is thought to use a signaling cascade comprised of 3 genetic modules. The global module includes the atypical cadherins Fat and Dachsous, and the golgi kinase Four-jointed to orient tissue polarity with the body axes. A core PCP signaling module comprised of Frizzled, Dishevelled and others are thought o generate cellular asymmetry within individual cells and propagate local polarity information. These two modules are thought to act sequentially or in parallel to regulate the tissue specific module to affect morphological polarization, in this case a distal growth of a hair on the apical domain of each wing epithelial cell. In contrast, the follicle epithelium (**B**) uses the atypical cadherin Fat2 and cell-matrix genes to establish global tissue polarity and generate cellular asymmetries by propagating planar information using a biomechanical mechanism through global tissue rotation. Cross talk between the follicle cells and a polarized ECM output enables rapid amplification of cellular asymmetries across the entire epithelium. It remains unclear how Fat2 and the cell-matrix genes interact (genetically and molecularly) to regulate follicle PCP and egg shape, though both do have an effect on the morphological output of polarization of the Collagen IV matrix (see Chapter 3). (**A**) from (Axelrod, 2009).

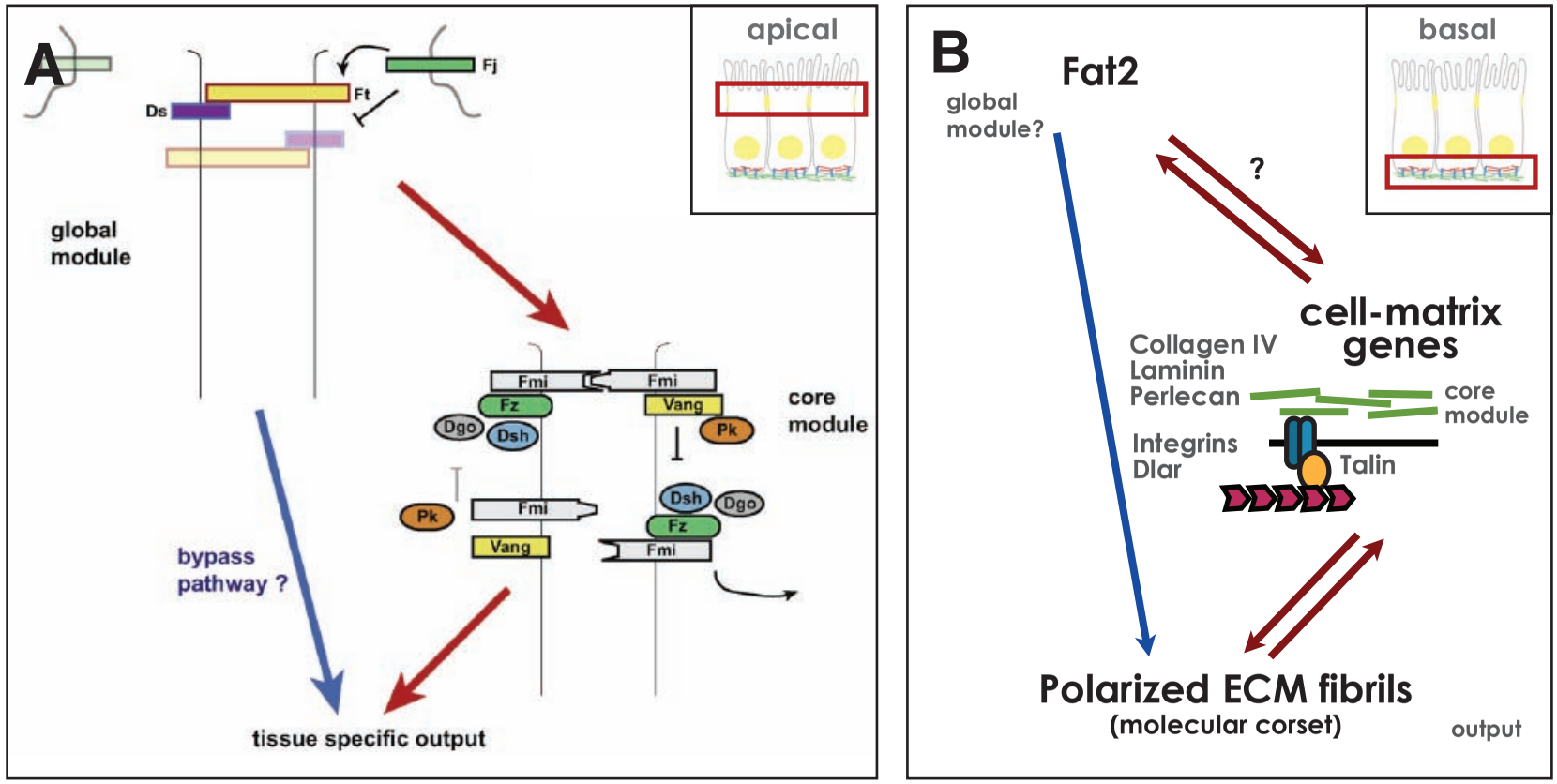
A
apical
Fj
Ft
Ds
global
module
Fmi
Fmi
Fz
Vang
Dgo
Dsh
Pk
core
module
Pk
Fmi
Dsh
Dgo
Fz
Vang
Fmi
bypass
pathway ?
tissue specific output
B
Fat2
global
module?
?
basal
cell-matrix
genes
Collagen IV
Laminin
Perlecan
core
module
Integrins
Dlar
Talin
Polarized ECM fibrils
(molecular corset)
output

Chapter 3

Furthering our understanding of
the cellular basis of *Drosophila* egg elongation

3.1 Abstract

The discovery of global tissue rotation to build a polarized extracellular matrix (ECM) to constrain tissue shape in the *Drosophila* follicle provides interesting novel insights to the mechanisms of morphogenesis, but also results in a conundrum. Tissue elongation thus far is known to occur through polarized changes in cell shape or cell neighbors when cell division is absent in the tissue, suggesting that these behaviors also occur during the rotation phase of follicle elongation and may contribute to total tissue elongation. Moreover, our mutant analysis from Chapter 2 indicates that global tissue rotation is the primary, but not only, behavior that accounts of elongation of the developing egg. To identify additional behaviors involved in the control of egg elongation, we performed morphometric analysis of living and fixed egg chambers and continued to characterize additional known round egg mutants. Surprisingly, live imaging analysis or preliminary morphometric analysis from fixed samples did not reveal obvious changes in polarized cell shape changes or cell intercalation. Our early studies may have been limited by our inability to resolve behaviors at the poles or by our inability to fully recapitulate follicle growth during live imaging. Improvements in techniques have been made more recently and are discussed for future studies. In addition, preliminary characterization of other known round egg mutants, *rhea/talin*, *Dpak, bola/Dlar* and *kugelei/fat2*, indicate that these genes may also be required for polarized global tissue rotation and for formation of a polarized ECM corset. Thus, identification of novel genes through continued screening strategies may help uncover additional behaviors that provide us with a better understanding of the cellular basis of egg elongation.

3.2 Introduction

The *Drosophila* follicle provides an interesting model tissue to study elongation, given its geometric topology as a closed chamber. Despite the discovery of polarized global tissue rotation and the emergence of a polarized ECM matrix to shape the follicle as a growing ellipsoid in Chapter 2, it remains unclear how follicle cells respond to this mechanical constraint during tissue elongation. A dogma within the morphogenesis community is that tissue elongation occurs through polarized cell shape changes and/or polarized cell intercalation (Blanchard et al., 2009). Whether these morphogenetic behaviors also occur and contribute to follicle elongation has not been determined. Our *mys* and *vkg* mutant data shown in Chapter 2 suggests that there are additional cellular mechanisms regulating *Drosophila* egg elongation, as both mutants showed wild type elongation rates during mid-oogenesis. In efforts to begin identifying additional morphogenetic behaviors controlling follicle elongation, morphometric analysis and further characterization of published round egg mutants were performed to better understand the cellular basis of elongation in this tissue.

3.3 Results

3.3.1 Live imaging reveals little change in cell neighbor relations during the rotation phase of follicle elongation

To determine whether polarized cell shape changes or cell intercalation occur during follicle rotation, we performed single and collective cell analysis of wild type follicles undergoing rotation. Qualitatively, there was limited evidence for changes in cell shape occurring during live imaging. Some evidence pointed towards the presence of cell intercalation, as transitory 4-cell T2 junctions typically found in intercalating epithelia of the germband (Bertet et al., 2004) were evident in fixed and live samples (Figure 3.1, A-A'). However, tracking individual cells to identify a true cell intercalation event, defined by a polarized type 1 to type 2 to type 3 junction transition (also known as T1 and T2 processes) (Bertet et al., 2004; Zallen and Zallen, 2004), revealed no obvious intercalation event in all cells tracked thus far. Partial type 1 to type 2 or partial type 2 to type 3 junction transitions were observed (Figure 3.1), indicative of junction disassembly or reassembly occurring in follicle cells, like that seen in the pupal wing morphogenesis (Classen et al., 2005). However, whether these junction transitions indicate polarized cell neighbor exchange was not clear from our live studies thus far.

3.3.2 Morphometric analysis of fixed specimens from the elongation phase also indicate limited changes in cell shape or cell neighbor exchange

The challenges in identifying cell shape or cell neighbor exchanges occurring during live imaging led us to address the question using morphometric analysis of fixed samples, which have been performed on other tissues undergoing elongation (Zallen and Zallen, 2004). One indication that cell intercalation has occurred in the *Drosophila* follicle may be to assess the relative number of follicle cells that occupy the planes comprising the maximal A-P length and maximal D-V length of each follicle (Figure 3.2, B). If relative shifts in follicle cell number occur from the maximal D-V plane to the maximal A-P plane (in the absence of cell division)

between two stages, then this indicates cell rearrangements must have occurred to account for the redistribution of cells and elongation of the tissue between those two stages.

Before performing this morphometric analysis, an *in silico* screen was performed amongst the GFP protein trap lines available in the Flytrap collection (Buszczak et al., 2007; Kelso et al., 2004; Morin et al., 2001; Quinones-Coello et al., 2007) to identify a marker of follicle cell nuclei that did not express in germline nuclei. This characteristic was important for post-imaging morphometric analysis using 3D/4D image analysis software. This led to the identification of a GFP protein trap in *CG10927* as a new marker of follicle cell nuclei (Figure 3.2, A). Using CG10927-GFP, follicles from stage 6 to stage 8 were analyzed for follicle cell numbers in the maximal A-P and D-V planes, and a subset of these follicles was analyzed for total follicle cell number. The results were ambiguous from independent experimental sets (Figure 3.2, C-D). While subtle changes in follicle cell number were seen between the two axes from stage 6 to 8, it remains unclear whether this is due to changes in cell rearrangement, incomplete cessation of follicle cell proliferation of stage 6 follicles analyzed, or within the biological variation of follicle cell distribution in stage 6 to stage 8 follicles. There were on average more follicle cells along the maximal A-P plane in stage 8 follicles compared to stage 6 or 7 follicles in independent experiments (from 5-15 cells), but the number of follicle cells in the maximal D-V plane were within a similar range between stage 6 and stage 8 follicles (Figure 3.2, C). Moreover, this study was confounded by using stage 6 follicles that had not ceased follicle cell proliferation completely, so some of these changes may be accounted for by an increase in cell number that resulted in increasing follicle cell number along the A-P axis. However, the few follicle cell divisions documented during my dissertation indicates that cell divisions are not always aligned with the elongating A-P axis (data not shown), so it is unclear whether oriented cell divisions can account for the follicle cell distributions observed from this analysis.

Another hallmark of intercalating tissues is an increase in variance in epithelial topology (Zallen and Zallen, 2004). Cellular topology can be defined by a statistical distribution in the frequency of n-sided cells observed in an epithelium. A typical static epithelium has a normal distribution around hexagonal cells, ranging from 5 to 7-sided cells and 67% of the epithelium having hexagonal shapes, as seen in stage 6 embryos prior to germband extension. However, during germband extension, the epithelium diverges from this distribution, resulting in a topology ranging from 3 to 8-sided cells, with only 38% of the cells having a hexagonal shape (Zallen and Zallen, 2004). Examination of the lateral region of stage 6 and stage 8 egg chambers (Figure 3.3, A-B') indicates that the follicle epithelium maintains a fairly normal distribution around hexagons, though a very small fraction (3%) of cells contact 8 neighbors by stage 8 (Figure 3.3, C-D), indicating possible shifts in cell neighbors occurring at this time. However, variance in epithelial topology can also occur from proliferating cells (Gibson et al., 2006), and given that stage 6 follicles analyzed have not completed follicle cell proliferation, it may be possible that this subtle shift in epithelial topology distribution is due to follicle cell proliferation.

Given the data thus far showing limited support for polarized cell intercalation, we next assessed whether polarized cell shape changes may be occurring during the rotation phase of follicle elongation. Individual follicle cells were outlined to measure the length of the major and minor axis of each cell, and to quantify cell orientation by plotting the orientation of the major axis of each follicle cell relative to the egg chamber A-P axis in rose diagrams (Appendix A). This

analysis revealed that follicle cells are elongating during stage 6 to 8 (Figure 3.3, E, G), and while cell orientation of the major axis of most cells is oriented along the circumferential axis at stage 6 (Figure 3.3, F), follicle cells shift their long axis orientation towards the A-P axis by stage 8 (Figure 3.3, H). As follicle cells increase their basal surface substantially between these stages (Figure 3.3, I), it indicates that individual follicle cell growth may be biased towards the A-P axis. However, whether these shifts are sufficient to account for the approximately 40% elongation that is occurring between these two stages has yet to be determined and may require mathematical modeling to answer this question.

3.3.3 Improvements in follicle imaging resolution can identify potential behaviors occurring at the poles

One possibility to explain our limited detection of cell shape changes and cell intercalation in the lateral region of elongating follicles is that the additional morphometric behaviors we seek to identify may be occurring at the follicle termini, which have been difficult to image with enough resolution until very recently. 4D time-lapse imaging of polarized follicle rotation provided clear documentation of the phenomenon, but provided poor z-resolution to analyze individual cells, particularly at the poles. Recent acquisition of new laser scanning confocal microscopes with improved scanning resolution and speed have enabled acquisition of high resolution images of stage 5 to stage 8 follicles for further morphometric analysis (Figure 3.4). However, morphometric analysis on these samples has yet to be performed.

3.3.4 rhea/talin mutants share similar phenotypes to *myospheroid/integrin βPS* mutants in egg shape morphogenesis

Another approach taken to identify additional morphogenetic behaviors involved in *Drosophila* follicle elongation was to further characterize published round egg mutants, identifying their period of requirement during oogenesis and analyzing their effects on global tissue rotation and polarization of the Collagen IV matrix. Preliminary results from four of these genes are presented below.

rhea/talin encodes a critical component of focal adhesions that links integrin receptors to the actin cytoskeleton (Nayal et al., 2004). Talin was first implicated in *Drosophila* oogenesis due to its role in regulating oocyte positioning during follicle formation in the germarium by regulating cadherin-transcription in an integrin-independent manner (Becam et al., 2005). This report also indicated that later during oogenesis, Talin can affect basal actin filament organization and lead to the production of round eggs (Becam et al., 2005), but no further characterization was made.

We first asked when *rhea* is required for egg shape. Examination of tissue mosaics for follicle cells carrying homozygous mutations of the null allele $rhea^{79a}$ (Brown et al., 2002) indicate that *rhea* mutants can yield round follicles as early as stage 6 (Figure 3.5, A; data not shown). How early this shape defect occurs is yet to be determined. In addition, *rhea* mutant follicles exhibit multilayering of follicle cells at poles and misoriented follicles, like that seen in *mys* mutant follicles. While mutations in *rhea* can result in oocyte mispositioning in young follicles (Becam et al., 2005), *rhea* seems to phenocopy *mys* in its temporal requirement for follicle shape during the rotation phase of oogenesis. Therefore, we next examined whether *rhea* mutants are capable

of polarized follicle rotation. We found that *rhea* mutant round follicles undergo off-axis rotation in the majority of samples from the four time-lapses taken thus far (Figure 3.5, B). We failed to see a complete block in follicle rotation as seen in *mys* mutant follicles. Next, we examined the organization of the Collagen IV matrix and actin cytoskeleton in round *rhea* mutants and found that both structures have off-axis polarization (Figure 3.5, A'-A"), consistent with the rotation defect seen from live imaging. In samples where clonal analysis could be made, it appears that *rhea* has a cell-autonomous defect in F-actin organization, aggregating to the periphery or showing aberrant aggregation of F-actin at cell edges (Figure 3.5, C arrow). Neighboring wild type cells, however, maintain polarized basal actin filaments and exhibit local tissue polarity alignment. The sample for this clonal analysis exhibited wild type shape, so no obvious loss of global tissue polarity has been observed so far in *rhea* mutant follicles. In summary, *rhea* appears to phenocopy *mys* in many respects, and the difference in off-axis rotation seen in the majority of *rhea* mutants may have to do with mutant clone size using different FRT chromosomes, although this has yet to be formally tested. Thus, Talin likely plays a critical role in facilitating linkage between integrins and the actin cytoskeleton to coordinate polarized global rotation and formation of the polarized Collagen IV matrix.

3.3.5 Mutations in dpak can affect polarized Collagen IV fibrillogenesis

p21-activated kinase (Pak) is a serine/threonine protein kinase known to interact with the small GTPases Rac and Cdc42 to regulate the structure of the actin cytoskeleton to control many cellular processes, including cell motility and morphogenesis (Szczepanowska, 2009). *Drosophila* Pak (dPak) was first implicated in the control of egg shape from an observation that females transheterozygous for strong *dpak* hypomorphic mutations resulted in female sterility. Analysis during oogenesis indicated these *dpak* mutants yield round follicles, follicle cell multilayering and invasion into the germline, with subsequent degeneration of these mutants prior to formation of a mature egg (Conder et al., 2007). Clonal analysis revealed that dPak is required to assemble basal actin filaments and have a non-autonomous effect on F-actin polarity in neighboring wild type cells (Conder et al., 2007).

Given the similarities in phenotypes observed with *mys* and *rhea*, we characterized $dpak^{6}/dpak^{11}$ transheterozygotes for their effect on Collagen IV polarity and fibrillogenesis. We confirmed that *dpak* hypomorphic transheterozygotes can yield round follicles, with most follicles show additional phenotypes including severe follicle cell multilayering and germline invasion, though a small minority have only mild defects in follicle shape (Figure 3.6, A-B). Examination of Collagen IV-GFP in these mutants indicated compromised Collagen IV polarity and fibrillogenesis, as round *dpak* mutants failed to show elongate oriented Collagen IV fibrils at stage 6 (Figure 3.6, C-C'). Moreover, this allelic combination seemed to have less severe effects on basal F-actin assembly as most mutant cells showed individual actin filament polarity but loss of global tissue polarity (Figure 3.6, C"). In contrast, more elongate $dpak^{6}/dpak^{11}$ mutants showed polarized Collagen IV fibrils and approximately wild type organization of basal F-actin and monopolar protrusions (Figure 3.5, D-D"). These data suggest that *dpak* is also involved in the genetic regulatory network regulating global tissue rotation and ECM fibrillogenesis, though direct analysis of these mutants for follicle rotation has yet to be made.

3.3.6 bola/Dlar may have limited effects on polarized ECM fibrillogenesis

Leukocyte antigen related (Lar) is a receptor-like tyrosine phosphatase that was initially shown to be involved in regulating the actin cytoskeleton of the developing nervous system in *Drosophila* embryos but also found to exhibit partial female sterile phenotypes (Bateman et al., 2001; Frydman and Spradling, 2001). Homozygous mutant females bearing a molecular null allele of *dlar* show variable penetrance in affecting egg shape – with 14-70% of mutants having an effect on follicle shape from mid-late oogenesis. Quantification of follicle aspect ratio suggest that *dlar* mutants show an initial defect around stage 7-8, though this an estimate since absolute follicle dimensions were used rather than stage of oogenesis in the report (Bateman et al., 2001). Thus, *dlar* may exhibit phenotypes on follicle rotation and ECM fibrillogenesis more similar to *vkg*, given its apparent later defect in follicle shape.

However, analysis of *dlar* mutants was difficult given its very low penetrance in our hands. We were not able to recover round *dlar* mutant follicles to assess polarized follicle rotation; however, one round mutant follicle was recovered to analyze *dlar*'s effect on Perlecan fibrillogenesis. Perlecan-GFP appeared to localize normally to the follicle basement membrane and showed generally polarized Perlecan fibrils, though not completely wild type in organization. Likewise, basal actin polarity seemed generally circumferentially polarized around the A-P axis, though aberrations in basal F-actin protrusion orientation was apparent in a subset of mutant follicle cells. These phenotypes resemble a similar breakdown occurring in basal F-actin and Perlecan fibril integrity of stage 7 *vkg* mutants. Further characterization of the temporal requirement of *dlar* and additional recovery of round mutant follicles for analysis of Perlecan matrix organization and integrity can help elucidate whether Dlar may play a role in maintaining ECM integrity with Collagen IV.

3.3.7 kugelei/fat2 show similar and unique defects in polarized Collagen IV fibrillogenesis

Recently, Fat2 has been identified to be the first gene involved in follicle planar cell polarity (PCP) and egg shape that is not a known component of cell-matrix interactions (Viktorinova et al., 2009; Viktorinova et al., 2011). *kugelei/fat2* appears to have a high penetrance in regulating follicle and egg shape, and like the cell-matrix proteins, Fat2 is thought to be localized at the basal surface of the follicular epithelium using a Fat2-GFP transgene to infer subcellular localization. Fat2-GFP in wild type mosaic follicles shows monopolar enrichment on dorsal or ventral faces of the basal surface, like that seen for actin-based protrusions. *fat2* mutants show no defect in individual follicle cell polarization of basal actin filaments but lack global tissue polarity, suggesting it may act as a global regulator of follicle PCP (Viktorinova et al., 2011) rather than generating the cellular asymmetries necessary for polarized follicle rotation, as seen from cell-autonomous defects of cell-matrix genes in tissue mosaics (Figure 2.16, 3.5). However, *fat2* mutant follicles appear to exhibit bipolar actin protrusions not discussed in the original report (Viktorinova et al., 2009), suggesting further characterization of *fat2* in the control of egg shape is necessary to better understand its function.

Preliminary analysis in our lab suggest that *fat2* may be required during the rotation phase of elongation (L. Yuan, unpublished observations). This suggests *fat2* may have effects on global tissue rotation and Collagen IV fibrillogenesis. Examination of Collagen IV-GFP in a $fat2^{103C}$ (Viktorinova et al., 2009) homozygous mutant background revealed that follicle shape was not as

severely affected as equivalent stage *mys* mutants (compare Figure 3.8, A to Figure 2.5), but a similar defect in polarized Collagen IV fibrillogenesis was seen (Figure 3.8, A'). Moreover, basal actin filaments were present, but not coordinately polarized across the whole tissue (Figure 3.8, A"). By stage 8, *fat2* mutants exhibited a clear defect in follicle shape and showed global defects in Collagen fibril orientation. Moreover, these *fat2* mutant follicles also exhibited aberrant Collagen IV-GFP aggregations that appeared to correspond to basal and basolateral follicle cell membranes (Figure 3.8, C-C"; data not shown). These results suggest that one potential role Fat2 may have is to help organize Collagen IV fibrillogenesis properly into the follicle basement membrane, and its loss can result in aberrant Collagen IV assembly at cell peripheries.

3.4 Discussion

3.4.1 The potential wealth of information from morphometric analysis of the elongating follicle

We have a strong desire to better understand the cellular response of the follicle epithelium during the rotation phase of elongation. The follicle epithelium must continue to grow anisotropically by exhibiting a net elongation of the entire epithelium under a mechanical constraint of a circumferentially polarized ECM. Whether this net anisotropic growth is due to polarized cell elongation of individual follicle cells or due to polarized cell rearrangements, and at earlier stages, due to oriented cell divisions, is not yet clear.

Preliminary analysis indicates that the follicle epithelium shares some hallmarks of cell intercalation. The presence of transitory 4-cell vertex type 2 junctions, which is thought to be an unstable but necessary configuration of epithelial cells undergoing neighbor exchange (Zallen and Zallen, 2004) and the emergence of a slight increase in variance in epithelial topology at stage 8 with some 8-sided cells suggested a low frequency of local cell rearrangements may be occurring in the lateral region of the follicle. However, proliferating epithelia also exhibit these hallmarks (Farhadifar et al., 2007; Gibson et al., 2006), so additional analysis is needed to resolve these ambiguities.

Of greater promise is the evidence that polarized cell shape changes within the follicle epithelium may be biased towards the elongating A-P axis during the rotation phase of follicle elongation. While increased sample size and statistics will increase the confidence of these preliminary results, a mathematical modeling approach may be needed in order to fully appreciate whether these subtle changes in cell shape have an additive effect of elongating the epithelium by 40% between stage 6 and 8. We have initiated a collaboration to apply mathematical models to the topology of the follicle epithelium during elongation, but these analyses are still underway (M. Roper, unpublished results).

Our initial morphometric analysis was not as informative as we had hoped due to several limitations in imaging capacity at the time – analysis in a fairly restricted part of the follicle epithelium, inability to track cells or cell clones over time due to a loss of visualization along the z-axis as clones move out of the view during rotation, and due to confounding proliferation issues from analysis of stage 6 follicles. It is possible that cell intercalation occurs in the lateral

region of the follicle but the kinetics of this cell rearrangement may be much slower in the *Drosophila* follicle than in other intercalating tissues; in other words, that the complete type 1 to type 2 to type3 junction transitions occur at a rate slower than the 45-60 minutes a clone of cells can be tracked from our current analyses of live time-lapse movies. As z-resolution is lost during 4D time-lapse imaging using conventional laser scanning confocal microscopes as a compromise with imaging speed, use of more sophisticated imaging systems like the light sheet scanning systems that enable selective plane illumination microscopy (SPIM) can collect high resolution images of egg chambers around the entire circumference, potentially in a live imaging context (Huisken and Stainier, 2009).

Our more recent developments towards a global, systematic analysis of the follicle epithelium show great promise in elucidating the topological changes occurring in the epithelium during the rotation phase of elongation. Our ability to resolve cell shapes and epithelial topology at follicle poles now enable us to decipher whether distinct cell behaviors occur at the poles compared to the follicle cells occupying the lateral region of the follicle. Use of newer technologies like SPIM may enable us to observe whether follicle cells exhibit different rates of follicle rotation in lateral versus terminal regions and may help point us to identify regions where cell rearrangements may occur. Given that some elongating tissues show multiple morphogenetic behaviors that under wild type conditions mask one another (Butler et al., 2009), identification of additional genes that may uncouple some of these cellular behaviors will be important to determine the relative contribution of global tissue rotation with other behaviors involved in follicle elongation. Also, it is important to recognize that some behaviors occur passively in response to forces generated elsewhere, so any changes in cell shape, cell neighbors or cell division orientation identified more explicitly may be occurring passively in response to the activity of global rotation that generates a mechanical ECM constraint on the follicle epithelium. There is great promise in studying the follicle epithelium as a novel closed system to study tissue elongation and it will be interesting to see what future studies uncover.

3.4.2 Additional published round egg mutants appear to be involved in polarized global tissue rotation and polarization of the fibrillar ECM

It is not surprising that the majority of published round egg mutants, known to play critical roles in cell-matrix interactions, are also involved in global tissue rotation and building a polarized extracellular matrix like *mys* and *vkg*. There are some subtle phenotypic differences, however, that are worth discussion.

Round *rhea* mutant follicles currently only exhibit off-axis rotation but not complete blockage of global tissue rotation like that seen in *mys* mosaic follicles. This may be due to a difference in mutant clone size as *rhea* and *mys* are located on chromosomes 3L and X, respectively, and use distinct FRTs that have different recombination frequencies. It is also possible that Talin, thought to be an essential effector of integrin signaling and function in *Drosophila* (Brown, 2000), may be compensated for in the follicle by other adaptor proteins that link integrins to the actin cytoskeleton. One possible alternate adaptor protein is Tensin (also known as *blistery, by*), which was reported to yield round eggs (Lee et al., 2003). Efforts to examine *tensin*'s role in the control of egg elongation were not fruitful, as we failed to reproduce the result described in (Lee et al., 2003) using two independently derived genetic null alleles, including the allele used by the

original authors. The questionable role that Tensin has in the control of follicle elongation is further weakened by its expression only late in oogenesis (Delon and Brown, 2009). In line with a previous study that has examined the evolution of focal complexes during mid to late oogenesis (Delon and Brown, 2009), it will be interesting to see how Talin and other adaptor proteins that form focal complexes are utilized earlier during global tissue rotation and mature into more stable complexes later in oogenesis to enable distinct types of cell-matrix interactions necessary to carry out the many processes occurring during oogenesis. We currently do not know the subcellular localization patterns of these focal complex proteins during the rotation phase, and future studies can provide valuable insights to focal complex evolution and function and may provide insights to the forces that mediate collective cell migration during follicle rotation.

Preliminary analysis of *fat2* mutant follicles indicates that Fat2 is required for polarized Collagen IV fibrillogenesis. Fat2 is the first gene implicated in controlling *Drosophila* egg shape that is not known to play a direct role in cell-matrix adhesions and has been suggested to function as a global regulator of follicle PCP (Viktorinova et al., 2011), like its other family member – Fat - functions in other tissues. It may be possible that Fat2 acts globally to orient the polarity of global tissue rotation, directly upstream of cell-matrix genes or in parallel to cell-matrix genes, to result in the misorientation of Collagen IV-GFP fibrils. However, Fat2 seems to have additional functions as well. The accumulation of Collagen IV-GFP at basal follicle cell peripheries is unique to *fat2* mutants compared to all other round egg mutants analyzed thus far. This suggests several alternate, though not mutually exclusive, roles for Fat2. Fat2 may be required to restrict cell-matrix adhesions to the basal surface that upon its loss, results in aberrant cell-matrix adhesions in the basolateral domain of follicle cells, resulting in Collagen IV-GFP accumulation in between lateral follicle cell membranes. More likely, Fat2 may instead be facilitating cell-cell adhesion at basolateral domains of neighboring follicle cells, restricting Collagen IV secretion towards the basal surface. Loss of Fat2 in this scenario may lead to loosened cell-cell contacts between follicle cells, enabling aberrant secretion of Collagen IV-GFP between follicle cells. These ideas can be tested by examining integrin and focal complex proteins to see if they show aberrant aggregation in lateral domains of follicle cells. In addition, using a marker of follicle plasma membranes (Neuroglian-GFP) rather than F-actin itself can be informative because there may be loosened cell-cell contacts at basolateral faces between neighboring follicle cells that is not apparent from the ectopic cortical F-actin localization in *fat2* mutants. This F-actin accumulation at cell peripheries, however, is phenotypically distinct from that of *mys* or *rhea* mutants, suggesting Fat2 may have a function that is independent of direct regulation of coordinated global tissue rotation. Moreover, *fat2* mutants exhibit subtle defects in follicle shape compared to *mys, rhea* or *dpak* mutants during the early rotation phase (L. Yuan, unpublished observations), suggesting that *fat2* may be involved in other cellular behaviors that may be occurring during the rotation phase of elongation instead of directly affecting rotation itself. It will be quite interesting to see whether *fat2* mutants are capable of polarized follicle rotation and where Fat2 will fit in with its role in regulating follicle PCP and egg shape.

Finally, it is worth noting that many of these published round egg mutants described in Chapter 2 and 3 show qualitative differences in epithelial topology compared to control genotypes. Continued progress in morphometric analysis of wild type and round egg mutants will provide novel insights to our understanding of the cellular basis of follicle elongation and will be an exciting area of future research in the morphogenesis community.

3.5 Materials & Methods

Drosophila genetics

The following alleles were used: *rhea*^{79a} (also known as *rhea*^{79}) from F. Schöck, *Dlar*^{bola1} and *Dlar*^{bola2} from A. Spradling (Frydman and Spradling, 2001), *fat2*^{58D} *FRT80B* and *fat2*^{103C} from C. Dahmann (Viktorinova et al., 2009), *by*^{2} from J. Chung (Lee et al., 2003), and *tensin*^{33c} from G. Tanentzapf (Becam et al., 2005). *dpak*^{6}, *dpak*^{11}, *e22c::GAL4 UAS::FLP, ubi::nls-GFP ubi::nls-GFP FRT2A* and *Df(2L)E55* were obtained from the Bloomington stock collection; information is available on Flybase (Tweedie et al., 2009). GFP protein traps in *indy* (YC0017), *CG10927* (ZCL3012) (Kelso et al., 2004), *vkg* (CC00791), and *trol* (CA06698) (Buszczak et al., 2007) were obtained from L. Cooley and M. Buszczak. Mosaic follicle cells were generated as previously described (Duffy et al., 1998). All crosses were performed at 25 ºC and adult females were fed on an abundant yeast diet for 2-7 days prior to dissection.

Experimental Genotypes:

Figure 3.1:
A. *w; indy-GFP*

Figure 3.2:
A-B. *w; CG10927-GFP; +*

Figure 3.3:
A-I. *w; indy-GFP*

Figure 3.4:
A. *w; indy-GFP*

Figure 3.5:
A. *yw/w; vkg-GFP/e22c::GAL4 UAS-FLP; rhea*^{79a} *FRT2A/ubi::nls-GFP ubi::nls-GFP FRT2A*
B. *w Nrg-GFP/w; e22c::GAL4 UAS-FLP/+; rhea*^{79a} *FRT2A/ubi::nls-GFP ubi::nls-GFP FRT2A*
C. *w; e22c::GAL4 UAS-FLP/+; rhea*^{79a} *FRT2A/ubi::nls-GFP ubi::nls-GFP FRT2A*

Figure 3.6:
A-B. *pak*^{6}*/pak*^{11}
C-D. *w/+; vkg-GFP/+; pak*^{6}*/pak*^{11}

Figure 3.7:
A. *w trol-GFP/+; Dlar*^{bola1}*/Df(2L)E55 rdo*^{1} *hk*^{1} *pr*^{1}

Figure 3.8:
A, C. *w; vkg-GFP; fat2*^{103C}*/fat2*^{103C}
B. *w; vkg-GFP; fat2*^{103C}*/TM6C*

Movie 3.1
w Nrg-GFP/w; e22c::GAL4 UAS-FLP/+; rhea^{79a} *FRT2A/ubi::nls-GFP ubi::nls-GFP FRT2A*

Fixation & Immunohistochemistry

All follicles were manually dissected from the epithelial muscle sheath as described (Prasad et al., 2007) to preserve follicle shape in Schneider's *Drosophila* medium (GIBCO) and fixed within 15 minutes using 4% formaldehyde in Schnieder's *Drosophila* medium supplemented with phalloidin (see below for dilution) to preserve basal F-actin structures in the follicle

epithelium. F-actin was visualized using phalloidin-TRITC (1:500, Sigma) or phalloidin-AlexaFluor 647 (1:30, Molecular Probes).

***Ex vivo* follicle culture**

Live imaging of cultured follicles were performed largely as described (Prasad et al., 2007) with the following modification. For egg chamber mounting, a 18x18 mm #1 cover glass (Fisher Sci.) was cushioned using high vacuum grease (Dow Corning) and gently placed over dissected follicles in 30 µl of culturing medium to reduce the working distance required for use with certain objective lenses.

Sample preparation for morphometric analysis

Sample preparation varied depending on the microscope used for imaging to avoid any compression of samples through the combined effects of the cover glass and objective lenses requiring a short working distance for optimal imaging. Ovarioles were mounted in a 0.5-1.0% low melting point agarose (Agarose, Type VII, Sigma) in phosphate-buffered saline (PBS) in a custom-made well built on glass slides for imaging on the upright LSM 5 Live (Zeiss) using a water dipping objective lens. Sterile PBS was used in lieu of water as the immersion medium for water dipping objective lenses; the lenses were thoroughly cleaned after each use to avoid salt accumulation on the lenses. In contrast, ovarioles were mounted in PBS alone or mounted in 0.5-1.0% low melting point agarose in PBS on 35mm bottom glass microwell dishes (MatTek Corp., part # P35G-1.5-14-C) for imaging on the inverted LSM 5 Live (Zeiss) using a water immersion objective lens. Samples securely embedded in agarose were then flooded with PBS in the culture dish to prevent desiccation of the sample during imaging.

Microscopy

Fixed and live time-lapse images were acquired on a TCS SL (Leica) using 16x/NA 0.5, 40x/NA 1.25 or 63x/NA 1.4 oil immersion lenses, a LSM 5 Live (Zeiss) using 20x/NA 0.5 or 40x/NA 0.8 water dipping lenses, a Axio Imager.M1 (Zeiss) using 10x/NA 0.3 air objective lens or a LSM 700 (Zeiss) using a 40x/NA 1.1 water immersion lens. For time-lapse imaging, 5 minute time points were acquired with a single xy plane.

Data Analysis

All experiments in this chapter are preliminary and have low sample sizes but have been performed on 2 or more independent dates. Data graphs are reported as histograms or mean $\pm$ standard deviation. Images were processed and assembled using Creative Suite 4 (Adobe), Volocity and Image J. Graphs were produced using Excel 2008 (Microsoft) or Igor Pro (WaveMetrics, Inc.) and rose diagrams were plotted using Rozeta 2.0 (Pazera-Software).

Morphometric Analysis

Cell tracking was performed using object tracking algorithms or manual object tracking in Volocity (Perkin Elmer). Morphometric analysis of the follicle epithelium was developed and performed using Volocity and Image J (NIH). Data quantification for follicle epithelial topology was performed on 30 x 30 µm regions in the lateral region of stage 6 or stage 8 follicles from follicles imaged using the sample preparation methods described above. Basal surfaces of individual follicle cells were outlined following xyz coordinates from cropped z-stacks in Image J to delineate individual cells (polygons). Polygons were then analyzed as a fitted ellipse to

obtain measurements for the following cell parameters: basal surface area, major axis (pixel and μm), minor axis (pixel and μm), follicle cell aspect ratio (pixel/pixel), and angle of major axis relative to the x (follicle A-P) axis (degree). Cell topology (n sides) was manually scored for each polygon.

Figure 3.1
There is little evidence for polarized cell intercalation during follicle rotation *ex vivo* from live cell imaging.

(**A**) A subset of follicles from live imaging videos have stereotypical type 2 junctions, where 4 cells meet at one vertex (**A'**, left). Tracking these type 2 junctions indicate some junctional remodeling occurring during follicle rotation (**A-A'**, middle-right) but no complete intercalation event, highlighted by a type 1 to type 2 to type 3 junction transition, has been observed from manual analysis of follicles undergoing rotation.

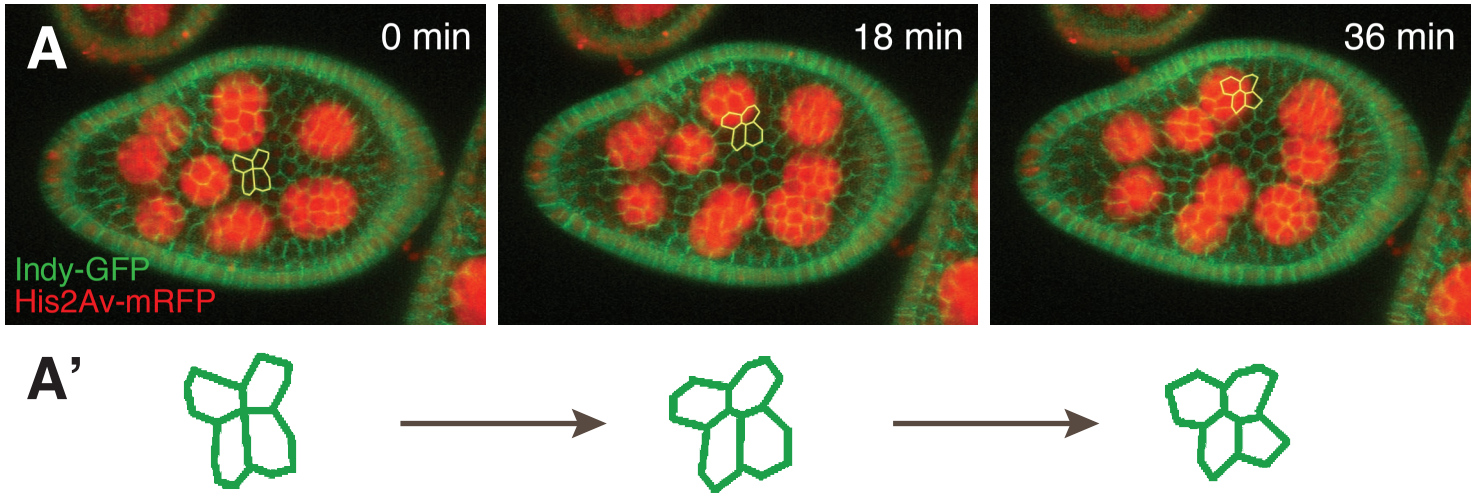
A
0 min
18 min
36 min
Indy-GFP
His2Av-mRFP
A'

Figure 3.2
Subtle shifts in the number of follicle cells along the major and minor planes of the follicle during elongation may or may not be indicative of cell rearrangements.

(**A**) CG10927-GFP marks follicle cell nuclei and was used for morphometric analysis (**B**) to determine the number of follicle cells occupying the maximal A-P plane (**B'**) or maximal D-V plane (**B"**) to determine whether shifts in follicle cell numbers occurred during the rotation phase of follicle elongation. Independent experimental data sets (**C-D**) indicate a potential increase in follicle cells along the A-P axis, but changes in total follicle cell number in the stages examined make it unclear whether cell rearrangements can account for these subtle shifts.

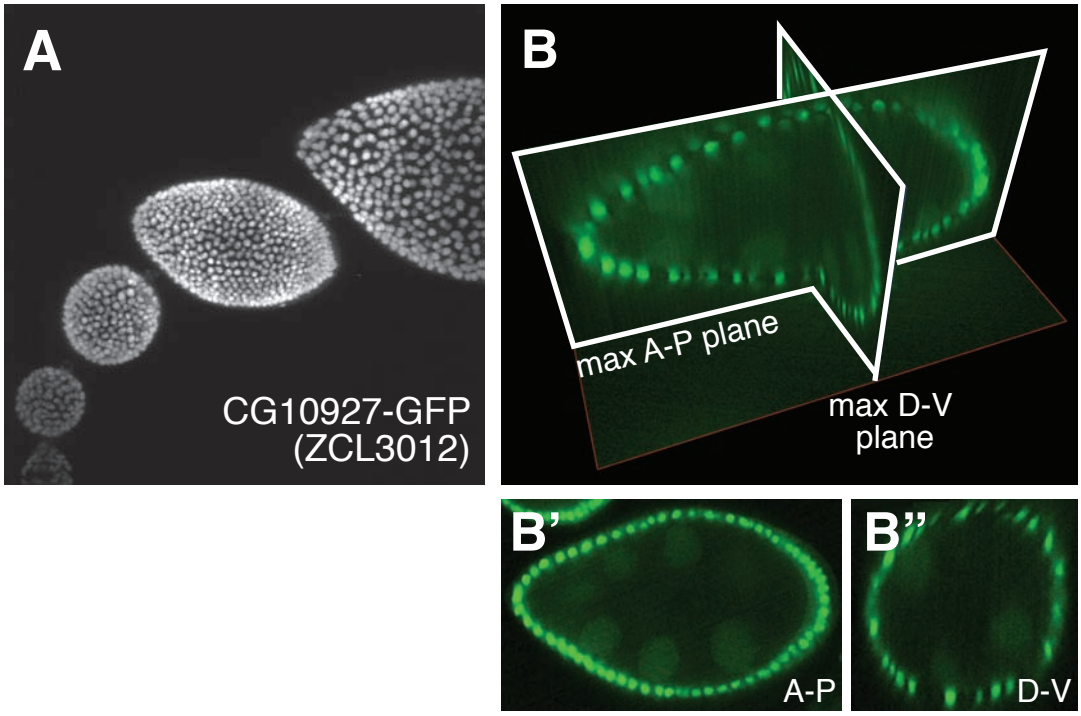

C

Stage	max A-P follicle cell #	max D-V follicle cell #	total follicle cell #	max A-P length (μm)	max D-V length (μm)
6	42	26	n.d.	79.2	65.4
6	36	27	n.d.	79.4	63.0
6	43	25	n.d.	76.0	62.4
6	47	29	662	91.0	66.1
6	49	33	613	92.7	70.9
8	60	29	794	180.6	104.3
8	59	30	n.d.	148.6	98.5
8	59	28	782	167.7	93.7

D

Stage	max A-P follicle cell #	max D-V follicle cell #
6	57	36
6	56	30
6	55	28
7	55	30
7	43	34
7	59	34
8	62	29
8	64	30
8	67	29
8	61	35

Figure 3.3
Subtle cell elongation and cell neighbor exchanges are observed in the lateral follicle epithelium during the rotation phase of elongation.

(**A-B**) Lateral regions of stage 6 and 8 follicles were used for morphometric analysis; higher magnification of basal follicle cell surface shown in (**A'-B'**). (**C-D**) Distribution of follicle cell topology of stage 6 (**C**) or stage 8 (**D**) follicles. Note that at both stages, a similar distribution around hexagons exists, although there is a slight increase in cell topology variance at stage 8 due to a small percentage (3%) of cells having 8 neighbors. (**E**) Most follicle cells in the lateral regions are elongate in the circumferential axis, orthogonal to the A-P axis (**F**), but more follicle cells increase their individual cell aspect ratio at stage 8 (**G**) and bias their long axis towards the A-P axis (**H**). (**I**) Basal surface area of follicle cells indicates a doubling of surface area from stage 6 to stage 8. Scale bar in (**A-B**) 10 μm, (**A'-B'**) 5 μm.

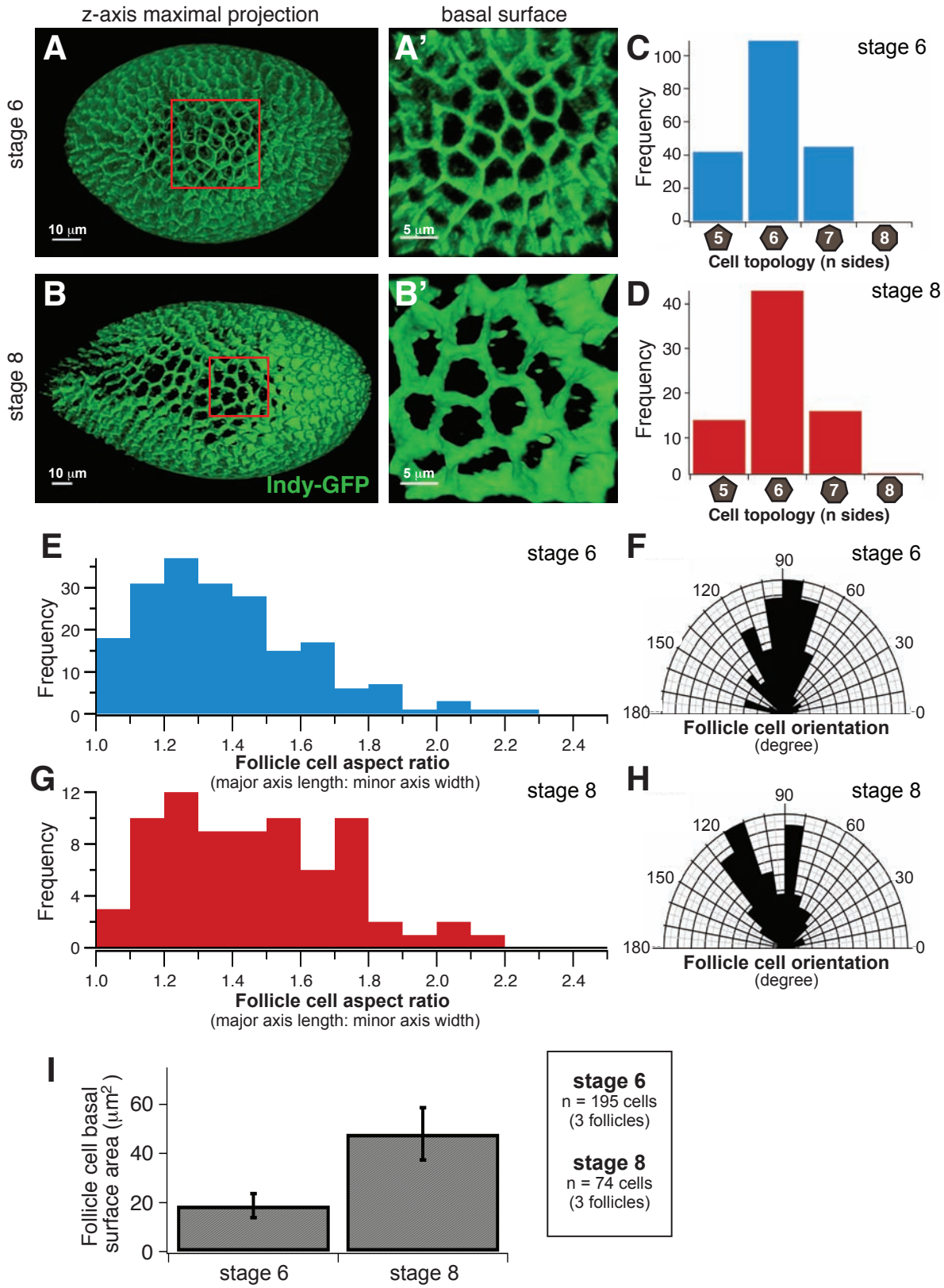
z-axis maximal projection
basal surface
stage 6
stage 8
A
A'
B
B'
10 μm
5 μm
Indy-GFP
C
stage 6
Frequency
Cell topology (n sides)
D
stage 8
E
Follicle cell aspect ratio
(major axis length: minor axis width)
F
Follicle cell orientation
(degree)
G
H
I
Follicle cell basal surface area (μm²)
stage 6
n = 195 cells
(3 follicles)
stage 8
n = 74 cells
(3 follicles)

Figure 3.4
Optimization of high resolution cellular imaging for morphometric analysis of the entire follicle epithelium.

(**A**) 96.36 μm z-stack projection of a stage 8 follicle expressing Indy-GFP, taken at 500 nm step intervals, highlights the newest improvements in cellular resolution at both the anterior and posterior poles of the follicle. Updates in imaging technology and minimal sample distortion during image acquisition by modifying sample preparation have enabled faster acquisition of images with great clarity like that shown here.

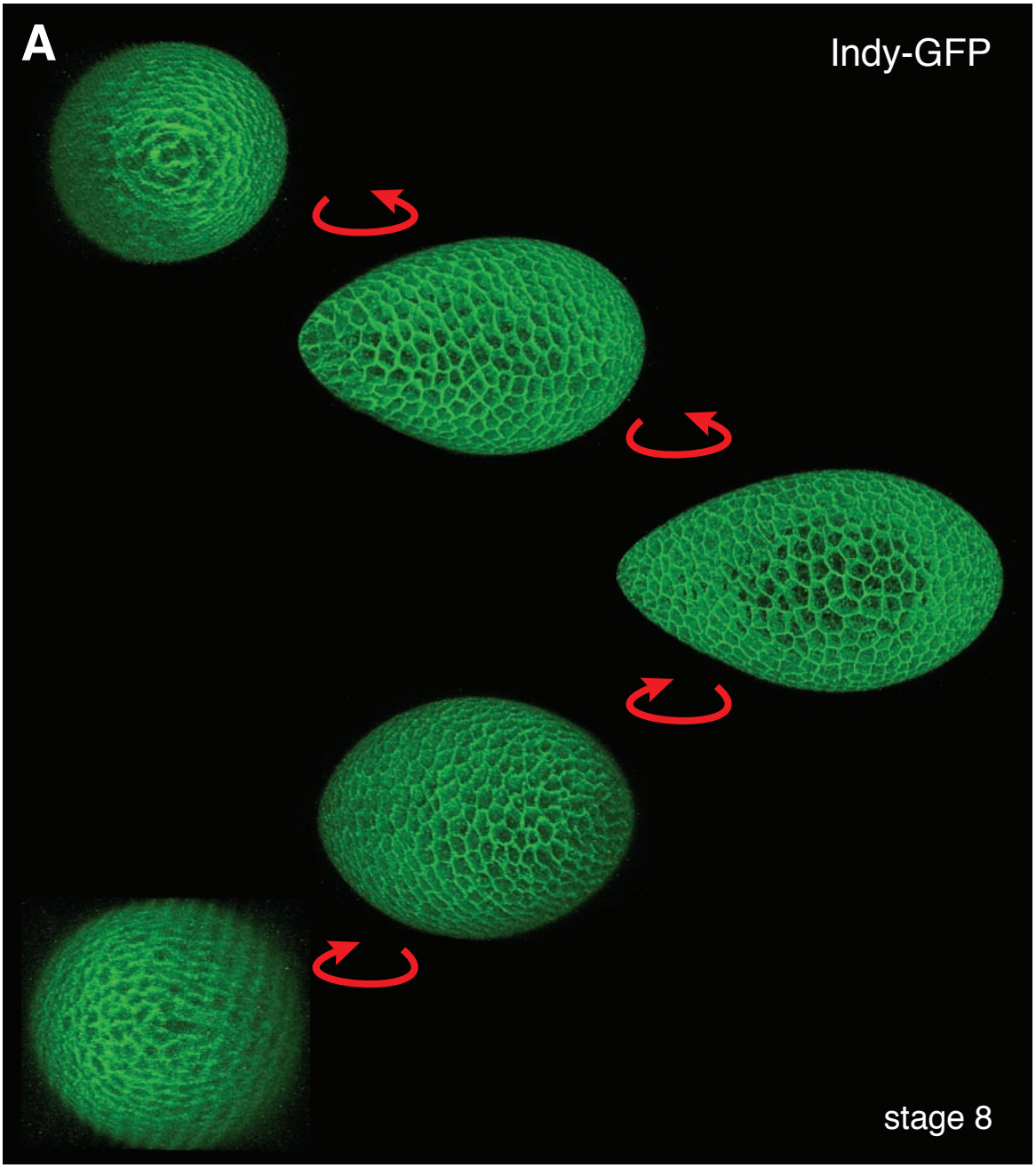
A
Indy-GFP
stage 8

Figure 3.5
***rhea/talin* mutant follicles exhibit defects in follicle shape, global tissue rotation, F-actin and Collagen IV polarity.**

(**A**) Stage 8 *rhea* mosaic round follicle shows that it is misoriented (arrow) relative to the A-P axis of the ovariole, which runs top to bottom in this image. Basal surface views of Collagen IV-GFP (**A'**) or basal actin filaments (**A"**) indicate off-axis polarization of both structures. (**B**) Time-lapse images of *rhea* mosaic round follicle (top) shows off-axis rotation in the plane of the image while a sibling control genotype (bottom) undergoes polarized follicle rotation. Asterisk notes mutant follicle cells; numbers mark internal nurse cell nuclei for tracking over time. The transparency of the number indicates its relative depth, where an increase in opacity indicates the nucleus is closer to the surface of the viewing plane. (**C**) Clonal analysis of *rhea* mutant follicle cells (GFP negative) indicates a cell-autonomous reduction in polarized basal actin filaments and aberrant aggregations of F-actin at cell peripheries (arrow). Neighboring wild type cells (green) still form polarized actin filaments. Note that this follicle has wild type follicle shape (**C'**, inset) and correspondingly, no effect on global tissue polarity was observed in this portion of the follicle. Grayscale of F-actin alone shown in (**C'**). Frames for (**B**) taken from Movie 3.1. Scale in (**A, B**) 50 μm, (**A'-A"**) and (**C-C'**) 10 μm.

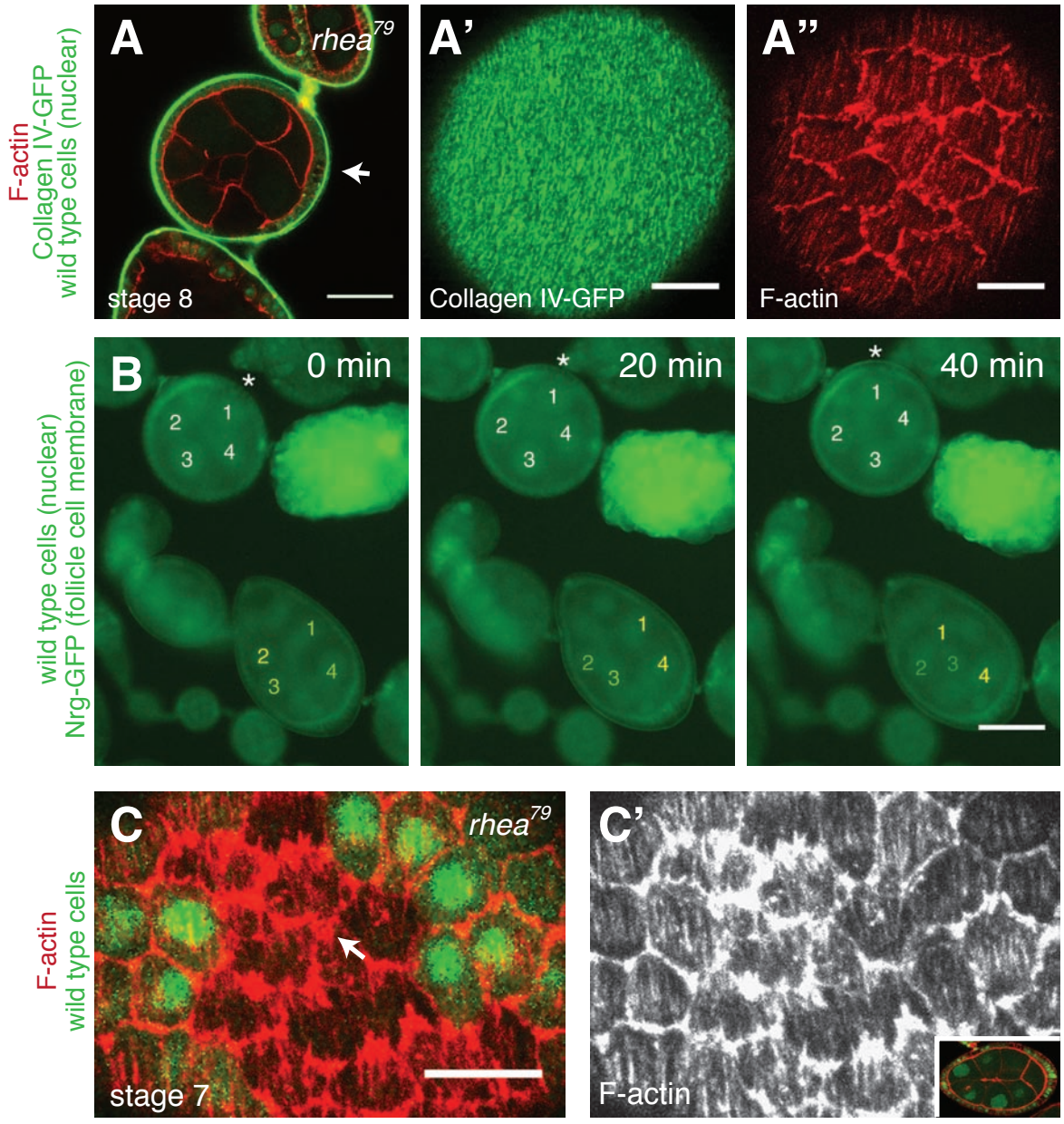
A
rhea79
stage 8
A'
Collagen IV-GFP
A''
F-actin
F-actin
Collagen IV-GFP
wild type cells (nuclear)
B
0 min
20 min
40 min
wild type cells (nuclear)
Nrg-GFP (follicle cell membrane)
C
rhea79
stage 7
C'
F-actin
F-actin
wild type cells

Figure 3.6
***pak* has variable effects on polarized Collagen IV fibrillogenesis.**

(**A-B**) *pak* hypomorphic transheterozygotes exhibit pleiotropic defects, including multilayering (asterisk) and invasion of follicle cells into the germline, misoriented follicles (arrow), and subsequent degeneration of late stage follicles, though survival to stage 11 can be observed on occasion (**B**). Round *pak* mutant follicles (**C-C"**) exhibit reduced Collagen IV-GFP fibrillogenesis and global tissue polarity defects in basal actin polarity, while more elongate *pak* mutant follicles (**D-D"**) exhibit polarized Collagen IV-GFP fibrillogenesis and a relatively polarized basal microfilament cytoskeleton, albeit some irregularities in epithelial topology. Scale in (**A-B**) 100μm; (**C-D**) 25μm; (**C'-C", D'-D"**) 10μm.

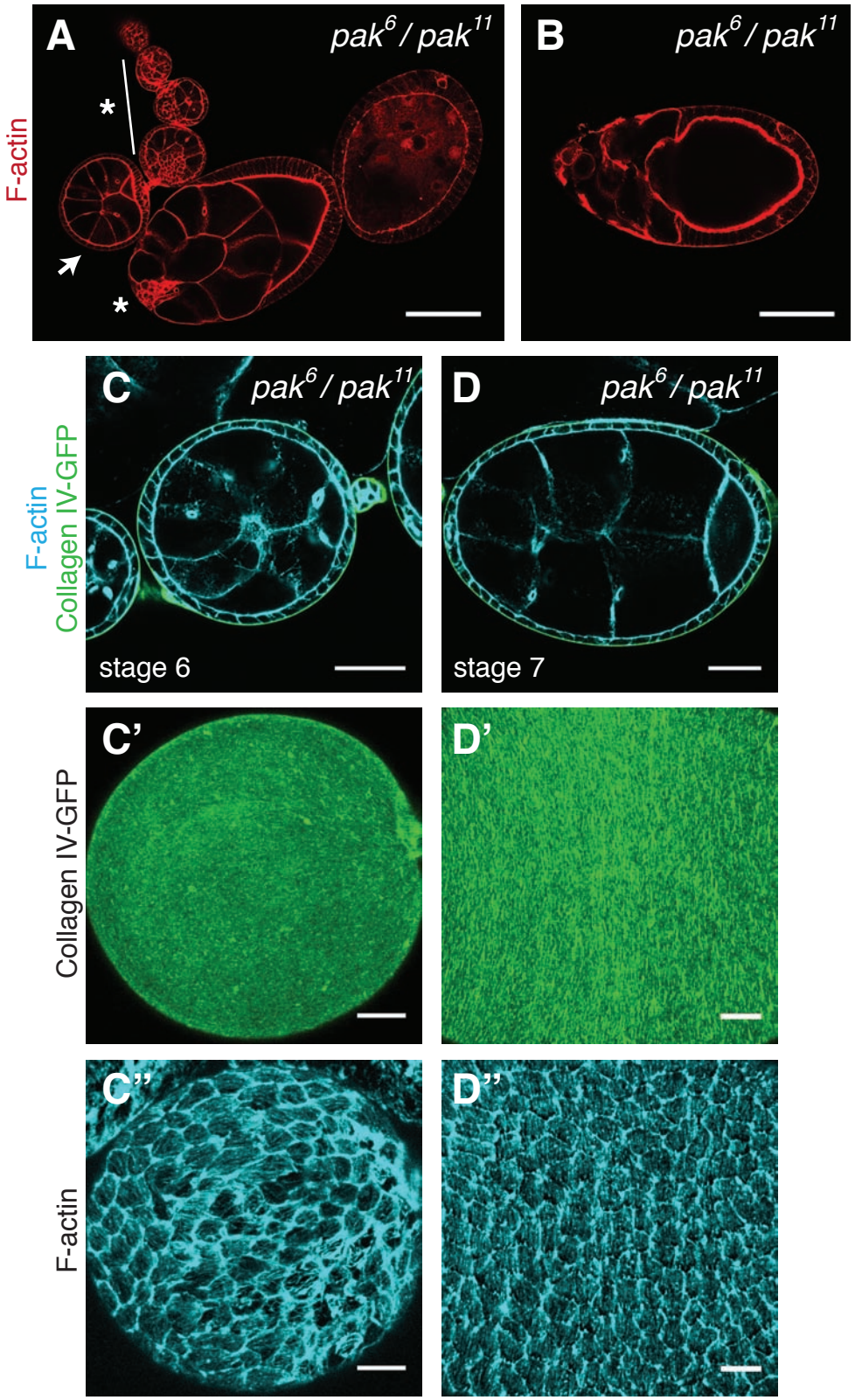
A
pak6 / pak11
B
pak6 / pak11
F-actin
C
pak6 / pak11
D
pak6 / pak11
F-actin
Collagen IV-GFP
stage 6
stage 7
C'
D'
Collagen IV-GFP
C''
D''
F-actin

Figure 3.7
***Dlar* may have subtle effects on ECM fibrillogenesis.**

(**A**) Stage 8 *Dlar* mutant round follicle shows normal deposition of Perlecan-GFP into the follicle basement membrane. Examination of the basal surface indicates that polarized Perlecan-GFP fibrils are still present (**A'**) although global polarity across the tissue is not as tightly coordinated as seen in wild type. Likewise, polarized actin filaments are seen at the basal surface (**A"**) but F-actin is also aberrantly enriched at cell cortices and may increase actin-rich protrusions on the basal surface. Scale in (**A**) 25μm; (**A'-A"**) 10μm.

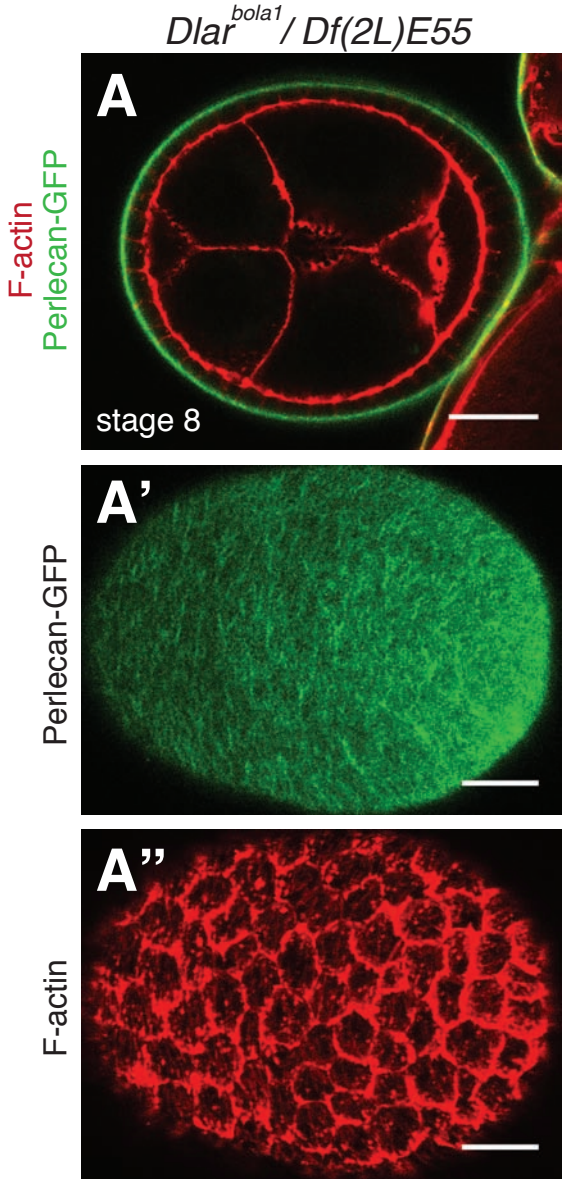
Dlar bola1 / Df(2L)E55
A
F-actin
Perlecan-GFP
stage 8
A'
Perlecan-GFP
A''
F-actin

Figure 3.8
***fat2* is required for polarized Collagen IV fibrillogenesis.**

(**A**) Stage 6 *fat2* mutant follicles show a defect in polarization of Collagen IV fibrils (**A'**) and a global loss of basal F-actin tissue polarity (**A"**). Note that some mutant follicle cells display aberrant F-actin accumulation at tricellular junctions. Comparison of heterozygote control (**B**) and *fat2* mutant follicles (**C**) indicates a defect in follicle shape and a more notable defect in Collagen IV fibrillogenesis (compare **C'** to **B'**). *fat2* mutant follicles also display aberrant accumulation of Collagen IV-GFP at basal cell peripheries (**C'**), concomitant with an up regulation of cortical F-actin (**C"**), giving *fat2* mutant follicle cells a rounded appearance (compare **C"** to **B"**). Scale in (**A**) 25μm; (**B-C**) 50μm; (**A'A", B'-B", C'-C"**) 10μm.

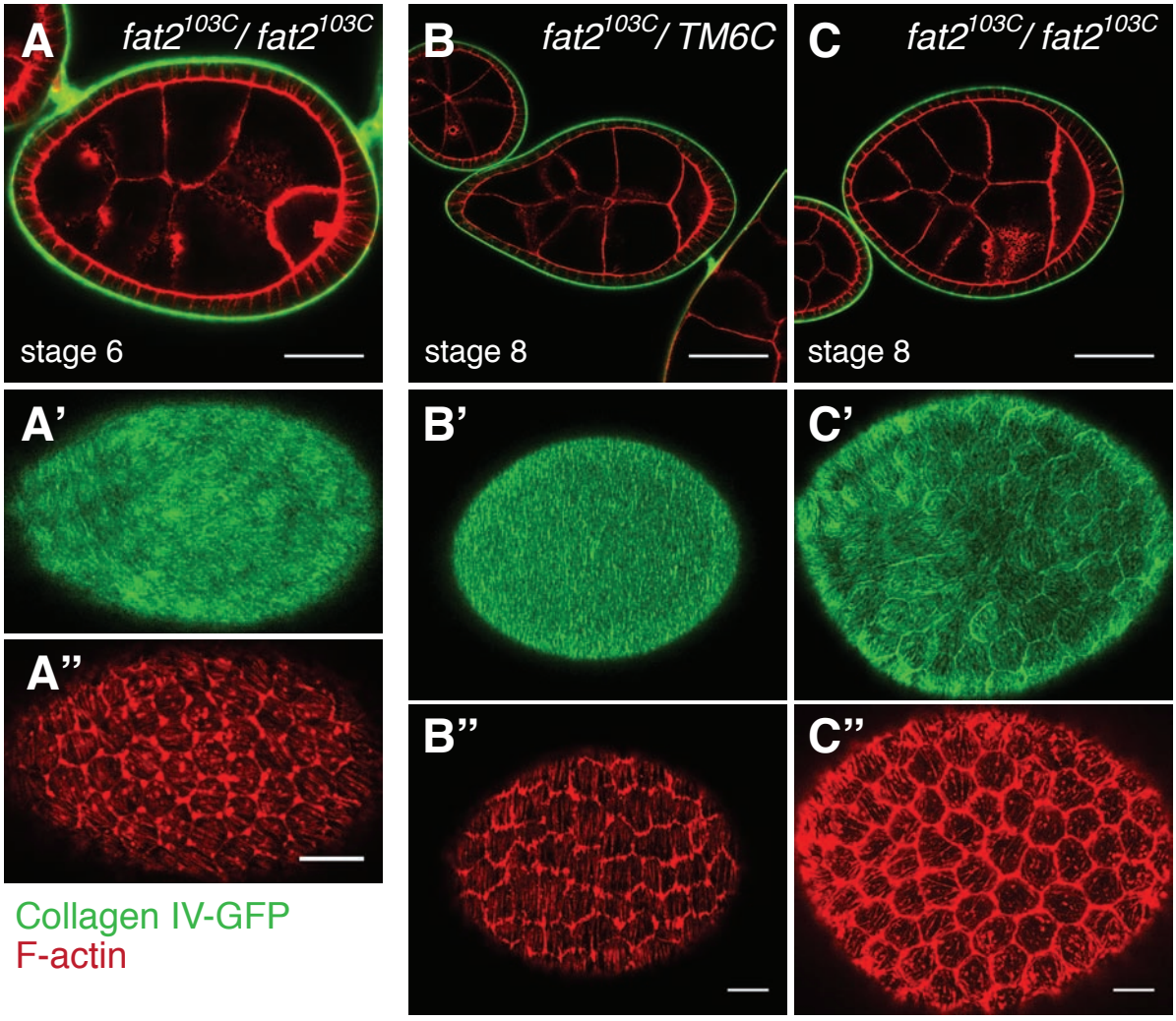
A
fat2103C/ fat2103C
stage 6
B
fat2103C/ TM6C
stage 8
C
fat2103C/ fat2103C
stage 8
A'
A''
B'
B''
C'
C''
Collagen IV-GFP
F-actin

Chapter 4

Investigating the source of planar cell polarity in the *Drosophila* follicle

4.1 Abstract

One of the greatest mysteries from the discovery of global tissue rotation is how this novel morphogenetic behavior is initiated. Analysis of the emergence of molecular planar cell polarity (PCP) of cell-matrix proteins compared to the emergence of polarized tissue rotation indicate a critical period in stage 5 when both molecular and morphological PCP are established in the *Drosophila* follicle. One possible polarizing source that has been previously proposed is the polar cells at the termini of each follicle, but experimental evidence has shown mixed evidence supporting their role as the polarizing source. To begin identifying a potential source of follicle PCP and follicle rotation, an *in silico* enhancer trap screen within the Flytrap collection was performed to identify developmental signaling pathways and other genes that may coincide in expression with the major elongation phase. This has led to the identification of the Notch/Delta signaling pathway as a putative regulator of follicle PCP and global tissue rotation, potentially providing an activation signal from the germline at stage 5. Interestingly, germline mutations in *liquid facets*, an epsin homolog required for Delta endocytosis and activation, result in round follicles, off-axis rotation, and loss of global tissue polarity in basal actin filaments. It will be exciting to perform follow up experiments further testing the role of Notch/Delta signaling in the control of follicle PCP and to elucidate the molecular and cellular basis of the initiation of global tissue rotation.

4.2 Introduction

The discovery of global tissue rotation raises several questions about how this morphogenetic behavior fits in with our general understanding of pattern formation during oogenesis. Of greatest curiosity is what signaling event initiates the emergence of follicle PCP and the onset of global tissue rotation. This requires a brief background on our current understanding of pattern formation during *Drosophila* oogenesis.

Drosophila oogenesis has been a powerful genetic system that has led to a detailed molecular understanding of how the antero-posterior (A-P) and dorso-ventral (D-V) axes are established by multiple signaling events mediated between the soma and germline over the last 25 years (Bastock and St Johnston, 2008; Roth and Lynch, 2009). Four key signaling events occur during oogenesis. First, signaling in the germarium mediated by follicle cells of neighboring, older egg chambers to establish A-P polarity within the germline cyst (Torres et al., 2003). During stages 5 to 7, signaling from the germline establishes A-P polarity within the follicle epithelium (Gonzalez-Reyes et al., 1995; Gonzalez-Reyes and St Johnston, 1998; Grammont and Irvine, 2002; Lopez-Schier and St Johnston, 2001; Xi et al., 2003). This is followed by reciprocal signaling by the posterior follicle cells at stage 6 to 7 to initiate D-V asymmetry in the oocyte to relocate the oocyte nucleus and key maternal components to the prospective dorso-anterior corner of the oocyte (Gonzalez-Reyes and St Johnston, 1994; Neuman-Silberberg and Schupbach, 1993; Poulton and Deng, 2007). Subsequently, signaling by the oocyte back to the follicle cells at stages 8-9 establish D-V polarity in the follicle, thereby completing polarization of both body axes of *Drosophila* by stage 10 of oogenesis (Gonzalez-Reyes et al., 1995; Montell et al., 1991).

In efforts toward the identification of a potential signaling source of follicle PCP and follicle rotation, characterization of the emergence of molecular PCP in the *Drosophila* follicle was performed, followed by an *in silico* enhancer trap screen within the Flytrap collection. A potential involvement of the Notch/Delta signaling at the early elongation phase from the enhancer trap screen is supported by defects in follicle shape, rotation and follicle PCP when a mutation in *liquid facets* (*lqf*) was used to block Delta activation in the germline. One hypothetical model is discussed to explain how Notch/Delta signaling may be regulating the onset of follicle rotation and I end by applying these findings to our growing understanding of the mechanisms that regulate tissue elongation of the developing egg.

4.3 Results

4.3.1 Molecular PCP and the onset of global tissue rotation both appear to emerge at stage 5 of oogenesis

Previous studies have found that molecular PCP can precede morphogenetic movements (Blankenship, 2006). Whether this also occurs in the *Drosophila* follicle remain unclear. Early studies had reported that actin filaments are present on the basal surface of young follicles and exhibit individual cell polarization, but do not show coordinated tissue polarity until stage 5 (Frydman and Spradling, 2001) (Appendix A). Likewise, a similar observation was made regarding the Collagen IV matrix during the early phase of follicle elongation (Haigo and Bilder,

2011). To better understand the emergence of follicle PCP at the molecular level, additional markers of cell-matrix components and the actomyosin network thought to mediate polarized follicle migration were examined during the early elongation phase of oogenesis.

Spaghetti squash (*sqh*) encodes the regulatory light chain of *Drosophila* non-muscle myosin II (MRLC) that is part of the actomyosin contractile network involved in regulating cell migration and morphogenesis in a variety of contexts (Rauzi et al., 2010; Vicente-Manzanares et al., 2009). Sqh is known to exhibit planar polarization in the *Drosophila* germband during convergent extension (Bertet et al., 2004; Blankenship, 2006) but its localization during follicle elongation is not well characterized. Examination of Sqh-GFP during the early phase of elongation found that its has similarities to basal actin filaments – both MRLC and F-actin show oriented fibrils within individual follicle cells but exhibit no clear tissue polarity (Figure 4.1, A). However, at stage 5, Sqh-GFP fibrils begins to show monopolar enrichment on either the dorsal or ventral faces of individual follicle cells with a clear tissue polarity apparent by stage 6 (Figure 4.1, B-C). Interestingly, these enrichments of Sqh-GFP are reminiscent of puncta seen with Fat2-GFP (Viktorinova et al., 2009), βPS integrin and Dlar (Bateman et al., 2001). It remains unclear to what subcellular structures these Sqh-GFP enrichments co-localize.

A second molecule examined thus far is the Perlecan matrix. Perlecan is a heparan sulfate proteoglycan that is one of the four core components of all basement membranes and is thought to help maintain basement integrity with Collagen IV (Yurchenco and Patton, 2009) to maintain stable tissue architecture (Haigo and Bilder, 2011; Schneider et al., 2006). Preliminary analysis of Perlecan-GFP during the early elongation phase suggests that the Perlecan matrix has a very similar timing in its fibrillar organization to that of Collagen IV (Figure 4.1, D-I). Perlecan-GFP is present in the germarium and young follicles with distinct puncta that appear to mature into elongate fibrils from stage 5 onward. Perlecan fibrils do not appear as crisp as Collagen IV fibrils and the limited samples analyzed at these early stages suggest that additional characterization of Perlecan-GFP is needed to confirm the polarization patterns described here.

In summary, all molecular markers examined thus far indicate that molecular PCP emerges at the same time as global tissue rotation at stage 5.

4.3.2 An in silico enhancer trap screen for dynamic expression patterns during follicle elongation identifies a potential role for Notch/Delta signaling

The lack of a clear molecular polarity prior to the onset of global tissue rotation led us to approach the question using a different strategy. The Flytrap collection was developed by several labs in an effort to perform high throughput protein trapping screens to study protein localization in live or fixed tissues without the need for antibodies (Buszczak et al., 2007; Kelso et al., 2004; Morin et al., 2001; Quinones-Coello et al., 2007). A transposable P element carrying an artificial exon encoding green fluorescent protein (GFP) flanked by splice acceptor and splice donor sights were randomly hopped into the *Drosophila* genome. GFP protein trap lines are generated upon insertion into intronic sequences that upon splicing into mature mRNAs and in-frame fusion, result in the expression of GFP at the endogenous locus. A number of the GFP protein trap lines are viable and fertile. Unexpectedly, this strategy also led to the production of 254 enhancer trap lines that had insertions within 500 nucleotides upstream of an

annotated gene (Figure 4.2, A). In these enhancer trap lines, the 5' transcriptional start site of the gene was able to activate transcription of the P element and the transposase encoded within this P element provided the starting methonine codon for translation of GFP (Quinones-Coello et al., 2007). Many of these enhancer trap lines have GFP expression during oogenesis.

From this enhancer trap collection, 18 enhancer trap lines were selected based on a dynamic change in expression of GFP during the early elongation phase of oogenesis (Figure 4.2, B). Interestingly, more than half of these lines are enhancer traps in genes that are direct components or targets of the Notch/Delta signaling pathway or in genes that have been genetically linked to Notch/Delta signaling (Figure 4.2, B bold). A number of these enhancer traps have been validated for expression during the major elongation phase of oogenesis (Figure 4.2, C-E). Some of these enhancer trap lines show strong up- or down-regulation of expression at stage 5, and a subset of these lines show a shift in expression where uniform expression is seen throughout the follicle epithelium up through stage 4-5 but become restricted to the anterior or posterior termini at stage 5 and later. These localization patterns are consistent with published expression patterns and the known role of Notch/Delta signaling required for follicle cell differentiation during this time (Assa-Kunik et al., 2007; Jordan et al., 2006; Larkin et al., 1999; Lopez-Schier and St Johnston, 2001; Ruohola et al., 1991).

4.3.3 Germline mutations in lqf perturb follicle shape, global tissue rotation, and basal microfilament polarity

The results from the *in silico* enhancer trap screen led us to revisit Notch/Delta signaling at stage 5. It is known that Delta protein levels are dramatically upregulated at stage 5 that trigger follicle cell differentiation and the cessation of follicle cell proliferation during stage 6-7 (Lopez-Schier and St Johnston, 2001). Interestingly, our lab has recently used the *Drosophila* ovary to examine endocytic regulation of Delta signaling during oogenesis and found that germline mutations in *liquid facets* (*lqf*) can result in round follicles (Windler and Bilder, 2010) (S. Windler, personal communication). Liquid facets is the *Drosophila* Epsin homolog that mediates Delta endocytosis necessary for its activation in signal sending cells and Notch activation in signal receiving cells (Overstreet et al., 2004; Wang and Struhl, 2004). These observations suggest that one potential source of follicle PCP and the onset of polarized follicle rotation may be a Delta activation signal sent from the germline at stage 5.

To begin testing this hypothesis, *lqf* germline clones were analyzed for their ability to undergo polarized follicle rotation and basal microfilament orientation (Figure 4.3). *lqf* germline clones were confirmed to show a defect in follicle shape during the elongation phase (Figure 4.3, A), with similarities to *fat2* mutants. Live imaging of *lqf* germline clones demonstrated an ability to rotate, though they appear to rotate off-axis from the A-P axis (Figure 4.3, B). Finally, examination of the basal F-actin cytoskeleton indicates irregularities in basal microfilament polarity. While actin filaments are present in all follicle cells and exhibit local polarity alignment, global tissue polarity seems impaired and off from the long A-P axis (Figure 4.3, C-E). Most notably, aberrations in basal actin-based protrusions were seen, where in many cells the protrusions seemed misoriented in many directions and often appeared to project bidirectionally at given cell-cell interfaces that lie parallel with the A-P axis.

4.4 Discussion

4.4.1 The emergence of follicle PCP

All migrating cells exhibit an intrinsic subcellular polarity necessary for migration (Ridley et al., 2003) and much attention has been given to the formation of actin-based protrusions at the leading edge of migration cells to break its cellular symmetry (Mitchison and Cramer, 1996; Ridley et al., 2003). However, more recent studies of cell migration in culture have found that cell rear retraction can trigger the initial break in cell symmetry to initiate cell migration in contexts where a guidance cue is absent (Cramer, 2010). While F-actin has been found to be the first molecule exhibiting planar polarity prior to polarized morphogenesis seen during germband extension, it seems that F-actin arises in planar polarization along with myosin II at the basal follicle cell surface and with basement membrane molecules at stage 5. Thus, it remains mysterious how the follicle epithelium breaks its initial symmetry to exhibit cellular and supracellular polarization during stage 5, alongside the emergence of polarized follicle rotation.

Part of the issue may be that we currently do not have enough temporal resolution during stage 5. Stage 5 of oogenesis spans 6 hours (Spradling, 1993), so we do not have the temporal and morphological resolution on the order of minutes like that of the early *Drosophila* embryo. Without additional morphological criteria aside from follicle size to delineate follicles, it may be difficult to improve our current understanding of the emergence of follicle PCP. However, one candidate molecule worth examining is Laminin, which is also known to exhibit planar polarization during the elongation phase (Bateman et al., 2001; Gutzeit et al., 1991) but has not been characterized at early stages. Laminin is worth considering because it is thought to be required for basement membrane assembly (Yurchenco and Patton, 2009), so it may form polarized fibrils in the follicle basement membrane before Perlecan or Collagen IV. Efforts to examine the Laminin matrix have been made using several Laminin antibodies without success. Concanavalin A, a plant lectin that binds to glycoproteins like Laminin, is a possible alternate readout of the Laminin matrix, but has not yet been used for analysis of young follicles in the early phase of elongation. Resolving this question will be of great interest to the cell-matrix community, as it is often contested which structure forms first – the ECM or the cytoskeleton (Brown, 2000).

4.4.2 Sources of follicle PCP

The effort to identify the source of follicle PCP was initiated a decade ago when F-actin was found to exhibit tissue polarity at stage 5 of oogenesis (Frydman and Spradling, 2001). In this report, basal actin filaments were found to first polarize circumferentially around the poles and spread this tissue polarity towards the center of each follicle by stage 6. Furthermore, some round egg mutants like *Dlar/bola* contain ectopic polar cell clusters at a small frequency that correlated with misoriented basal microfilaments (Frydman and Spradling, 2001). This led to the hypothesis that the polar cells may provide the polarizing cue to initiate basal actin PCP. This hypothesis was tested by ectopic expression of Hedgehog (Hh) to induce ectopic polar cells, with the prediction that basal actin polarity surrounding the ectopic polar cells would reorient circumferentially around the clone. However, only some follicles with ectopic polar cells

reoriented actin filaments while others had no effect. Thus, it remains unclear whether polar cells can act as a source of follicle PCP.

An alternate hypothesis from the preliminary results of this chapter suggests that the source of follicle PCP may originate from the germline upon elevated Delta expression at stage 5. While it remains unclear what prompts this upregulation in Delta expression at stage 5, it may be related to a unique chromatin remodeling of the nurse cell polytene chromosomes into chromosomal blobs that then become more disperse by stage 6 (Dej and Spradling, 1999). The defects in follicle shape, off-axis rotation and perturbations in basal microfilament polarity in *lqf* germline clones suggests the necessity of Delta activation in the germline at stage 5 for follicle PCP and for proper orientation of global tissue rotation by the follicle. Confirmation of the requirement of Delta germline signaling will be important to follow up on, and use of a temperature sensitive $delta^{RF}$ allele that fails to reach the cell surface at a restrictive temperature (Delwig and Rand, 2007) may be useful as an independent method to determine whether Delta signaling is necessary for the emergence of follicle PCP and polarized tissue rotation. Likewise, whether Delta signaling is sufficient to induce follicle PCP at the molecular and morphological levels can be performed by ectopic expression of Delta in the germline (Jordan et al., 2006) and examination of stage 4 or younger follicles for polarized actomyosin, basement membrane molecules and premature polarized follicle rotation.

If Delta signaling from the germline is found to be necessary and sufficient for follicle PCP and global tissue rotation, what might a potential mechanism be? While we reported in chapter 2 that polarized global tissue rotation does not occur until mid-stage 5 (Haigo and Bilder, 2011), younger follicles did exhibit some signs of movement, although not convincingly in one direction (Figure 2.1, blue dashed line). It also remained unclear whether these young follicle movements were due to twisting of the anterior tip of the ovariole, which has been observed in several time-lapse movies (data not shown). These early, uncoordinated follicle movements are consistent with the presence of actin filaments on the basal surface that have yet to exhibit tissue polarity and the presence of a non-fibrillar basement membrane, and may reflect early isotropic growth of follicles during stages 1 to 4 of oogenesis. However, a sudden pulse of Delta signaling from the germline at stage 5 may be sufficient to transiently enable follicle cells to coordinate movement in a circumferential direction orthogonal to the A-P axis, committing to one chiral orientation or the other by random chance, manifested by the monopolar orientation of actin protrusions on the leading edge and the emergence of monopolar localization of non-muscle myosin II on the lagging edge. Planar mechanotransduction through the follicle basement membrane can rapidly amplify and reinforce the direction of movement started by the initial polarizing event. Notch/Delta signaling has been involved in many binary cell fate decisions (Axelrod, 2010; Fortini, 2009), so it is not far reaching to speculate that a similar binary switch may be used in the follicle to trigger follicle PCP and polarized follicle rotation, that is quickly reinforced and amplified by cell-matrix interactions to propagate global tissue polarity in the *Drosophila* follicle. Moreover, that many morphogenetic processes during *Drosophila* oogenesis require cross-talk between the germline and soma increase the support for Delta germline signaling as a potential polarizing source for follicle PCP. Whether the initial break in symmetry is mediated by a feedback loop as seen in lateral inhibition of other tissues, or why symmetry is broken orthogonal to the A-P axis are unclear, but the latter may coincide with other signaling events that are patterning the follicle epithelium along with Notch/Delta signaling during this

critical stage of oogenesis. It also remains unclear how this proposed Notch/Delta signaling interfaces with the proposed global tissue polarity regulator function ascribed to Fat2. It is apparent that much work remains to be done regarding the source of follicle PCP and it will be a very interesting active area of future research.

4.4.3 Concluding remarks: an emerging cellular and molecular framework for the elongation of the Drosophila egg

I hope that the results and discussion enclosed within this dissertation provide a new framework to think about the cellular and molecular mechanisms underlying tissue elongation of the developing egg (Figure 4.4). At the start of my dissertation, we did not have a defined phase of follicle elongation during oogenesis. We did not know the molecular mechanism underlying the necessity of cell-matrix genes in the control of *Drosophila* egg shape. As my dissertation now ends, we have identified a novel morphogenetic behavior – polarized global tissue rotation – that builds an oriented fibrillar ECM corset to constrain circumferential growth and promote elongation of the developing egg along the A-P axis. We have explored how this unexpected behavior fits in with conventional behaviors that elongate developing tissues. We learned about the challenges of working with a three-dimensional epithelial chamber but through it all, have made progress towards a cellular understanding of the behaviors underlying follicle elongation. We can place the requirement of cell-matrix genes and planar polarity of basal actin filaments with a requirement for collective cell migration of the follicle epithelium during global tissue rotation. We have thus provided new insights to a relatively simple, but age-old question of how one generates an ellipsoid shaped egg.

Some of our findings challenge current perspectives on metazoan morphogenesis. Global tissue rotation is a novel polarized morphogenetic behavior required for tissue elongation and is the first collective cell migration with an obvious individual cell polarity and tissue polarity, but with no obvious collective cell polarity with leader and follower cells. The relatively concomitant emergence of molecular PCP with the onset of global tissue rotation raises the possibility that different mechanisms of PCP establishment and propagation may occur in different tissues. Thus, it is a prime time to study the mechanisms underlying *Drosophila* egg elongation, and future studies will continue to expand our understanding of tissue polarity, morphogenesis and development in all metazoans.

4.5 Materials & Methods

Drosophila genetics

The following stocks were used: *lqf^{L71}FRT80B, hs::FLP;;ovo^{D1} FRT80B* (Windler and Bilder, 2010), *sqh^{AX3}; sqh-GFP* (also known as RLC-GFP or Sqh-GFP) (Royou et al., 2004), *miR279-Stinger* was a gift from E. Lai (Sloan-Kettering). GFP protein traps in *vkg* (CC00791), *trol* (CA06698) (Buszczak et al., 2007) and GFP enhancer traps (Kelso et al., 2004; Quinones-Coello et al., 2007) were obtained from L. Cooley and M. Buszczak. Germline mutant clones were generated as previously described (Windler and Bilder, 2010) with two hour heat shocks at 37ºC for two consecutive days of L1-L3 larvae. All crosses were performed at 25 ºC and adult females were fed on an abundant yeast diet for 2-7 days prior to dissection.

Experimental Genotypes:

Figure 4.1:

A-C. *sqh^{AX3}; sqh-GFP*
D-F. *y w; vkg-GFP*
G, I. *y w trol-GFP*
H. *y w trol-GFP/w; ubi::EGFP FRT40A; GR1::GAL4 UAS-FLP/+*

Figure 4.2:

C. *w peb::GFP(YB0041)*
D. *w;; emc::GFP (YB0067)*
E. *w; Sin3A::GFP;+ (P01869)*

Figure 4.3:

A-E. *y w hs::FLP;; lqf^{L71} FRT80B/ovo^{D1} FRT80B*
B. *w; miR279-Stinger/+; indy-GFP/+*

Movie 4.1

y w hs::FLP;; lqf^{L71} FRT80B/ovo^{D1} FRT80B (GFP negative follicles)
w; miR279-Stinger/+; indy-GFP/+ (GFP positive follicles used as control genotype)

Fixation & Immunohistochemistry

All follicles were manually dissected from the epithelial muscle sheath as described (Prasad et al., 2007) to preserve follicle shape in Schneider's *Drosophila* medium (GIBCO) and fixed within 15 minutes using 4% formaldehyde in Schnieder's *Drosophila* medium supplemented with phalloidin (see below for dilution) to preserve basal F-actin structures in the follicle epithelium. F-actin was visualized using phalloidin-TRITC (1:500, Sigma) or phalloidin-AlexaFluor 647 (1:30, Molecular Probes).

Ex vivo follicle culture

Live imaging of cultured follicles were performed largely as described (Prasad et al., 2007) with the following modification. For egg chamber mounting, a 18x18 mm #1 cover glass (Fisher Sci.) was cushioned using high vacuum grease (Dow Corning) and gently placed over dissected follicles in 30 µl of culturing medium to reduce the working distance required for use with certain objective lenses.

Microscopy
Fixed and live time-lapse images were acquired on a TCS SL (Leica) using 16x/NA 0.5, 40x/NA 1.25 or 63x/NA 1.4 oil immersion lenses, or an Axio Imager.M1 (Zeiss) using 10x/NA 0.3 air objective lens. For time-lapse imaging, 5 minute time points were acquired with a single xy plane.

Data Analysis
All experiments in this chapter are preliminary and have low sample sizes. Some experiments have only been performed on 1 experimental date. Images were processed and assembled using Creative Suite 4 (Adobe) and Image J.

Figure 4.1
Molecular PCP in the *Drosophila* follicle emerges at stage 5.

(**A-C**) The myosin II regulatory light chain (MRLC-GFP; green) exhibit localization patterns similar to F-actin. MRLC-GFP is present as puncta and fibrils at the basal surface of stage 4 follicles, but begin to show monopolar orientation at stage 5 (arrows). Clear monopolar enrichment in individual follicle cells exhibit a clear circumferential orientation by stage 6 (**C**). F-actin (red) outlines follicle cell membrane. Collagen IV-GFP (**D-F**) and Perlecan-GFP (**G-I**) form discrete puncta (asterisks) at early stages that begin to mature into elongate fibrils at stage 5 (arrows). Polarized fibrils are clearly apparent by stage 6. (**A-I**) 10μm.

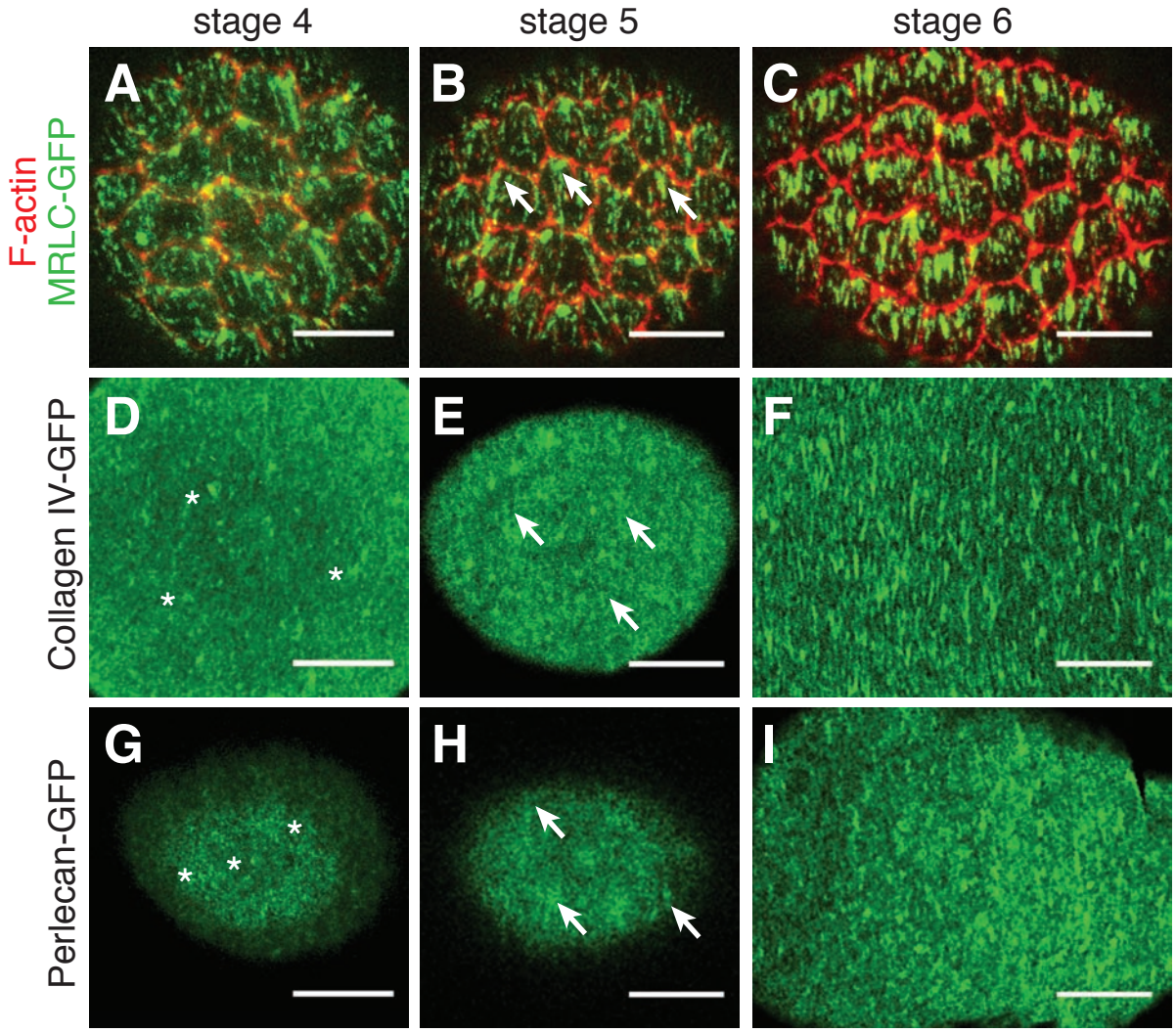
stage 4
stage 5
stage 6
F-actin
MRLC-GFP
Collagen IV-GFP
Perlecan-GFP
A
B
C
D
E
F
G
H
I

Figure 4.2
***In silico* enhancer trap screen for putative signaling pathways and other genes that may be involved in follicle planar polarity and the onset of polarized follicle rotation .**

(**A**) Diagram depicting GFP enhancer traps in the Flytrap collection. A P element containing GFP exon flanked by splice acceptor and splice donor sites (green triangle) in close proximity to a gene's 5' transcription start site (black arrow) can result in transcription of the P element transposase and GFP. GFP expression occurs from translation initiation using a Met initiation codon from the transposase within the P element. (**B**) 18 GFP enhancer trap lines selected for dynamic expression patterns during the early elongation phase of oogenesis. (**C-E**) GFP enhancer trap expression is validated in representative lines shown here. **(A**) adapted from (Kelso et al., 2004).

A

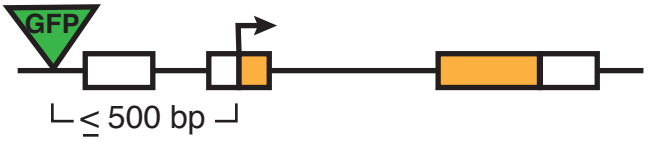

B

Flytrap Line	Enhancer trap location	Flytrap Line	Enhancer trap location
P01432	*Sema-1a/CG18405 (2L)*	YB0144	*Atg13/CG7331 (3R)*
P01869	***Sin3A/CG8815 (2R)***	YB0217	***emc/CG1007 (3L)***
YB0018	***inx2/CG4590 (X)***	YB0242	*meso18E/CG14233 (X)*
YB0031	***inx2/CG4590 (X)***	YB0295	*Jupiter/CG31363 (3R)*
YB0040	***emc/CG1007 (3L)***	YD0178	*ci/CG2125 (4)*
YB0041	***peb/CG12212 (X)***	YD0415	***stg/CG1395 (3R)***
YB0058	***Sin3A/CG8815 (2R)***	YD0614	*scyl/CG7590 (3L)*
YB0067	***emc/CG1007 (3L)***	ZCL1408	*CG32676 (X)*
YB0141	***Dl/CG3619 (3R)***	ZCL2879	*Pka-R2/CG15862 (2R)*

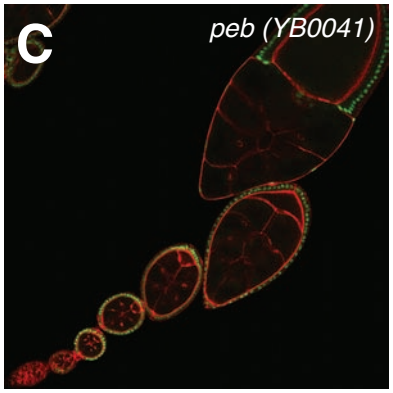

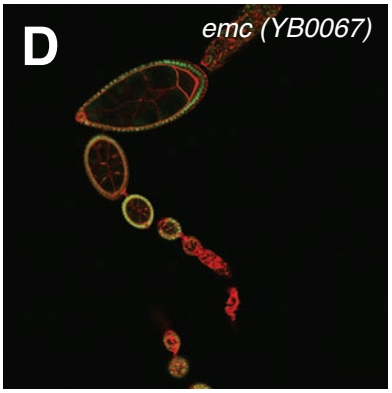

Figure 4.3
***lqf* germline clones show defects in follicle shape, exhibit off-axis rotation, and perturbations in basal actin protrusions and global tissue polarity.**

(**A**) *lqf* germline clones show defects in follicle shape. F-actin (cyan). (**B**) Live imaging of *lqf* germline clones (GFP negative) show off-axis rotation. Note that controls (GFP positive) undergo normal polarized global rotation. Numbers mark internal nurse cell nuclei for tracking over time. The transparency of the number indicates its relative depth, where an increase in opacity indicates the nucleus is closer to the surface of the viewing plane. (C-E) Basal microfilament organization in *lqf* germline clones. Note misorientation of basal actin protrusions, bipolar protrusions at given cell-cell interfaces, and off-axis orientation of actin filaments relative to the follicle A-P axis. F-actin (cyan). Frames for (**B**) taken from Movie 4.1. Scale in (**A-B**) 10μm; (**C**) 25 μm.

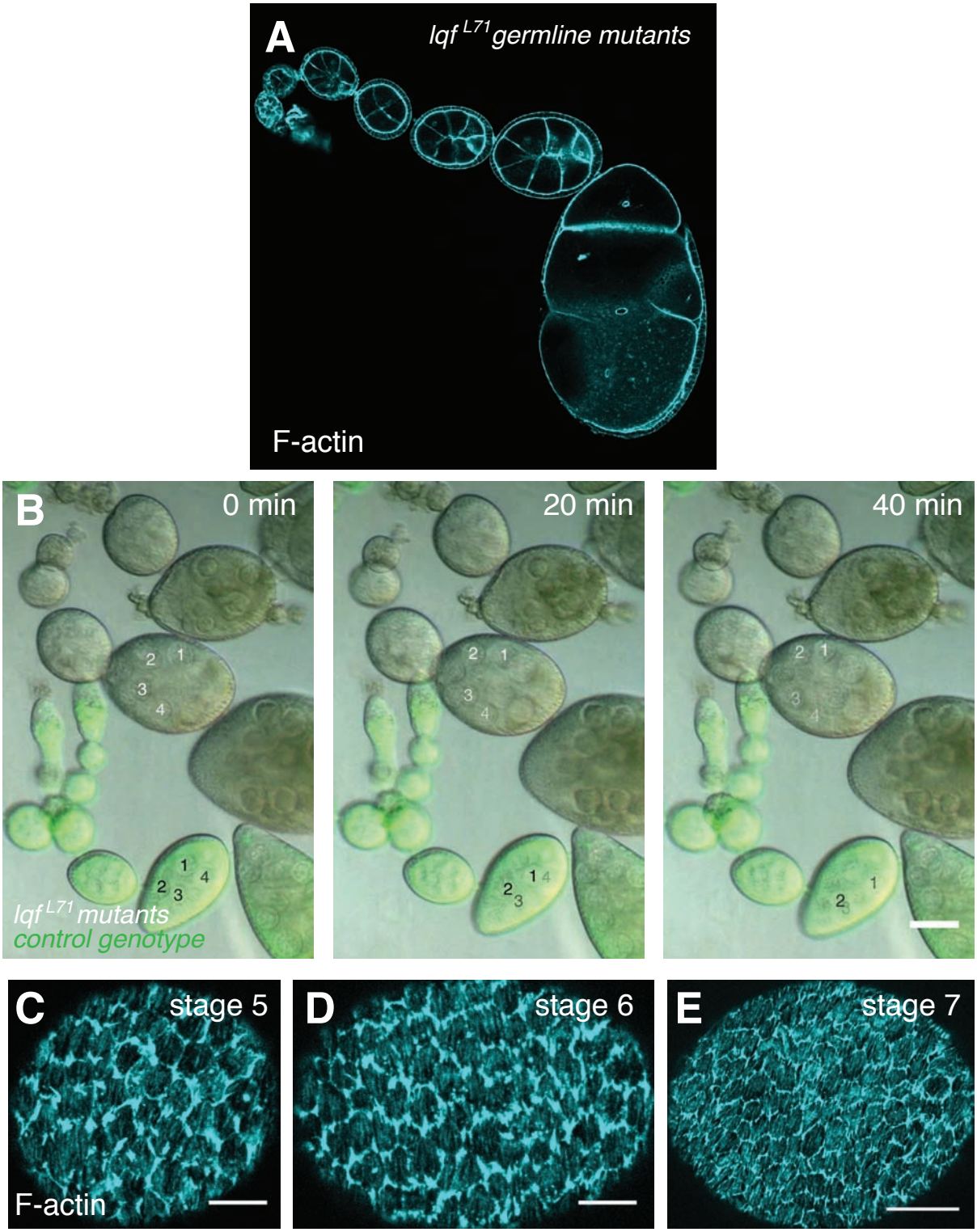
A
lqf L71 germline mutants
F-actin
B
0 min
20 min
40 min
lqf L71 mutants
control genotype
C
stage 5
F-actin
D
stage 6
E
stage 7

Figure 4.4
Working model for the cellular and molecular regulation of *Drosophila* egg elongation.

We update our current understanding of *Drosophila* oogenesis (**A-B**) with the incorporation of follicle elongation (magenta). The major phase of follicle elongation occurs from stage 5-9 and accounts for 74% of total elongation (solid line). (**C**) The discovery of global tissue rotation (lavender) and its function to build a polarized fibrillar ECM (green) is thought to account for the majority of follicle elongation. Other potential morphogenetic behaviors are included in parentheses. It is thought a critical polarizing cue to establish follicle PCP and trigger the onset of global tissue rotation occurs at stage 5 (red arrow). Genes encoding published round egg mutants or putative candidate genes thought to regulate other key events are color matched with their proposed function in (**B**). (**A-B**) adapted from (Horne-Badovinac and Bilder, 2005).

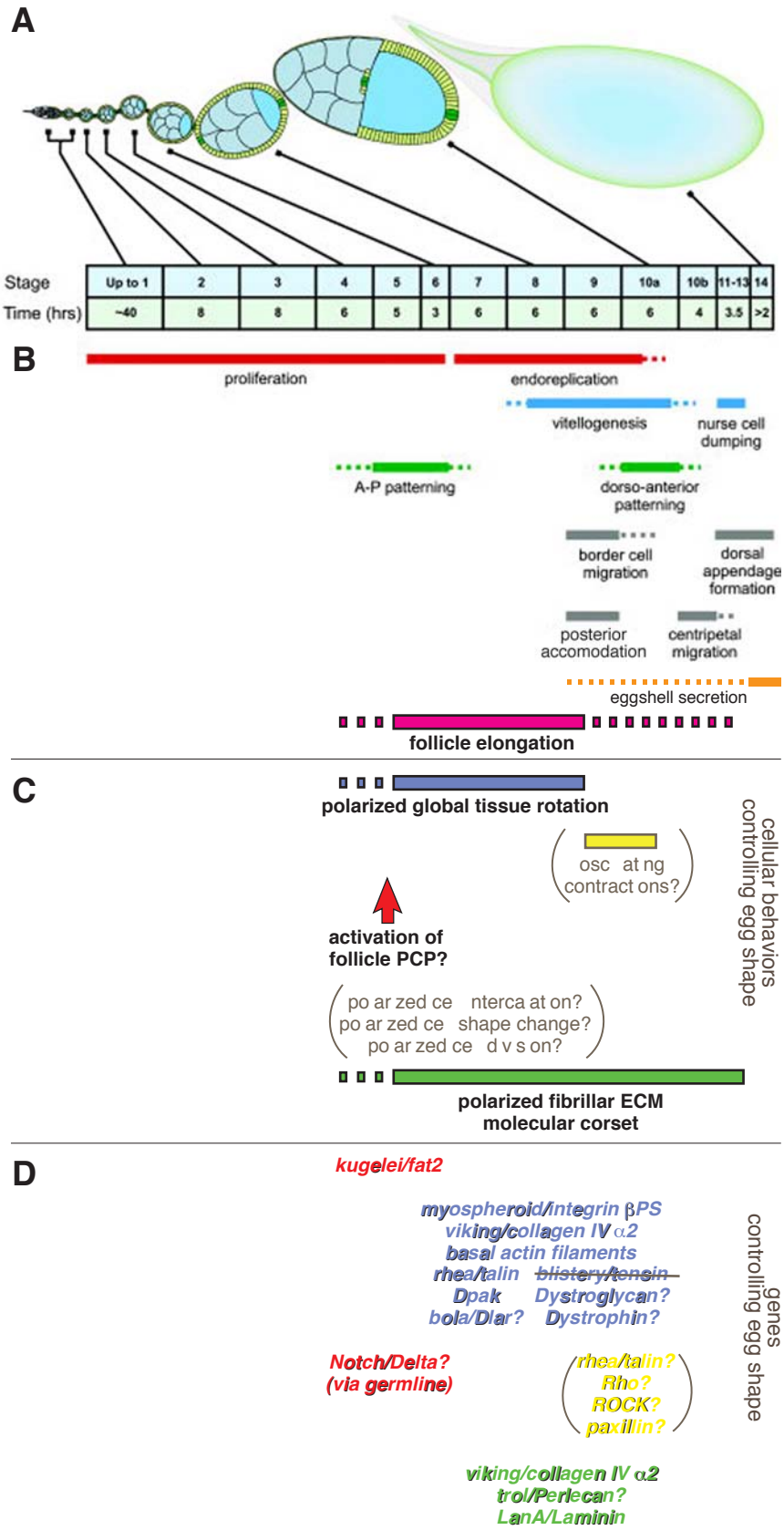
A
Stage
Time (hrs)
Up to 1
~40
2
8
3
8
4
6
5
5
6
3
7
6
8
6
9
6
10a
6
10b
4
11-13
3.5
14
>2
B
proliferation
endoreplication
vitellogenesis
nurse cell dumping
A-P patterning
dorso-anterior patterning
border cell migration
dorsal appendage formation
posterior accomodation
centripetal migration
eggshell secretion
follicle elongation
C
polarized global tissue rotation
osc at ng contract ons?
activation of follicle PCP?
po ar zed ce nterca at on?
po ar zed ce shape change?
po ar zed ce d v s on?
polarized fibrillar ECM molecular corset
cellular behaviors controlling egg shape
D
kugelei/fat2
myospheroid/integrin βPS
viking/collagen IV α2
basal actin filaments
rhea/talin
blistery/tensin
Dpak
Dystroglycan?
bola/Dlar?
Dystrophin?
Notch/Delta?
(via germline)
rhea/talin?
Rho?
ROCK?
paxillin?
viking/collagen IV α2
trol/Perlecan?
LanA/Laminin
genes controlling egg shape

References

Adams, D. S., Keller, R. and Koehl, M. A. R. (1990). The Mechanics of Notochord Elongation, Straightening and Stiffening in the Embryo of Xenopus-Laevis. *Development* **110**, 115-130.

Aigouy, B., Farhadifar, R., Staple, D. B., Sagner, A., Roper, J. C., Julicher, F. and Eaton, S. (2010). Cell flow reorients the axis of planar polarity in the wing epithelium of Drosophila. *Cell* **142**, 773-86.

Almuedo-Castillo, M., Salo, E. and Adell, T. (2011). Dishevelled is essential for neural connectivity and planar cell polarity in planarians. *Proceedings of the National Academy of Sciences of the United States of America* **108**, 2813-2818.

Andrew, D. and Ewald, A. (2010). Morphogenesis of epithelial tubes: Insights into tube formation, elongation, and elaboration. *Dev Biol* **341**, 34-55.

Assa-Kunik, E., Torres, I. L., Schejter, E. D., St Johnston, D. and Shilo, B. Z. (2007). Drosophila follicle cells are patterned by multiple levels of Notch signaling and antagonism between the Notch and JAK/STAT pathways. *Development* **134**, 1161-1169.

Axelrod, J. D. (2009). Progress and challenges in understanding planar cell polarity signaling. *Semin Cell Dev Biol* **20**, 964-71.

Axelrod, J. D. (2010). Delivering the lateral inhibition punchline: it's all about the timing. *Sci Signal* **3**, pe38.

Axelrod, J. D., Miller, J. R., Shulman, J. M., Moon, R. T. and Perrimon, N. (1998). Differential recruitment of Dishevelled provides signaling specificity in the planar cell polarity and Wingless signaling pathways. *Genes & Development* **12**, 2610-2622.

Baena-Lopez, L. A., Baonza, A. and Garcia-Bellido, A. (2005). The orientation of cell divisions determines the shape of Drosophila organs. *Curr Biol* **15**, 1640-4.

Bastock, R. and St Johnston, D. (2008). Drosophila oogenesis. *Current Biology* **18**, R1082-R1087.

Bastock, R. and Strutt, D. (2007). The planar polarity pathway promotes coordinated cell migration during Drosophila oogenesis. *Development* **134**, 3055-64.

Bateman, J., Reddy, R., Saito, H. and Van Vactor, D. (2001). The receptor tyrosine phosphatase Dlar and integrins organize actin filaments in the Drosophila follicular epithelium. *Curr Biol* **11**, 1317-27.

Becam, I., Tanentzapf, G., Lepesant, J., Brown, N. and Huynh, J. (2005). Integrin-independent repression of cadherin transcription by talin during axis formation in Drosophila. *Nat Cell Biol* **7**, 510-6.

Bertet, C., Sulak, L. and Lecuit, T. (2004). Myosin-dependent junction remodelling controls planar cell intercalation and axis elongation. *Nature* **429**, 667-71.

Bianco, A., Poukkula, M., Cliffe, A., Mathieu, J., Luque, C., Fulga, T. and Rorth, P. (2007). Two distinct modes of guidance signalling during collective migration of border cells. *Nature* **448**, 362-5.

Blanchard, G. B., Kabla, A. J., Schultz, N. L., Butler, L. C., Sanson, B., Gorfinkiel, N., Mahadevan, L. and Adams, R. J. (2009). Tissue tectonics: morphogenetic strain rates, cell shape change and intercalation. *Nat Methods* **6**, 458-64.

Blankenship, J. T. (2006). Multicellular rosette formation links planar cell polarity to tissue morphogenesis. *Dev Cell* **11**, 459-70.

Bozec, L., van der Heijden, G. and Horton, M. (2007). Collagen fibrils: nanoscale ropes. *Biophys J* **92**, 70-5.

Brittle, A. L., Repiso, A., Casal, J., Lawrence, P. A. and Strutt, D. (2010). Four-Jointed Modulates Growth and Planar Polarity by Reducing the Affinity of Dachsous for Fat. *Current Biology* **20**, 803-810.

Brown, N. H. (2000). An integrin chicken and egg problem: which comes first, the extracellular matrix or the cytoskeleton? *Curr Opin Cell Biol* **12**, 629-33.

Brown, N. H., Gregory, S. L., Rickoll, W. L., Fessler, L. I., Prout, M., White, R. A. and Fristrom, J. W. (2002). Talin is essential for integrin function in Drosophila. *Dev Cell* **3**, 569-79.

Buszczak, M., Paterno, S., Lighthouse, D., Bachman, J., Planck, J., Owen, S., Skora, A. D., Nystul, T. G., Ohlstein, B., Allen, A. et al. (2007). The carnegie protein trap library: a versatile tool for Drosophila developmental studies. *Genetics* **175**, 1505-31.

Butler, L., Blanchard, G. B., Kabla, A., Lawrence, N., Welchman, D., Mahadevan, L., Adams, R. and Sanson, B. (2009). Cell shape changes indicate a role for extrinsic tensile forces in Drosophila germ-band extension. *Nat Cell Biol* **11**, 859-64.

Caddy, J., Wilanowski, T., Darido, C., Dworkin, S., Ting, S. B., Zhao, Q. A., Rank, G., Auden, A., Srivastava, S., Papenfuss, T. A. et al. (2010). Epidermal Wound Repair Is Regulated by the Planar Cell Polarity Signaling Pathway (vol 19, pg 138, 2010). *Developmental Cell* **19**, 353-353.

Cant, K., Knowles, B. A., Mooseker, M. S. and Cooley, L. (1994). Drosophila Singed, a Fascin Homolog, Is Required for Actin Bundle Formation during Oogenesis and Bristle Extension. *Journal of Cell Biology* **125**, 369-380.

Chen, W. S., Antic, D., Matis, M., Logan, C. Y., Povelones, M., Anderson, G. A., Nusse, R. and Axelrod, J. D. (2008). Asymmetric homotypic interactions of the atypical cadherin Flamingo mediate intercellular polarity signaling. *Cell* **133**, 1093-1105.

Chen, X. and Gumbiner, B. M. (2006). Crosstalk between different adhesion molecules. *Current Opinion in Cell Biology* **18**, 572-578.

Chuong, C. M. and Richardson, M. K. (2009). Pattern formation today. *Int J Dev Biol* **53**, 653-8.

Classen, A. K., Anderson, K. I., Marois, E. and Eaton, S. (2005). Hexagonal packing of Drosophila wing epithelial cells by the planar cell polarity pathway. *Dev Cell* **9**, 805-17.

Clay, M. R. and Halloran, M. C. (2011). Regulation of cell adhesions and motility during initiation of neural crest migration. *Curr Opin Neurobiol* **21**, 17-22.

Collier, S. and Gubb, D. (1997). Drosophila tissue polarity requires the cell-autonomous activity of the fuzzy gene, which encodes a novel transmembrane protein. *Development* **124**, 4029-4037.

Colognato, H., Winkelmann, D. A. and Yurchenco, P. D. (1999). Laminin polymerization induces a receptor-cytoskeleton network. *J Cell Biol* **145**, 619-31.

Concha, M. L. and Adams, R. J. (1998). Oriented cell divisions and cellular morphogenesis in the zebrafish gastrula and neurula: a time-lapse analysis. *Development* **125**, 983-94.

Conder, R., Yu, H., Zahedi, B. and Harden, N. (2007). The serine/threonine kinase dPak is required for polarized assembly of F-actin bundles and apical-basal polarity in the Drosophila follicular epithelium. *Dev Biol* **305**, 470-82.

Cooley, L., Verheyen, E. and Ayers, K. (1992). Chickadee Encodes a Profilin Required for Intercellular Cytoplasm Transport during Drosophila Oogenesis. *Cell* **69**, 173-184.

Cortes, F., Daggett, D., Bryson-Richardson, R. J., Neyt, C., Maule, J., Gautier, P., Hollway, G. E., Keenan, D. and Currie, P. D. (2003). Cadherin-mediated differential cell adhesion controls slow muscle cell migration in the developing zebrafish myotome. *Developmental Cell* **5**, 865-876.

Cramer, L. P. (2010). Forming the cell rear first: breaking cell symmetry to trigger directed cell migration. *Nature Cell Biology* **12**, 628-632.

da Silva, S. M. and Vincent, J. P. (2007). Oriented cell divisions in the extending germband of Drosophila. *Development* **134**, 3049-54.

Davidson, L. A., Dzamba, B. D., Keller, R. and Desimone, D. W. (2008). Live Imaging of Cell Protrusive Activity, and Extracellular Matrix Assembly and Remodeling During Morphogenesis in the Frog, Xenopus laevis. *Developmental Dynamics* **237**, 2684-2692.

Davidson, L. A., Marsden, M., Keller, R. and Desimone, D. W. (2006). Integrin alpha5beta1 and fibronectin regulate polarized cell protrusions required for Xenopus convergence and extension. *Curr Biol* **16**, 833-44.

Dej, K. J. and Spradling, A. C. (1999). The endocycle controls nurse cell polytene chromosome structure during Drosophila oogenesis. *Development* **126**, 293-303.

Delon, I. and Brown, N. (2009). The integrin adhesion complex changes its composition and function during morphogenesis of an epithelium. *J Cell Sci* **122**, 4363-74.

Delwig, A. and Rand, M. D. (2007). Loss-of-function in the Delta(RF) allele is due to a failure of the delta protein to reach the cell surface. *Fly* **1**, 190-193.

Deng, W. M., Schneider, M., Frock, R., Castillejo-Lopez, C., Gaman, E. A., Baumgartner, S. and Ruohola-Baker, H. (2003). Dystroglycan is required for polarizing the epithelial cells and the oocyte in Drosophila. *Development* **130**, 173-84.

Duffy, J., Harrison, D. and Perrimon, N. (1998). Identifying loci required for follicular patterning using directed mosaics. *Development* **125**, 2263-71.

Elgar, M. A. and Heaphy, L. J. (1989). Covariation between Clutch Size, Egg Weight and Egg Shape - Comparative Evidence for Chelonians. *Journal of Zoology* **219**, 137-152.

Elul, T. and Keller, R. (2000). Monopolar protrusive activity: A new morphogenic cell behavior in the neural plate dependent on vertical interactions with the mesoderm in Xenopus. *Developmental Biology* **224**, 3-19.

Elul, T., Koehl, M. A. R. and Keller, R. (1997). Cellular mechanism underlying neural convergent extension in Xenopus laevis embryos. *Developmental Biology* **191**, 243-258.

Ettensohn, C. A. (1985). Gastrulation in the Sea-Urchin Embryo Is Accompanied by the Rearrangement of Invaginating Epithelial-Cells. *Developmental Biology* **112**, 383-390.

Ewald, A. J., Brenot, A., Duong, M., Chan, B. S. and Werb, Z. (2008). Collective epithelial migration and cell rearrangements drive mammary branching morphogenesis. *Dev Cell* **14**, 570-81.

Farhadifar, R., Roper, J. C., Algouy, B., Eaton, S. and Julicher, F. (2007). The influence of cell mechanics, cell-cell interactions, and proliferation on epithelial packing. *Current Biology* **17**, 2095-2104.

Fernandez-Minan, A., Martin-Bermudo, M. D. and Gonzalez-Reyes, A. (2007). Integrin signaling regulates spindle orientation in Drosophila to preserve the follicular-epithelium monolayer. *Curr Biol* **17**, 683-8.

Fortini, M. E. (2009). Notch signaling: the core pathway and its posttranslational regulation. *Dev Cell* **16**, 633-47.

Friedl, P. and Gilmour, D. (2009). Collective cell migration in morphogenesis, regeneration and cancer. *Nat Rev Mol Cell Biol* **10**, 445-57.

Frydman, H. and Spradling, A. (2001). The receptor-like tyrosine phosphatase lar is required for epithelial planar polarity and for axis determination within drosophila ovarian follicles. *Development* **128**, 3209-20.

Gibson, M. C., Patel, A. B., Nagpal, R. and Perrimon, N. (2006). The emergence of geometric order in proliferating metazoan epithelia. *Nature* **442**, 1038-1041.

Gilbert, A. B. (1979). Female genital organs. In *Form and Function in Birds*, vol. 1 (ed. A. S. King and J. McLelland), pp. 237-360. London: Academic Press Inc.

Gong, Y., Mo, C. and Fraser, S. (2004). Planar cell polarity signalling controls cell division orientation during zebrafish gastrulation. *Nature* **430**, 689-93.

Gonzalez-Reyes, A., Elliott, H. and St Johnston, D. (1995). Polarization of Both Major Body Axes in Drosophila by Gurken-Torpedo Signaling. *Nature* **375**, 654-658.

Gonzalez-Reyes, A. and St Johnston, D. (1994). Role of Oocyte Position in Establishment of Anterior-Posterior Polarity in Drosophila. *Science* **266**, 639-642.

Gonzalez-Reyes, A. and St Johnston, D. (1998). Patterning of the follicle cell epithelium along the anterior-posterior axis during Drosophila oogenesis. *Development* **125**, 2837-46.

Grammont, M. (2007). Adherens junction remodeling by the Notch pathway in Drosophila melanogaster oogenesis. *J Cell Biol* **177**, 139-50.

Grammont, M. and Irvine, K. D. (2002). Organizer activity of the polar cells during Drosophila oogenesis. *Development* **129**, 5131-5140.

Grant, P. R. (1982). Variation in the size and shape of Darwin's finch eggs. *The Auk* **99**, 15-23.

Guan, X., Middlebrooks, B. W., Alexander, S. and Wasserman, S. A. (2006). Mutation of TweedleD, a member of an unconventional cuticle protein family, alters body shape in Drosophila. *Proc Natl Acad Sci U S A* **103**, 16794-9.

Gubb, D. and Garcia-Bellido, A. (1982). A Genetic-Analysis of the Determination of Cuticular Polarity during Development in Drosophila-Melanogaster. *Journal of Embryology and Experimental Morphology* **68**, 37-57.

Gumbiner, B. M. (2005). Regulation of cadherin-mediated adhesion in morphogenesis. *Nature Reviews Molecular Cell Biology* **6**, 622-634.

Gupta, T. and Schupbach, T. (2003). Cct1, a phosphatidylcholine biosynthesis enzyme, is required for Drosophila oogenesis and ovarian morphogenesis. *Development* **130**, 6075-87.

Gutzeit, H. (1990). The microfilament pattern in the somatic follicle cells of mid-vitellogenic ovarian follicles of Drosophila. *Eur J Cell Biol* **53**, 349-56.

Gutzeit, H. (1992). Organization and in vitro activity of microfilament bundles associated with the basement membrane of Drosophila follicles. *Acta Histochem Suppl* **41**, 201-210.

Gutzeit, H., Eberhardt, W. and Gratwohl, E. (1991). Laminin and basement membrane-associated microfilaments in wild-type and mutant Drosophila ovarian follicles. *J Cell Sci* **100**, 781-8.

Gutzeit, H. and Haas-Assenbaum, A. (1991). The somatic envelopes around the germ-line cells of polytrophic insect follicles: structural and functional aspects. *Tissue Cell* **23**, 853-65.

Gutzeit, H. O. (1980). YOLK SYNTHESIS IN OVARIAN FOLLICLES OF DROSOPHILA. *Wilhelm Rouxs Archives of Developmental Biology* **189**, 221-224.

Gutzeit, H. O. (1986). THE ROLE OF MICROFILAMENTS IN CYTOPLASMIC STREAMING IN DROSOPHILA FOLLICLES. *Journal of Cell Science* **80**, 159-169.

Gutzeit, H. O. and Gehring, W. J. (1979). LOCALIZED SYNTHESIS OF SPECIFIC PROTEINS DURING OOGENESIS AND EARLY EMBRYOGENESIS IN DROSOPHILA-MELANOGASTER. *Wilhelm Rouxs Archives of Developmental Biology* **187**, 151-165.

Gutzeit, H. O., Vonseydlitzkurzbach, E. and Neuschroer, R. (1993). How Drosophila (Diptera, Drosophilidae) Follicles Become Spatially Organized and Obtain Their Ovoid Shape. *International Journal of Insect Morphology & Embryology* **22**, 335-347.

Haas, P. and Gilmour, D. (2006). Chemokine signaling mediates self-organizing tissue migration in the zebrafish lateral line. *Dev Cell* **10**, 673-80.

Haigo, S. L. and Bilder, D. (2011). Global tissue revolutions in a morphogenetic movement controlling elongation. *Science* **331**, 1071-4.

Halder, G. and Johnson, R. L. (2011). Hippo signaling: growth control and beyond. *Development* **138**, 9-22.

Hammerschmidt, M., Pelegri, F., Mullins, M. C., Kane, D. A., Brand, M., vanEeden, F. J. M., FurutaniSeiki, M., Granato, M., Haffter, P., Heisenberg, C. P. et al. (1996). Mutations

affecting morphogenesis during gastrulation and tail formation in the zebrafish, Danio rerio. *Development* **123**, 143-151.

Hardin, J. (1989). Local Shifts in Position and Polarized Motility Drive Cell Rearrangement during Sea-Urchin Gastrulation. *Developmental Biology* **136**, 430-445.

Hardin, J. D. and Cheng, L. Y. (1986). The Mechanisms and Mechanics of Archenteron Elongation during Sea-Urchin Gastrulation. *Developmental Biology* **115**, 490-501.

Hartenstein, V. and Camposortega, J. A. (1985). Fate-Mapping in Wild-Type Drosophila-Melanogaster .1. The Spatio-Temporal Pattern of Embryonic-Cell Divisions. *Wilhelm Rouxs Archives of Developmental Biology* **194**, 181-195.

He, L., Wang, X. B., Tang, H. L. and Montell, D. J. (2010). Tissue elongation requires oscillating contractions of a basal actomyosin network. *Nature Cell Biology* **12**, 1133-U40.

Heisenberg, C. P., Tada, M., Rauch, G. J., Saude, L., Concha, M. L., Geisler, R., Stemple, D. L., Smith, J. C. and Wilson, S. W. (2000). Silberblick/Wnt11 mediates convergent extension movements during zebrafish gastrulation. *Nature* **405**, 76-81.

Herlands, R. L. and Bode, H. R. (1974). Nematocyte Migration in Hydra Influenced by Tissue Polarity. *Nature* **248**, 387-390.

Horne-Badovinac, S. and Bilder, D. (2005). Mass transit: epithelial morphogenesis in the Drosophila egg chamber. *Dev Dyn* **232**, 559-74.

Huisken, J. and Stainier, D. Y. R. (2009). Selective plane illumination microscopy techniques in developmental biology. *Development* **136**, 1963-1975.

Irvine, K. and Wieschaus, E. (1994). Cell intercalation during Drosophila germband extension and its regulation by pair-rule segmentation genes. *Development* **120**, 827-41.

Johnstone, I. L. (1994). The cuticle of the nematode Caenorhabditis elegans: a complex collagen structure. *Bioessays* **16**, 171-8.

Jordan, K. C., Schaeffer, V., Fischer, K. A., Gray, E. E. and Ruohola-Baker, H. (2006). Notch signaling through Tramtrack bypasses the mitosis promoting activity of the JNK pathway in the mitotic-to-endocycle transition of Drosophila follicle cells. *Bmc Developmental Biology* **6**, -.

Kametani, Y. and Takeichi, M. (2007). Basal-to-apical cadherin flow at cell junctions. *Nature Cell Biology* **9**, 92-U118.

Keller, R. (2002). Shaping the vertebrate body plan by polarized embryonic cell movements. *Science* **298**, 1950-4.

Keller, R. (2006). Mechanisms of elongation in embryogenesis. *Development* **133**, 2291-302.

Keller, R., Davidson, L., Edlund, A., Elul, T., Ezin, M., Shook, D. and Skoglund, P. (2000). Mechanisms of convergence and extension by cell intercalation. *Philosophical Transactions of the Royal Society B-Biological Sciences* **355**, 897-922.

Keller, R., Shih, J. and Sater, A. (1992). The cellular basis of the convergence and extension of the Xenopus neural plate. *Dev Dyn* **193**, 199-217.

Keller, R. E. (1984). The Cellular Basis of Gastrulation in Xenopus-Laevis - Active, Postinvolution Convergence and Extension by Mediolateral Interdigitation. *American Zoologist* **24**, 589-603.

Keller, R. E., Danilchik, M., Gimlich, R. and Shih, J. (1985). The Function and Mechanism of Convergent Extension during Gastrulation of Xenopus-Laevis. *Journal of Embryology and Experimental Morphology* **89**, 185-209.

Kelso, R., Buszczak, M., Quinones, A., Castiblanco, C., Mazzalupo, S. and Cooley, L. (2004). Flytrap, a database documenting a GFP protein-trap insertion screen in Drosophila melanogaster. *Nucleic Acids Res* **32**, D418-20.

King, R. (1970). Ovarian Development in Drosophila melanogaster. New York: Academic Press.

King, R. C. and Vanoucek, E. G. (1960). Oogenesis in adult Drosophila melanogaster. X. Studies on the behavior of the follicle cells. *Growth* **24**, 333-338.

Kinoshita, N., Iioka, H., Miyakoshi, A. and Ueno, N. (2003). PKC delta is essential for Dishevelled function in a noncanonical Wnt pathway that regulates Xenopus convergent extension movements. *Genes & Development* **17**, 1663-1676.

Kochav, S. and Eyalgila, H. (1971). BILATERAL SYMMETRY IN CHICK EMBRYO DETERMINATION BY GRAVITY. *Science* **171**, 1027-29.

Koehl, M. A. R., Quillin, K. J. and Pell, C. A. (2000). Mechanical design of fiber-wound hydraulic skeletons: The stiffening and straightening of embryonic notochords. *American Zoologist* **40**, 28-41.

Kolahi, K. S., White, P. F., Shreter, D. M., Classen, A. K., Bilder, D. and Mofrad, M. R. (2009). Quantitative analysis of epithelial morphogenesis in Drosophila oogenesis: New insights based on morphometric analysis and mechanical modeling. *Dev Biol* **331**, 129-39.

Kondo, S. and Miura, T. (2010). Reaction-diffusion model as a framework for understanding biological pattern formation. *Science* **329**, 1616-20.

Larkin, M. K., Deng, W. M., Holder, K., Tworoger, M., Clegg, N. and Ruohola-Baker, H. (1999). Role of Notch pathway in terminal follicle cell differentiation during Drosophila oogenesis. *Development Genes and Evolution* **209**, 301-311.

Larue, L., Ohsugi, M., Hirchenhain, J. and Kemler, R. (1994). E-Cadherin Null Mutant Embryos Fail to Form a Trophectoderm Epithelium. *Proceedings of the National Academy of Sciences of the United States of America* **91**, 8263-8267.

Lawrence, P. A. (1966). Gradients in Insect Segment - Orientation of Hairs in Milkweed Bug Oncopeltus Fasciatus. *Journal of Experimental Biology* **44**, 607-&.

Lawrence, P. A. and Shelton, P. M. J. (1975). Determination of Polarity in Developing Insect Retina. *Journal of Embryology and Experimental Morphology* **33**, 471-486.

Lee, S., Cho, K., Kim, E. and Chung, J. (2003). blistery encodes Drosophila tensin protein and interacts with integrin and the JNK signaling pathway during wing development. *Development* **130**, 4001-10.

Lopez-Schier, H. and St Johnston, D. (2001). Delta signaling from the germ line controls the proliferation and differentiation of the somatic follicle cells during Drosophila oogenesis. *Genes Dev* **15**, 1393-405.

Ma, D., Amonlirdviman, K., Raffard, R. L., Abate, A., Tomlin, C. J. and Axelrod, J. D. (2008). Cell packing influences planar cell polarity signaling. *Proceedings of the National Academy of Sciences of the United States of America* **105**, 18800-18805.

Ma, D., Yang, C. H., McNeill, H., Simon, M. A. and Axelrod, J. D. (2003). Fidelity in planar cell polarity signalling. *Nature* **421**, 543-7.

Mahajanmiklos, S. and Cooley, L. (1994). The Villin-Like Protein Encoded by the Drosophila Quail Gene Is Required for Actin Bundle Assembly during Oogenesis. *Cell* **78**, 291-301.

Mangold, O. (1920). Fragen der regulation und Determination an umgeordneten Furchungsstadien und verschmolzenen Keimen von Triton. *Arch. EntwMech. Org.* **47**.

Mao, K. M., Murakami, A., Iwasawa, A. and Yoshizaki, N. (2007). The asymmetry of avian egg-shape: an adaptation for reproduction on dry land. *Journal of Anatomy* **210**, 741-748.

Margolis, J. and Spradling, A. (1995). Identification and behavior of epithelial stem cells in the Drosophila ovary. *Development* **121**, 3797-807.

Marsden, M. and DeSimone, D. W. (2003). Integrin-ECM interactions regulate cadherin-dependent cell adhesion and are required for convergent extension in Xenopus. *Current Biology* **13**, 1182-1191.

Millot, A. (1897-1904). "Oeufs" (Eggs), from Nouveau Larousse Illustré, (ed., pp. "Oeufs" (Eggs). Paris: Librarie Larousse.

Mirouse, V., Christoforou, C., Fritsch, C., St Johnston, D. and Ray, R. (2009). Dystroglycan and perlecan provide a basal cue required for epithelial polarity during energetic stress. *Dev Cell* **16**, 83-92.

Mitchison, T. J. and Cramer, L. P. (1996). Actin-based cell motility and cell locomotion. *Cell* **84**, 371-379.

Miyamoto, D. M. and Crowther, R. J. (1985). Formation of the Notochord in Living Ascidian Embryos. *Journal of Embryology and Experimental Morphology* **86**, 1-17.

Montell, D. J., Keshishian, H. and Spradling, A. C. (1991). Laser Ablation Studies of the Role of the Drosophila Oocyte Nucleus in Pattern-Formation. *Science* **254**, 290-293.

Montell, D. J., Rorth, P. and Spradling, A. C. (1992). slow border cells, a locus required for a developmentally regulated cell migration during oogenesis, encodes Drosophila C/EBP. *Cell* **71**, 51-62.

Morin, X., Daneman, R., Zavortink, M. and Chia, W. (2001). A protein trap strategy to detect GFP-tagged proteins expressed from their endogenous loci in Drosophila. *Proc Natl Acad Sci U S A* **98**, 15050-5.

Munro, E. M. and Odell, G. M. (2002). Polarized basolateral cell motility underlies invagination and convergent extension of the ascidian notochord. *Development* **129**, 13-24.

Nakayama, Y. and Kohno, K. (1974). Number and Polarity of Ependymal Cilia in Central Canal of Some Vertebrates. *Journal of Neurocytology* **3**, 449-458.

Nayal, A., Webb, D. J. and Horwitz, A. F. (2004). Talin: an emerging focal point of adhesion dynamics. *Current Opinion in Cell Biology* **16**, 94-98.

Neuman-Silberberg, F. S. and Schupbach, T. (1993). The Drosophila Dorsoventral Patterning Gene Gurken Produces a Dorsally Localized Rna and Encodes a Tgf-Alpha-Like Protein. *Cell* **75**, 165-174.

Niewiadomska, P., Godt, D. and Tepass, U. (1999). DE-cadherin is required for intercellular motility during Drosophila oogenesis. *Journal of Cell Biology* **144**, 533-547.

O'Reilly, A. M., Lee, H. H. and Simon, M. A. (2008). Integrins control the positioning and proliferation of follicle stem cells in the Drosophila ovary. *J Cell Biol* **182**, 801-15.

Orr, W. C., Galanopoulos, V. K., Romano, C. P. and Kafatos, F. C. (1989). A Female Sterile Screen of the Drosophila-Melanogaster X-Chromosome Using Hybrid Dysgenesis - Identification and Characterization of Egg Morphology Mutants. *Genetics* **122**, 847-858.

Overstreet, E., Fitch, E. and Fischer, J. A. (2004). Fat facets and liquid facets promote Delta endocytosis and Delta signaling in the signaling cells. *Development* **131**, 5355-5366.

Paredez, A., Somerville, C. and Ehrhardt, D. (2006). Visualization of cellulose synthase demonstrates functional association with microtubules. *Science* **312**, 1491-5.

Park, W. J., Liu, J., Sharp, E. J. and Adler, P. N. (1996). The Drosophila tissue polarity gene inturned acts cell autonomously and encodes a novel protein. *Development* **122**, 961-9.

Parthasarathy, R., Sheng, Z. T., Sun, Z. Y. and Palli, S. R. (2010). Ecdysteroid regulation of ovarian growth and oocyte maturation in the red flour beetle, Tribolium castaneum. *Insect Biochemistry and Molecular Biology* **40**, 429-439.

Poschl, E., Schlotzer-Schrehardt, U., Brachvogel, B., Saito, K., Ninomiya, Y. and Mayer, U. (2004). Collagen IV is essential for basement membrane stability but dispensable for initiation of its assembly during early development. *Development* **131**, 1619-28.

Poulton, J. S. and Deng, W. M. (2007). Cell-cell communication and axis specification in the Drosophila oocyte. *Developmental Biology* **311**, 1-10.

Prasad, M., Jang, A., Starz-Gaiano, M., Melani, M. and Montell, D. (2007). A protocol for culturing Drosophila melanogaster stage 9 egg chambers for live imaging. *Nat Protoc* **2**, 2467-73.

Prasad, M. and Montell, D. (2007). Cellular and molecular mechanisms of border cell migration analyzed using time-lapse live-cell imaging. *Dev Cell* **12**, 997-1005.

Quesada-Hernandez, E., Caneparo, L., Schneider, S., Winkler, S., Liebling, M., Fraser, S. E. and Heisenberg, C. P. (2010). Stereotypical cell division orientation controls neural rod midline formation in zebrafish. *Curr Biol* **20**, 1966-72.

Quinones-Coello, A. T., Petrella, L. N., Ayers, K., Melillo, A., Mazzalupo, S., Hudson, A. M., Wang, S., Castiblanco, C., Buszczak, M., Hoskins, R. A. et al. (2007). Exploring strategies for protein trapping in Drosophila. *Genetics* **175**, 1089-104.

Rauzi, M., Lenne, P. F. and Lecuit, T. (2010). Planar polarized actomyosin contractile flows control epithelial junction remodelling. *Nature* **468**, 1110-U515.

Ridley, A. J., Schwartz, M. A., Burridge, K., Firtel, R. A., Ginsberg, M. H., Borisy, G., Parsons, J. T. and Horwitz, A. R. (2003). Cell migration: Integrating signals from front to back. *Science* **302**, 1704-1709.

Robinson, D. N. and Cooley, L. (1997). Examination of the function of two kelch proteins generated by stop codon suppression. *Development* **124**, 1405-1417.

Rodriguez, A., Zhou, Z., Tang, M., Meller, S., Chen, J., Bellen, H. and Kimbrell, D. (1996). Identification of immune system and response genes, and novel mutations causing melanotic tumor formation in Drosophila melanogaster. *Genetics* **143**, 929-40.

Rorth, P. (2009). Collective cell migration. *Annu Rev Cell Dev Biol* **25**, 407-29.

Roszko, I., Sawada, A. and Solnica-Krezel, L. (2009). Regulation of convergence and extension movements during vertebrate gastrulation by the Wnt/PCP pathway. *Seminars in Cell & Developmental Biology* **20**, 986-997.

Roth, S. and Lynch, J. A. (2009). Symmetry Breaking During Drosophila Oogenesis. *Cold Spring Harbor Perspectives in Biology* **1**, -.

Royou, A., Field, C., Sisson, J. C., Sullivan, W. and Karess, R. (2004). Reassessing the role and dynamics of nonmuscle myosin II during furrow formation in early Drosophila embryos. *Mol Biol Cell* **15**, 838-50.

Ruohola, H., Bremer, K. A., Baker, D., Swedlow, J. R., Jan, L. Y. and Jan, Y. N. (1991). Role of Neurogenic Genes in Establishment of Follicle Cell Fate and Oocyte Polarity during Oogenesis in Drosophila. *Cell* **66**, 433-449.

Saburi, S., Hester, I., Fischer, E., Pontoglio, M., Eremina, V., Gessler, M., Quaggin, S. E., Harrison, R., Mount, R. and McNeill, H. (2008). Loss of Fat4 disrupts PCP signaling and oriented cell division and leads to cystic kidney disease. *Nat Genet* **40**, 1010-5.

Samakovlis, C., Hacohen, N., Manning, G., Sutherland, D. C., Guillemin, K. and Krasnow, M. A. (1996). Development of the Drosophila tracheal system occurs by a series of morphologically distinct but genetically coupled branching events. *Development* **122**, 1395-407.

Sausedo, R. A. and Schoenwolf, G. C. (1993). Cell Behaviors Underlying Notochord Formation and Extension in Avian Embryos - Quantitative and Immunocytochemical Studies. *Anatomical Record* **237**, 58-70.

Sausedo, R. A. and Schoenwolf, G. C. (1994). Quantitative-Analyses of Cell Behaviors Underlying Notochord Formation and Extension in Mouse Embryos. *Anatomical Record* **239**, 103-112.

Schmidt, S. and Friedl, P. (2010). Interstitial cell migration: integrin-dependent and alternative adhesion mechanisms. *Cell and Tissue Research* **339**, 83-92.

Schneider, M., Khalil, A. A., Poulton, J., Castillejo-Lopez, C., Egger-Adam, D., Wodarz, A., Deng, W. M. and Baumgartner, S. (2006). Perlecan and Dystroglycan act at the basal side of the Drosophila follicular epithelium to maintain epithelial organization. *Development* **133**, 3805-15.

Schoenwolf, G. C. and Alvarez, I. S. (1989). Roles of Neuroepithelial Cell Rearrangement and Division in Shaping of the Avian Neural Plate. *Development* **106**, 427-439.

Schupbach, T. and Wieschaus, E. (1991). Female sterile mutations on the second chromosome of Drosophila melanogaster. II. Mutations blocking oogenesis or altering egg morphology. *Genetics* **129**, 1119-36.

Segalen, M., Johnston, C. A., Martin, C. A., Dumortier, J. G., Prehoda, K. E., David, N. B., Doe, C. Q. and Bellaiche, Y. (2010). The Fz-Dsh planar cell polarity pathway induces oriented cell division via Mud/NuMA in Drosophila and zebrafish. *Dev Cell* **19**, 740-52.

Shih, J. and Keller, R. (1992a). Cell motility driving mediolateral intercalation in explants of Xenopus laevis. *Development* **116**, 901-14.

Shih, J. and Keller, R. (1992b). Patterns of cell motility in the organizer and dorsal mesoderm of Xenopus laevis. *Development* **116**, 915-30.

Shimada, Y., Yonemura, S., Ohkura, H., Strutt, D. and Uemura, T. (2006). Polarized transport of Frizzled along the planar microtubule arrays in Drosophila wing epithelium. *Developmental Cell* **10**, 209-222.

Simon, M. A., Xu, A. G., Ishikawa, H. O. and Irvine, K. D. (2010). Modulation of Fat:Dachsous Binding by the Cadherin Domain Kinase Four-Jointed. *Current Biology* **20**, 811-817.

Simons, M. and Mlodzik, M. (2008). Planar Cell Polarity Signaling: From Fly Development to Human Disease. *Annual Review of Genetics* **42**, 517-540.

Skoglund, P. and Keller, R. (2010). Integration of planar cell polarity and ECM signaling in elongation of the vertebrate body plan. *Curr Opin Cell Biol* **22**, 589-96.

Slack, J. M. W. (2006). Essential developmental biology. Malden, MA: Blackwell Pub.

Smart, I. H. (1991). Egg shape in birds. In *Egg incubation: its effects on embryonic development in birds and reptiles*, (ed. D. C. Deeming and M. W. J. Ferguson), pp. 101-116. Cambridge: Cambridge University Press.

Sokol, S. Y. (1996). Analysis of dishevelled signalling pathways during Xenopus development. *Current Biology* **6**, 1456-1467.

Solnica-Krezel, L., Stemple, D. L., Mountcastle-Shah, E., Rangini, Z., Neuhauss, S. C. F., Malicki, J., Schier, A. F., Stainier, D. Y. R., Zwartkruis, F., Abdelilah, S. et al. (1996). Mutations affecting cell fates and cellular rearrangements during gastrulation in zebrafish. *Development* **123**, 67-80.

Spemann, H. (1902). Entwicklungsphysiologische Studien am Triton - Ei II. *Arch. EntwMech.* **15**, 448-534.

Spradling, A. (1993). Developmental genetics of oogenesis. In *The development of Drosophila melanogaster*, (ed. M. Bate and A. Martinez-Arias), pp. 1-70. New York: CSHL Press.

Stanger, B. Z. (2008). Organ size determination and the limits of regulation. *Cell Cycle* **7**, 318-24.

Steinmetz, P. R. H., Zelada-Gonzales, F., Burgtorf, C., Wittbrodt, J. and Arendt, D. (2007). Polychaete trunk neuroectoderm converges and extends by mediolateral cell intercalation. *Proceedings of the National Academy of Sciences of the United States of America* **104**, 2727-2732.

Szczepanowska, J. (2009). Involvement of Rac/Cdc42/PAK pathway in cytoskeletal rearrangements. *Acta Biochimica Polonica* **56**, 225-234.

Tada, M. and Kai, M. (2009). Noncanonical Wnt/PCP Signaling During Vertebrate Gastrulation. *Zebrafish* **6**, 29-40.

Taylor, N. G. (2008). Cellulose biosynthesis and deposition in higher plants. *New Phytol* **178**, 239-52.

Tearle, R. and Nusslein-Volhard, C. H. (1988). Tubingen mutants and stocklist. In *Drosophila Inform. Service*, vol. 66 (ed. P. W. Hedrick), pp. 209-269.

Theisen, H., Purcell, J., Bennett, M., Kansagara, D., Syed, A. and Marsh, J. L. (1994). Dishevelled Is Required during Wingless Signaling to Establish Both Cell Polarity and Cell Identity. *Development* **120**, 347-360.

Torres, I. L., Lopez-Schier, H. and St Johnston, D. (2003). A notch/delta-dependent relay mechanism establishes anterior-posterior polarity in Drosophila. *Developmental Cell* **5**, 547-558.

Tree, D. R. P., Shulman, J. M., Rousset, R., Scott, M. P., Gubb, D. and Axelrod, J. D. (2002). Prickle mediates feedback amplification to generate asymmetric planar cell polarity signaling. *Cell* **109**, 371-381.

Tucker, J. B. and Meats, M. (1976). Microtubules and control of insect egg shape. *J Cell Biol* **71**, 207-17.

Tweedie, S., Ashburner, M., Falls, K., Leyland, P., McQuilton, P., Marygold, S., Millburn, G., Osumi-Sutherland, D., Schroeder, A., Seal, R. et al. (2009). FlyBase: enhancing Drosophila Gene Ontology annotations. *Nucleic Acids Res* **37**, D555-9.

Ueda, M., Koshino-Kimura, Y. and Okada, K. (2005). Stepwise understanding of root development. *Curr Opin Plant Biol* **8**, 71-6.

Vicente-Manzanares, M., Ma, X. F., Adelstein, R. S. and Horwitz, A. R. (2009). Non-muscle myosin II takes centre stage in cell adhesion and migration. *Nature Reviews Molecular Cell Biology* **10**, 778-790.

Viktorinova, I., Konig, T., Schlichting, K. and Dahmann, C. (2009). The cadherin Fat2 is required for planar cell polarity in the Drosophila ovary. *Development* **136**, 4123-32.

Viktorinova, I., Pismen, L. M., Aigouy, B. and Dahmann, C. (2011). Modelling planar polarity of epithelia: the role of signal relay in collective cell polarization. *J R Soc Interface*.

Vinson, C. R. and Adler, P. N. (1987). Directional Non-Cell Autonomy and the Transmission of Polarity Information by the Frizzled Gene of Drosophila. *Nature* **329**, 549-551.

Vladar, E. K., Antic, D. and Axelrod, J. D. (2009). Planar Cell Polarity Signaling: The Developing Cell's Compass. *Cold Spring Harbor Perspectives in Biology* **1**, -.

Vogt, W. (1922a). Die Einrollung und Streckung der Urmundlippen bei Triton nach Versuchen mit einer neuen Methode embryonaler transplantation. *Verh. dt. Zool. Ges.* **27**, 49-51.

Vogt, W. (1922b). Opertiv bewirkte "Exogastrulation" bei Triton und ihre Bedeutung fur die Theorie der Wirbeltiergastrulation. *Anat. Anz. Erg.* **55**, 53-64.

Waddington, C. H. (1940). Organizers and Genes. Cambridge: Cambridge University Press.

Wallingford, J. (2005). Neural tube closure and neural tube defects: studies in animal models reveal known knowns and known unknowns. *Am J Med Genet C Semin Med Genet* **135C**, 59-68.

Wallingford, J. B. (2010). Planar cell polarity signaling, cilia and polarized ciliary beating. *Current Opinion in Cell Biology* **22**, 597-604.

Wallingford, J. B., Rowning, B. A., Vogeli, K. M., Rothbacher, U., Fraser, S. E. and Harland, R. M. (2000). Dishevelled controls cell polarity during Xenopus gastrulation. *Nature* **405**, 81-5.

Wang, W. D. and Struhl, G. (2004). Drosophila epsin mediates a select endocytic pathway that DSL ligands must enter to activate notch. *Development* **131**, 5367-5380.

Wang, X., Harris, R. E., Bayston, L. J. and Ashe, H. L. (2008). Type IV collagens regulate BMP signalling in Drosophila. *Nature* **455**, 72-7.

Wang, Y. S. and Nathans, J. (2007). Tissue/planar cell polarity in vertebrates: new insights and new questions. *Development* **134**, 647-658.

Warga, R. M. and Kimmel, C. B. (1990). Cell Movements during Epiboly and Gastrulation in Zebrafish. *Development* **108**, 569-580.

Weber, G. F., Bjerke, M. A. and DeSimone, D. W. (2011). Integrins and cadherins join forces to form adhesive networks. *Journal of Cell Science* **124**, 1183-1193.

Wei, Y. and Mikawa, T. (2000). Formation of the avian primitive streak from spatially restricted blastoderm: evidence for polarized cell division in the elongating streak. *Development* **127**, 87-96.

Weisblat, D. A., Zackson, S. L., Blair, S. S. and Young, J. D. (1980). Cell lineage analysis by intracellular injection of fluorescent tracers. *Science* **209**, 1538-41.

Went, D. (1978). Oocyte maturation without follicular epithelium alters egg shape in a Dipteran insect. *J Exp Zool* **205**, 149-155.

Went, D. F. and Junquera, P. (1981). Embryonic development of insect eggs formed without follicular epithelium. *Dev Biol* **86**, 100-10.

Wieschaus, E., Audit, C. and Masson, M. (1981). A Clonal Analysis of the Roles of Somatic-Cells and Germ Line during Oogenesis in Drosophila. *Developmental Biology* **88**, 92-103.

Wigglesworth, V. B. (1940). Local and general factors in the development of "pattern" in Rhodnius prolixus (hemiptera). *Journal of Experimental Biology* **17**, 180-U9.

Williams-Masson, E. M., Heid, P. J., Lavin, C. A. and Hardin, J. (1998). The cellular mechanism of epithelial rearrangement during morphogenesis of the Caenorhabditis elegans dorsal hypodermis. *Developmental Biology* **204**, 263-276.

Windler, S. L. and Bilder, D. (2010). Endocytic Internalization Routes Required for Delta/Notch Signaling. *Current Biology* **20**, 538-543.

Xi, R. W., McGregor, J. R. and Harrison, D. A. (2003). A gradient of JAK pathway activity patterns the anterior-posterior axis of the follicular epithelium. *Developmental Cell* **4**, 167-177.

Yang, C. H., Axelrod, J. D. and Simon, M. A. (2002). Regulation of Frizzled by fat-like cadherins during planar polarity signaling in the Drosophila compound eye. *Cell* **108**, 675-688.

Yin, C., Kiskowski, M., Pouille, P. A., Farge, E. and Solnica-Krezel, L. (2008). Cooperation of polarized cell intercalations drives convergence and extension of presomitic mesoderm during zebrafish gastrulation. *Journal of Cell Biology* **180**, 221-232.

Yurchenco, P. D. and Patton, B. L. (2009). Developmental and Pathogenic Mechanisms of Basement Membrane Assembly. *Current Pharmaceutical Design* **15**, 1277-1294.

Zallen, J. A. (2007). Planar polarity and tissue morphogenesis. *Cell* **129**, 1051-63.

Zallen, J. A. and Wieschaus, E. (2004). Patterned gene expression directs bipolar planar polarity in Drosophila. *Developmental Cell* **6**, 343-355.

Zallen, J. A. and Zallen, R. (2004). Cell-pattern disordering during convergent extension in Drosophila. *Journal of Physics-Condensed Matter* **16**, S5073-S5080.

Zarnescu, D. C. and Thomas, G. H. (1999). Apical spectrin is essential for epithelial morphogenesis but not apicobasal polarity in Drosophila. *Journal of Cell Biology* **146**, 1075-1086.

Zhu, X. and Stein, D. (2004). RNAi-mediated inhibition of gene function in the follicle cell layer of the Drosophila ovary. *Genesis* **40**, 101-8.

Appendix A

Supplemental Information

This appendix provides supplementary information to Chapters 2 to 4 that add to the general knowledge on follicle elongation, other aspects of oogenesis or provide technical details that were non-essential for the understanding the general logic of the chapters. It is written as a series of topics supported with images and/or discussion that may be read in any order.

Chapter 2

A.2.1 The rate of polarized follicle rotation varies by stage:

The rate of polarized follicle rotation was measured by manually tracking individual or groups of follicle cells from a minimum of 3 time points using Volocity. Due to subtle shifts in follicles along one of the x, y or z axes during the time-lapse, these velocity estimates are prone to some experimental error in calculation and was not included in the main text. Interestingly, the average follicle cell velocity from live imaging correlates somewhat with the percent elongation that occurs during that stage from fixed samples.

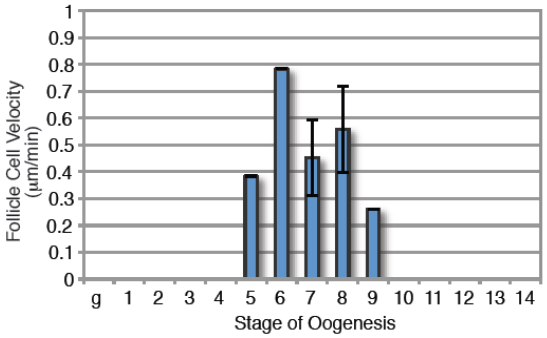

A.2.2 Interfollicular stalk cells can accommodate rotation of adjacent follicles

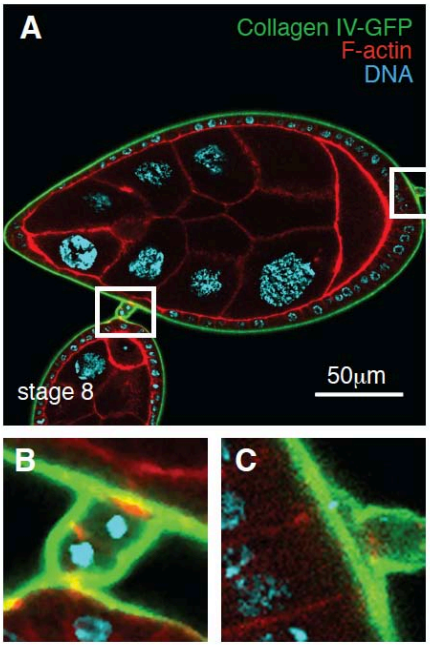

Those familiar with ovarian structure often wonder what the stalk cells do during follicle rotation. Time-lapse imaging reveals that the interfollicular stalk cells can accommodate rotation of adjacent follicles (see Movie 2.3). Closer analysis of the stalk cells from fixed samples reveals that they are in contact with the follicle basement membrane but not in direct contact with follicle cells.

(**A**) Stage 8 follicle expressing Collagen IV-GFP (green) reveals that stalk cells connecting adjacent follicles are in a distinct tissue compartment from rotating follicles due to their direct contact with the basement membrane. F-actin (red), DNA (cyan). Higher magnification of stalk cells contacting the follicle basement membrane in (**B-C**).

A.2.3 Planar polarity of F-actin is not always polarized orthogonal to the long A-P axis

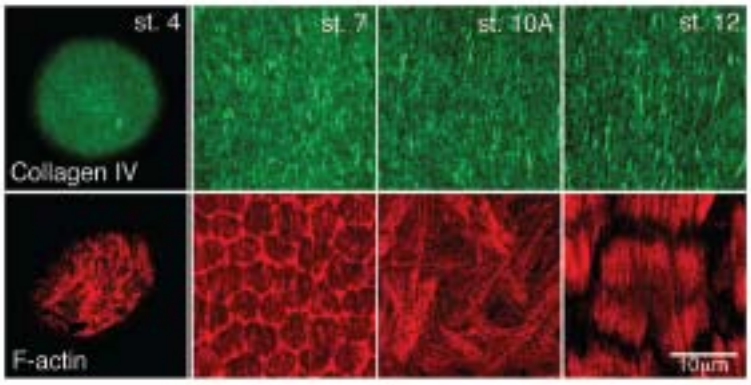

Early studies characterizing the basal actin cytoskeleton and Collagen IV matrix revealed that actin filaments are not always oriented orthogonal to the long A-P axis (bottom). This was not apparent at the beginning of my dissertation because most published reports report stage 6-8 or stage 12 follicles. Careful reading of Gutzeit's works revealed that he too recognized that actin filaments are not always circumferentially oriented, leading him to question F-actin as the molecular corset. This experiment helped me develop my primary hypothesis that perhaps the ECM instead acts as a molecular corset, as Collagen IV is the only basement membrane molecule that establishes and maintains this fibrillar organization during the entire elongation phase.

A.2.4 What percentage of the tissue needs to be mutant to see a round follicle phenotype?

This was a difficult question to answer for the longest time because the standard laser scanning microscope (LSM) primarily used for this project (Leica TCS SL) has very slow image acquisition speeds. Scanning an entire follicle would take 3-4 hours and this was not feasible given the high usage of this microscope. Access to a Zeiss 5 Live fast scanning microscope dramatically improved image acquisition speed, enabling whole follicle scans with good resolution in 8-20 minutes.

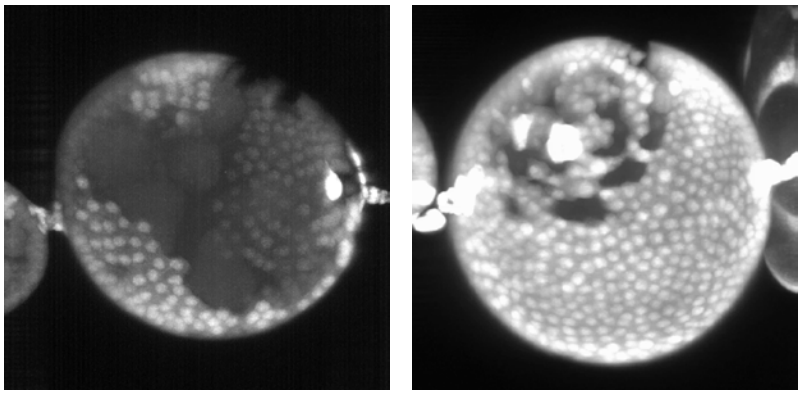

For *mys*^{XG43} null follicle cell clones, approximately one-third of the follicle is mutant in the round follicles analyzed (left). The mutant clone (marked by the absence of GFP (white)) usually occupies one large region and can reside anywhere in the follicle epithelium (e.g., mutant clones are not always found at follicle poles). However, clones can occupy as little as 5-10% of the follicle epithelium (right) and still yield a round follicle phenotype.

For *vkg*^{ICO} null follicles, the majority (>90%) of the follicle epithelium must be mutant in order to see a round follicle phenotype. This makes sense given that *vkg* encodes Collagen IV, an extracellular molecule. Analysis on *vkg*'s function was performed on follicles that were completely mutant for *vkg*.

A.2.5 Fertilized round vkg^{ICO} *mutant eggs can go through embryogenesis and hatch as larvae*

Consistent with observations made on other round egg mutants like *seg*, formation of a round egg is not incompatible with normal embryonic development. This *vkg*^{ICO} round egg was found inside an adult female uterus with a larvae hatching out upon dissection.

A.2.6 Follicle cells are the primary (but not only) source of the follicle basement membrane

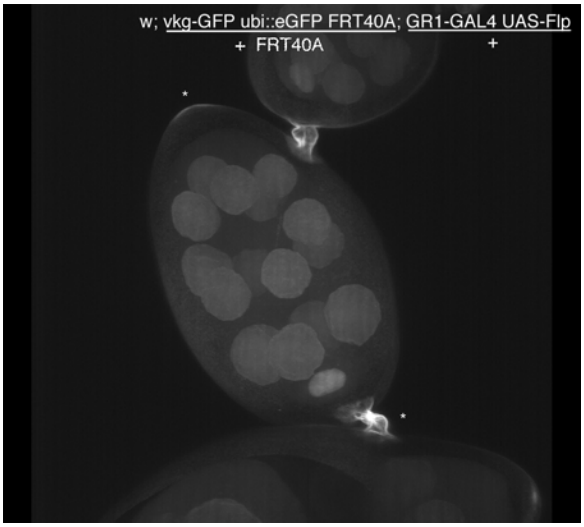

One question that was of concern when studying a gene encoding an extracellular matrix (ECM) molecule was whether the tissue being targeted is the only source tissue for ECM deposition. Hemocytes are major sources of basement membrane production during embryogenesis and larval stages, but its contribution to follicle basement membrane in the adult was unknown.

This preliminary experiment was part of one strategy taken to identify source cells by genetically linking them to the production of Collagen IV-GFP. By generating tissue mosaics in a wild type background, I can select for follicles whose epithelium are completely unmarked and yield unlabelled Collagen IV (left). This enables me to determine whether other cell types might be contributing to the follicle basement membrane. This image of an ovariole where all follicle cells are unlabelled indicate that the basement membrane surrounding the stalk cells are deposited by non-follicle cell source tissues. The higher level of Collagen IV-GFP at the anterior tip of the stage 7 follicle shown seems to be a historical mark when that portion of the basement membrane was in direct contact with the stalk cells. Note that no fibrillar Collagen IV-GFP is seen, indicating that follicle cells are the only source that produces the fibrillar Collagen IV matrix. Closer examination of the sample reveals a faint amount of Collagen IV-GFP in the lateral region of the follicle. This is speculated to be the "basal matrix" I discuss in the text, which I observe overlying the germarium and stage 1-4 follicles.

A.2.7 Is there a pattern to Collagen fibrillogenesis?

In depth analysis has not been performed on this question, but examination of follicles where the source cells are linked to the production of Collagen IV-GFP and span across the A-P axis show an interesting gradient in Collagen IV-GFP deposition across this axis (right), where it seems like there is more Collagen IV-GFP deposited in the center of the follicle and less at the poles. This may suggest that as the follicle grows during the elongation phase, the historically oldest part of the basement membrane is in the middle region, and the follicle grows outward towards the poles. It remains unclear how new ECM fibrils get incorporated into the existing basement membrane – through intercalation or biased deposition towards the poles. These patterns also provide some insights to the non-autonomy in ECM deposition seen at clone borders from tissue mosaic analysis and suggest some this non-autonomy may be due to growth patterns of the follicle and follicle basement membrane that occur during the elongation phase.

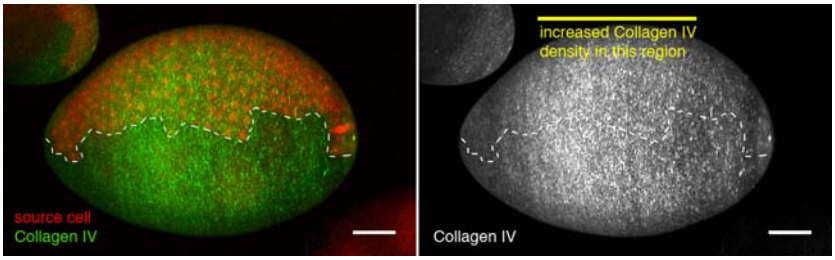

A.2.8 The basement membrane surrounding other tissues do not form a polarized, fibrillar Collagen IV matrix.

Type IV Collagens are typically not associated with the formation of fibrils; this organization is associated with type I Collagens in vertebrates. Thus, the observation that *Drosophila* Collagen IV forms fibrils in the follicle basement membrane was a bit surprising. Examination of basement membranes underlying other tissues indicates that Collagen IV forms a more traditional mesh-like network in other tissues, as shown here in the 3rd larval instar wing imaginal disc (left).

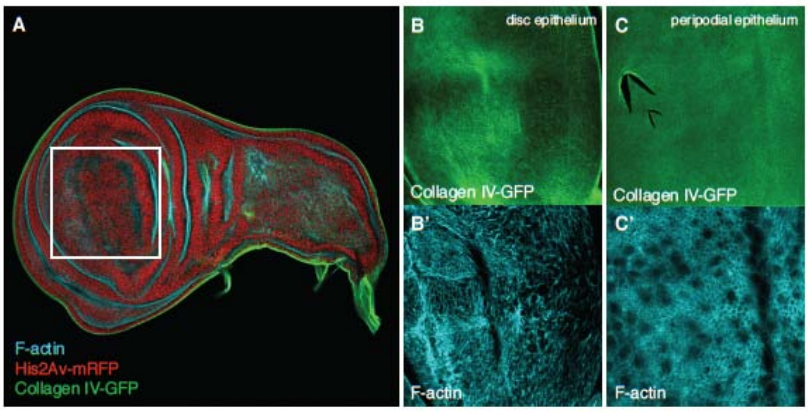

A.2.9 Collagen IV-GFP maximum fibrillar length or fibrillar density does not significantly differ between mys mutant mosaic follicles and wild type controls.

(**A**) Maximal length and (**B**) fibrillar density of the Collagen IV matrix in *mys* mutant mosaic follicles and wild type control samples shown in Fig. 2.14.

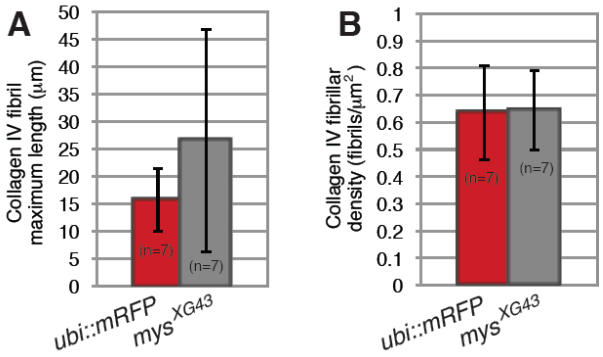

A.2.10 Follicle cell multilayering does not affect follicle shape.

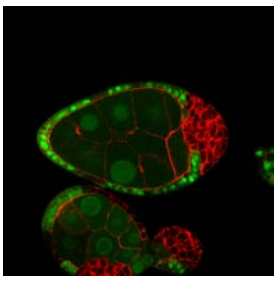

One concern examining *mys* mosaic follicles was that *mys* has pleiotropic effects during oogenesis, including a requirement to maintain follicle cells as a monolayer epithelium (Fernandez-Minan et al., 2007). For the analyses on *mys* performed in this dissertation, only follicles that maintain an epithelial monolayer were used for data quantification. In addition, the following control was performed: *rab5* mutant follicle cell clones exhibit strong multilayering phenotypes but have no notable effect on follicle shape (left).

A.2.11 Polarized follicle rotation is observed in other Drosophilid species but is not observed in more basally derived insects (grasshoppers and milkweed bugs).

In efforts to appreciate the generality of global tissue rotation in metazoans, I examined whether other insects undergo polarized follicle rotation to determine whether polarized rotation is conserved among insects that produce ellipsoid eggs. Species were selected to provide broad coverage across the Drosophilid and Insecta phylogenies.

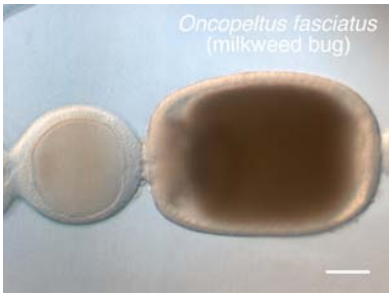

Both *Drosophila* species undergo polarized rotation. Interestingly, the rate of polarized follicle rotation seems to correlate with the extent of elongation seen at equivalent stages between the different Drosophilid species. However, quantification of the rate of follicle rotation was not made due to the low resolution using brightfield microscopy for these time-lapses.

In contrast, polarized follicle rotation was not readily detected in either the grasshopper or milkweed bug, although small cells seems to be actively moving around the follicle that did not appear to be the follicle epithelium. Some limitations in optimal culturing conditions or the imaging setup for these insect follicles restrict the information that can be obtained from brightfield time-lapse imaging. Interestingly, grasshopper follicles have circumferentially oriented actin filaments around elongate follicles. Whether these follicles also exhibit a polarized ECM has not been determined but would be interesting to follow up.

A.2.12 Coordinated basal actomyosin polarity is thought to underlie collective cell migration during global tissue rotation

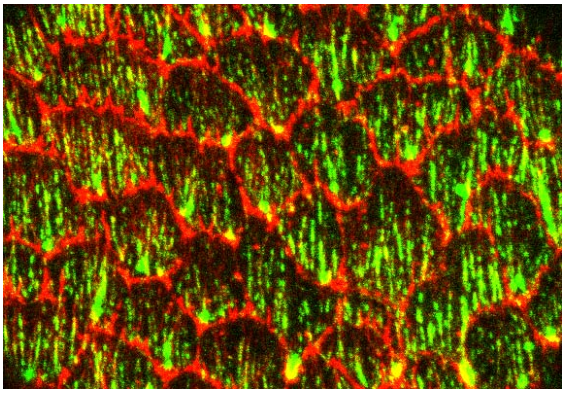

Here is a basal surface view from a stage 8 follicle supporting our view that basal actomyosin contractile forces are generated by follicle cells in the direction of motility to exert traction through focal adhesions on to the basement membrane. Note monopolar F-actin protrusions (red) appear to be at the leading edge while Myosin II regulatory light chain (MRLC-GFP, green) appears to be on the lagging edge, consistent with other polarized cells undergoing cell migration. However, these observations come from fixed samples and have yet to be examined under live conditions. Measurements of forces have not been tackled in our lab and have yet to be performed in this system.

A.2.13 Efforts to image polarized follicle rotation in vivo have been unsuccessful

Several attempts were made to image polarized follicle rotation in intact ovaries or *in vivo* performing open abdomen surgery on an adult female (right). No time-lapse provided interpretable data sets due to strong contractions from the ovarian muscles, gut and/or dorsal vessel. Efforts to block ovarian muscle contractions using the Nox inhibitor diphenylene iodinium (DPI; Sigma) were not successful.

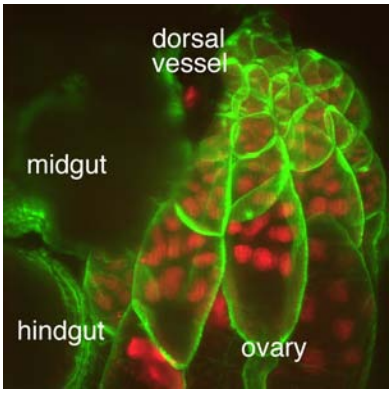

A.2.14 Additional details for Collagen IV-GFP fibril analysis

The flow diagram below provides more information on the steps taken to process each sample for Collagen IV-GFP fibril analysis for data generated in Figure 2.9 and Figure 2.14:

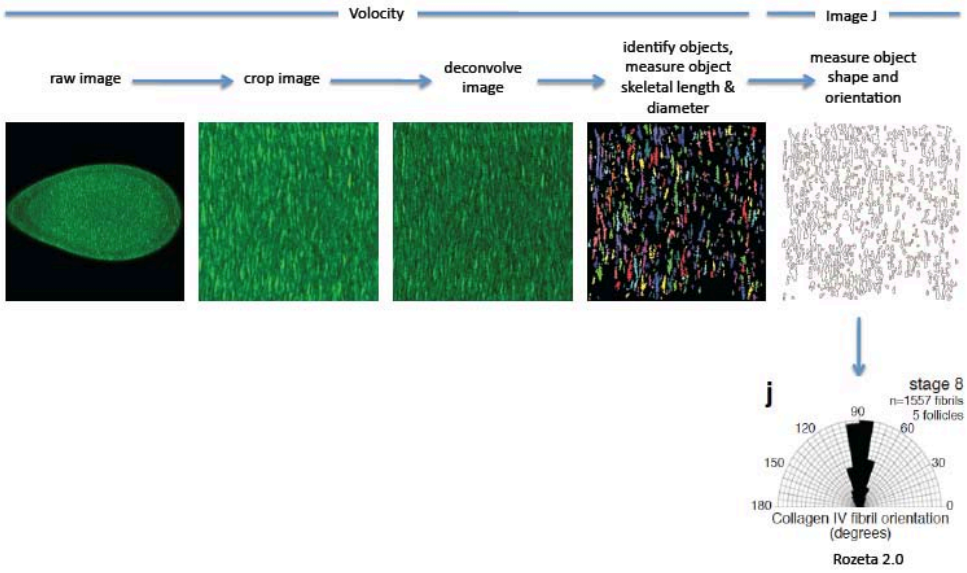

Chapter 3

A.3.1 Additional details for morphometric analysis of follicle epithelial topology

Images of raw images (left column) and traced (middle column) cells used for epithelial topology analysis. The image on the right depicts two potential indicators of individual follicle shape using ImageJ: Fit Ellipse (blue circle) or Feret's Diameter (pink line). Empirical studies found that Fit Ellipse most closely approximated cell shape and cell orientation for most cells used. Thus, Fit Ellipse was further developed for a protocol to analyze follicle epithelial topology.

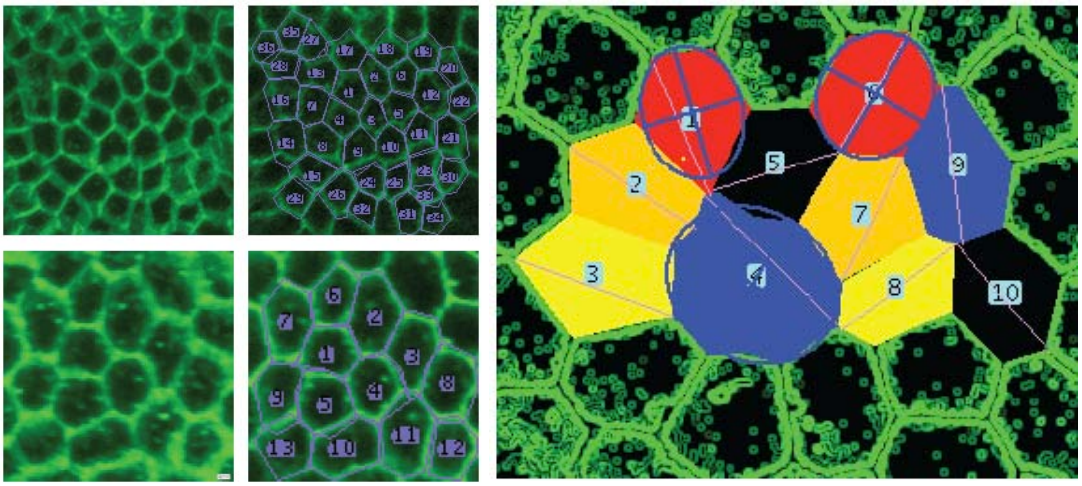

Appendix B

Supplemental Movies

This appendix provides movie captions to supplemental movies presented in Chapters 2 to 4. Movies will be stored on a DVD that will be filed with this dissertation as supplementary materials. Movies 2.2 to 2.9 are available online as supporting online material with the *Science* publication associated with Chapter 2. Visit:

http://www.sciencemag.org/content/331/6020/1071/suppl/DC1.

For access to all movies, please direct requests to the U.C. Berkeley Graduate Division, my Ph.D. dissertation advisor David Bilder, or myself.

Movie 2.1
Live imaging of developing follicles in culture can recapitulate *in vivo* follicle cell behaviors. 3D live imaging of ovarioles expressing Indy-GFP to mark follicle epithelia plasma membranes, imaged at a sagittal view. Stage 6, left; stage 9, middle; stage 10A, bottom right. This proof of principle experiment demonstrates that border cell migration occurs faithfully in the stage 9 follicle under our laboratory conditions (middle). Of note, however, is the younger stage 6 follicle (left, arrow) that is part of the major elongation phase and appears to be undergoing some directional movement during the time course of the movie. This movie is a prelude to the discovery of polarized follicle cell movement seen in Movie 2.2. Movie length is 4 hours with 2 minute time points.

Movie 2.2
The follicle epithelium undergoes a polarized, concerted migration perpendicular to the long A-P axis. 3D live imaging of stage 8-9 follicle expressing Indy-GFP to mark follicle epithelia plasma membranes, imaged at the basal surface. The follicle epithelium is seen moving perpendicular to the long A-P axis but stops towards the end of the movie when border cell migration has begun. Movie length is 4 hours with 2 minute time points.

Movie 2.3
Global tissue rotation coincides with the major elongation phase of oogenesis. 4D live imaging of an ovariole expressing His2Av-mRFP and Indy-GFP. 87 μm maximal projection. In stage 6 and 7 follicles, large polyploid germline nuclei (red) are seen rotating in concert with the follicle epithelium (green), while stage 4 and stage 9 follicles do not rotate. Note also that the stage 6 and stage 7 follicles are rotating with opposite chirality. Movie length is 3 hours with 5 minute time points.

Movie 2.4
The follicle epithelium moves against a static basement membrane. 4D live imaging of stage 8 follicle expressing myristolated mRFP (red) in follicle epithelia and Collagen IV-GFP (green) to highlight the fibrillar Collagen IV matrix, imaged at the basal surface. 26μm maximal projection. Follicle cells can be seen moving past static Collagen IV fibrils. Note that intracellular Collagen IV puncta can be seen moving within follicle cells against static Collagen IV fibrils within the basement membrane. Merge is to the left, Collagen IV-GFP is in the upper right, myristolated-mRFP is in the bottom right. Movie length is 38 minutes with 2 minute time points.

Movie 2.5
***mys* mutant follicles fail to undergo polarized rotation.** 3D live imaging of a round stage 8 *mys* mutant mosaic follicle expressing Indy-GFP. mys^{XG43} cells are identified by a lack of cellular GFP. The follicle does not rotate. Movie length is 2 hours with 2 minute time points.

Movie 2.6
Control genotype for *mys* mutant follicles undergo polarized follicle rotation. 3D live imaging of stage 7 sibling control genotype for Supplementary Movie 4. All follicle cells are wild type, indicated by intracellular GFP. The follicle rotates normally. Movie length is 2 hours with 2 minute time points.

Movie 2.7
A minor percentage of *mys* mutant follicles undergo off-axis rotation. 3D live imaging of a round stage 7 *mys* mutant mosaic follicle that undergoes off-axis rotation. All follicle cells express Indy-GFP. mys^{XG43} cells are identified by a lack of intracellular GFP. Movie length is 2 hours with 2 minute time points.

Movie 2.8
***vkg* mutant follicles fail to undergo polarized rotation when they first exhibit a defect in follicle shape at stage 8.** 3D live imaging of a stage 8 *vkg* mutant follicle expressing Indy-GFP. All follicle cells are mutant for vkg^{ICO}, indicated by a lack of intracellular GFP. The follicle does not rotate. Movie length is 2 hours with 2 minute time points.

Movie 2.9
Control genotype for *vkg* mutant follicles undergo polarized follicle rotation. 3D live imaging of stage 8 sibling control genotype for Supplementary Movie 7. All follicle cells are wild type, indicated by intracellular GFP. The follicle rotates normally. Movie length is 2 hours with 2 minute time points.

Movie 3.1
***rhea* mutant mosaic follicles undergo off-axis rotation.** 3D live imaging of ovarioles that are tissue mosaic for *rhea*. All follicle cells express Neuroglian-GFP. $rhea^{79a}$ cells are identified by a lack of intracellular GFP. Note the round *rhea* mosaic follicle in the center of the movie; it undergoes off-axis rotation. A sibling wild type control below exhibits normal polarized rotation. Movie length is 2.6 hours with 5 minute time points.

Movie 4.1
***lqf* germline mutant follicles undergo off-axis rotation.** 3D live imaging of ovarioles that are germline mutant for the epsin homolog *lqf*. lqf^{L71} germline mutants are identified by a lack of GFP. Ovarioles from a control genotype (green) were included as a positive control for polarized follicle rotation. Note the rounder *lqf* germline mutant follicles in the center of the movie undergo off-axis rotation. Wild type controls below exhibit normal polarized rotation. Movie length is 3 hours with 5 minute time points.